Coventry University

DOCTOR OF PHILOSOPHY

Automotive Tyre Fault Detection

Ersanilli, Vincent Emile

Award date:
2015

Awarding institution:
Coventry University

Link to publication

General rights
Copyright and moral rights for the publications made accessible in the public portal are retained by the authors and/or other copyright owners and it is a condition of accessing publications that users recognise and abide by the legal requirements associated with these rights.

- Users may download and print one copy of this thesis for personal non-commercial research or study
- This thesis cannot be reproduced or quoted extensively from without first obtaining permission from the copyright holder(s)
- You may not further distribute the material or use it for any profit-making activity or commercial gain
- You may freely distribute the URL identifying the publication in the public portal

Take down policy
If you believe that this document breaches copyright please contact us providing details, and we will remove access to the work immediately and investigate your claim.

Download date: 04. May. 2023

Automotive Tyre Fault Detection.

Ersanilli, V.

Submitted version deposited in the institutional repository June 2016

Original citation:
Ersanilli, V. (2015) Automotive Tyre Fault Detection. Unpublished PhD Thesis. Coventry: Coventry University Jaguar Land Rover.

Copyright © and Moral Rights are retained by the author. A copy can be downloaded for personal non-commercial research or study, without prior permission or charge. This item cannot be reproduced or quoted extensively from without first obtaining permission in writing from the copyright holder(s). The content must not be changed in any way or sold commercially in any format or medium without the formal permission of the copyright holders.

Some materials have been removed from this thesis due to third party copyright. Pages where material has been removed are clearly marked in the electronic version. The unabridged version of the thesis can be viewed at the Lanchester Library, Coventry University.

Automotive Tyre Fault Detection

Vincent Ersanilli B.Sc. M.Sc.

A thesis submitted in partial fulfilment of

the University's requirement for the

degree of Doctor of Philosophy.

January 2015

Control Theory and Applications Centre

Coventry University

in collaboration with Jaguar Land Rover,

Whitley, Coventry, UK

Summary

The focus of the work in this thesis is concerned with the investigation and development of indirect measurement techniques. The methodology adopted is a combination of practical experimental, analytical deductive reasoning and simulation studies. This has led to proposals for a number of indirect tyre pressure monitoring systems, which are able to detect pressure loss under specific circumstances. The outcome overall is a proposal for a new supervisory system comprising of a modular framework, allowing various algorithms and techniques to be implemented in a complementary manner as they emerge and data sources become available.

A number of contributions to the field have been made, which to the knowledge of the author, provide potential for further algorithm development and are imminently applicable given the above. The methods include a tyre pressure diagnosis via a wheel angular velocity comparator, the development of a model-based tyre pressure diagnosis via application of an unknown input observer and a parameter estimation scheme, a model-based tyre pressure diagnosis approach via an enhanced Kalman filter configured to estimate states including the input, a model-based tyre pressure diagnosis via cautious least squares, an investigation and critique of the effects of the choice of sampling interval on discrete-time models and estimation thereof. It is considered, that the extensive literature review provides a valuable historic insight into the tyre fault detection problem.

It is clear, from the development and testing of the algorithms (and also the literature), that no single indirect pressure detection method is able to reliably detect changes in all driving scenarios which the regulations typically stipulate (depending on jurisdiction). In the absence of any information about the road input, the majority of the detection work must be shouldered by the wheel angular velocity comparator algorithm. As image recognition and sensor technology develops, it becomes possible to make estimates about the road surface and this removes some of the uncertainty on the input of the model-based parameter estimation approaches.

Further work is detailed which goes some way towards realising the next steps in a development cycle suitable for a vehicle manufacturer to take through to the implementation stage.

Acknowledgements

Primarily I would like to acknowledge my wife, Lubomira, for the many things she has sacrificed while I worked on this thesis. Luba's moral and logistical support has been unrelenting.

I also acknowledge the significant contribution made by Professor Keith Burnham, who taught me much of what I know about control engineering. His enthusiasm for the subject has inspired me to pursue this path.

Other notable contributions come from the research staff and students at the Control Theory and Applications Centre (CTAC) and the friendly and capable staff at Jaguar Land Rover, who were instrumental in my data collection experiments and endlessly helpful.

Table of Contents

List of figures

List of tables

List of Symbols

A	matrix
X	observation matrix
u_{fc}	continuous time filtered input
B_s	Damper constant
k_s	Suspension spring constant
k_t	Tyre spring constant
m_s	Sprung mass
m_{us}	Un-sprung mass
x_r	Road input displacement
x_s	Sprung mass displacement
x_{us}	Un-sprung mass displacement
x	state variable
$\dot{x}$	first derivative of x
y_{fc}	continuous time filtered output
α	continuous time denominator coefficient
β	continuous time numerator coefficient
δ	discrete time delay
ε_L	CLS fault detection lower bound
ε_U	CLS fault detection upper bound
ζ	damping ratio
$\hat{\theta}$	estimated parameter vector
θ	parameter vector
θ_s	CLS safe parameter vector
λ	forgetting factor
ξ	additive noise
π	pi
σ	variance
Σ	sum
τ	continuous time delay
ϕ	observation vector
ω_n	natural frequency
ω_d	damped natural frequency

Nomenclature and Terminology

On examination of the fault detection and condition monitoring literature, it is apparent that consensus does not exist on the terminology used by the community of this discipline. In order to clarify terms this thesis shall adhere to the terminology descriptions defined by The SAFEPROCESS Technical Committee (Simani et al. 2003) with some additional terms for automotive specific descriptions and acronyms. The following list, while not exhaustive, attempts to define the common terms in the literature and in this thesis. It should be considered as a snapshot appropriate at the time of writing, as the list will evolve, as new techniques emerge and are classified.

States and Signals

Fault

An unpermitted deviation of at least one characteristic property or parameter of the system from the acceptable, usual or standard condition.

Failure

A permanent interruption of a system's ability to perform a required function under specified operating conditions.

Malfunction

An intermittent irregularity in the fulfilment of a system's desired function.

Error

A deviation between a measured or computed value of an output variable and its true or theoretically correct one.

Disturbance

An unknown and uncontrolled input acting on a system.

Residual

A fault indicator based on a deviation between measurements and model-equation-based computations.

Symptom

A change of an observable quantity from normal behaviour.

Functions

Fault detection

Determination of faults present in a system and the time of detection.

Fault isolation

Determination of the kind, location and time of detection of a fault. Follows fault detection.

Fault identification

Determination of the size and time-variant behaviour of a fault. Follows fault isolation.

Fault diagnosis

Determination of the kind, size, location and time of detection of a fault. Follows fault detection. Includes fault detection and identification.

Monitoring

A continuous real-time task of determining the conditions of a physical system, by recording information, recognising and indicating anomalies in the behaviour.

Supervision

Monitoring a physical system and taking appropriate actions to maintain the operation in the case of a fault.

Models

Quantitative model

Use of static and dynamic relations among system variables and parameters in order to describe a system's behaviour in quantitative mathematical terms.

Qualitative model

Use of static and dynamic relations among system variables in order to describe a system's behaviour in qualitative terms such as causalities and IF-THEN rules.

Diagnostic model

A set of static and/or dynamic relations which link specific input variables, the symptoms, to specific output variables, the faults.

Analytical redundancy

Use of more (not necessarily identical) ways to determine a variable, where one way uses a mathematical process model in analytical form.

System properties

Reliability

Ability of a system to perform a required function under stated conditions, within a given scope, during a given period of time.

Safety

Ability of a system not to cause danger to persons or equipment or the environment.

Availability

Probability that a system or equipment will operate satisfactorily and effectively at any point of time.

Time dependency of faults

Abrupt fault

Fault modelled as stepwise function. It represents bias in the monitored signal.

Incipient fault

Fault modelled by using ramp signals. It represents drift of the monitored signal.

Intermittent fault

Combination of impulses with different amplitudes.

Fault terminology

Additive fault

Influences a variable by an addition of the fault itself. They may represent, e.g., offsets of sensors.

Multiplicative fault

Are represented by the product of a variable with the fault itself. They can appear as parameter changes within a process.

Automotive terminology

ABS

Anti-locking Brake System

ADAS

Advanced Driver Assistance Systems, typically image recognition based systems that are intended to reduce the workload of the driver or increase safety e.g. collision mitigation braking

CAFE

Corporate Average Fuel Economy

CAN

Controller Area Network.

LS-CAN

Low speed CAN. Fault tolerant implementation for physically large networks and/or harsh environments. ISO standard ISO11898-3

MS-CAN

Medium Speed CAN is not a recognised specification but generally acknowledged to be ~250kbit/s in automotive engineering applications, for the purpose of non-safety critical control such as interior lights and functionality

HS-CAN

High Speed CAN (typically 500kbit/s, up to 1Mbit/s). SAE standard J2284-3, ISO standard ISO11898-2

CAN data frame

A data frame carries data from a transmitter to the receivers.

Curb weight

Mass of the vehicle with no occupants or additional load.

Distributed functionality

Functions are dependent on multiple controllers. The ABS depends on the wheel speed sensor but many other functions may also depend on the same signal, such as odometer and satellite navigation.

DTC

Diagnostic Trouble Code. SAE standard J2012 defines the trouble codes and their definition

ESC

Electronic Stability Control. See ESP

ESP

Electronic Stability Program. ESP is a trade mark of Bosch GmbH for a system that utilise the ABS system for the purposes of vehicle steering correction in the event of loss of traction, typically over-under-steer events.

GVW

Gross Vehicle Weight. Maximum permissible vehicle weight.

OBD/OBD-II

On-Board Diagnostics. Regulatory mandated standards for a vehicles self-diagnostic and reporting functions. Various standards set by SAE and ISO exist that define how OBD is

implemented in the vehicle and through the interface (SAE J1962, commonly referred to as the 'J1962 connector') that exists in the drivers footwell.

OEM

Original Equipment Manufacturer.

Safety critical

Safety critical is a term typically used to refer to a subset of systems on the vehicle whose function, if it were to fail, would be deemed an immediate threat to safety e.g. brake system.

Steering angle

The angular displacement of the steering wheel broadcast on the CAN as a degree value typically in the range 430° to -430°

TPMS

Tyre Pressure Monitoring System. A set of sensors placed in the air space of the road wheels of a vehicle directly sample the air pressure. Referred to as 'direct' in this thesis

TREAD

The Transportation Recall Enhancement, Accountability and Documentation (or TREAD) Act is a United States federal law. It was drafted in response to fatalities related to Ford Explorers fitted with Firestone tyres.

Miscellaneous terminology and acronyms

BAE

British Aerospace Engineering

CLS

Cautious Least Squares. The method of constraining the solution space of the estimation of a parametric model using least squares. The model and associated covariance matrix is reset to its original state (parameters) when a particular threshold has been transgressed.

CSV

Comma Separated Values. A non-standardised but widely recognised file format where data (numbers and text) is stored in plain-text form with commas or semi-colons used as delimiters. This format is favoured for data acquisition due to its compatibility with software tools, such as MATLAB.

CT

Continuous Time. Transfer function models in the frequency domain are functions of 's'

DAQ

Data Acquisition. A device that is designed to acquire and store data in a systematic way for future analysis

DFT

Discrete Fourier Transform

DSC

Digital Signal Controller (CPU)

DSP

Digital Signal Processor

DT

Discrete Time. Transfer function models in the time domain are functions of 'z'

ECU

Electronic Control Unit. Embedded automotive control, often deployed in distributed functionality systems with a CAN

EEPROM

Electrically Erasable Programmable Read Only Memory

EMS

Engine Management System, an ECU in the vehicle HS-CAN

EN

Euclidean Norm $\|x\| \coloneqq \sqrt{x_1^2 + \cdots + x_n^2}$

ETI

Elapsed Time Indicator

FFT (fft)

Fast Fourier Transform

FMEA

Failure Mode and Effects Analysis. A mainly subjective and qualitative analysis of failure modes and their effects upon system function. Intended as a measure to improve system reliability.

Freeware

Software that is usually developed by enthusiasts or a community, typically open source and freely available on the internet

FTA

Fault Tree Analysis. In the context of automotive engineering the FTA is usually based on the DTC list and provides a description of the conditions that cause the DTC to occur.

GPS

Global Positioning System. Basis of satellite navigation

I2C

MEPHM internal communications protocol

I/O

Input/Output

IFFT (ifft)

Inverse Fast Fourier Transform

LIDAR

Lidar is sensing technology that determines distance by illuminating the target with a laser and measuring the reflected portion of the light.

MEMS

Micro Electro-Mechanical System

MEPHM

Micro-Electronic Prognostic Health Monitor, product of BAE Systems. A vibration and temperature a data logger with CAN interface and FFT capability

PCB

Printed Circuit Board

PSD

Power Spectral Density

RLS

Recursive Least Squares

RS-232

Serial Communication Protocol

SF

Sampling Frequency

TF

Transfer Function

UNECE

The United Nations Economic Commission for Europe (UNECE or ECE) Transport Division is the provider of secretariat services to the World Forum for Harmonisation of Vehicle Regulations (WP.29). The World Forum has incorporated into its regulatory framework the technological innovations of vehicles to make them safer and more environmentally sound.

Chapter 1.

Introduction and outline of approach

1.1. Background and motivation

It is not clear what singularly motivated the original development of tyre pressure monitoring systems (TPMS), but there are practical considerations owing to the effect tyre pressure has on

- Safety (Smith, T. and Knight 2005, Brewer and Rice, R. S. 1983, Li, L. et al. 2005)
- Vehicle dynamics, handling and comfort (Pacejka 2006b)
- Brake effectiveness (Shyrokau and Wang, D. 2013)
- Rolling resistance and hence, efficiency (Clark and Dodge 1979)
- Tyre lifespan (Sivinski 2012).

The technology required to implement a direct TPMS had existed for quite some time by the 1980s. Whilst the novelty involved in the creation of a direct measurement solution is not significant, there are a number of non-trivial engineering challenges to overcome such as

- Operating a sensor in the harsh environment of a vehicle tyre
- Managing energy consumption such that the sensor battery life is acceptable
- Reliably transmitting data to the electronic control unit (ECU)
- Interpreting the sensor measurement data in the presence of unknown disturbances (road shocks and temperature variation)
- Interpreting the sensor measurement data in the presence of unknown disturbances (road shocks and temperature variation)
- Ensuring long term reliability, particularly of the sensors.

It is possible that the motivation for the initial systems was a marketing tactic to differentiate the brands and products of the original equipment manufacturers (OEM) who had invested in the technology.

TPMS technology was first introduced to the European market as an optional feature for luxury passenger vehicles in the 1980s. The first series-production passenger vehicle to adopt a TPMS was the Porsche 959 in 1986, featuring a direct measurement system, utilising radio frequency (RF) transmitters to get the tyre pressure measurement across the rotating boundary of the

wheel and into the data acquisition system that resides in an ECU. The ECU interprets the pressure signal, allowing for disturbances such as tyre deflection and thermal effects, and transmits the tyre pressure onto the vehicles data bus so that the instrument cluster can display the tyre pressure for the convenience of the driver. The Peugeot 607, launched in October 1999, was equipped with a TPMS as a standard feature. Following Peugeot-Citroën, Renault launched the Laguna II in 2000, which could be argued as the advent of the first mass-produced vehicle to be equipped with TPMS as a standard feature. These systems were all based on the same principle of operation as the Porsche 959, namely direct TPMS.

In the United States, a Schrader TPMS was used for the 1997 Corvette developed by General Motors. The vehicle also featured a Goodyear run-flat tyre and wheel system. This is a conventional RF based TPMS with the capability to detect tyre pressure at any wheel with warnings for both high and low pressure.

At this point in the development of TPMS by various OEM, advancements in the safety aspects of vehicles and rising fuel costs led to an increased interest in TPMS as a means of benefitting from the points listed in the opening paragraph. Despite the fact that most drivers know that having correct pressures is important, different studies have shown that many vehicles still run with under-inflated tyres. A study from Sweden (Sturmhoebel 2012), for instance, provides an example. The study showed that 20% of the vehicles sampled had tyres that were underinflated by 20% or more. The survey results have been mirrored in other countries (Singh et al. 2009).

This item has been removed due to 3rd Party Copyright. The unabridged version of the thesis can be viewed in the Lanchester Library Coventry University.

Figure 1.1 A fully inflated tyre (upper) vs a 70% inflated tyre (lower) (Marsh, 2004)

TPMS will not prevent every tyre failure and does not automatically control the tyre pressures to the correct level. However, they can provide early warnings if one or more of the tyres loses pressure, and also help the driver to maintain the correct tyre pressure level in all tyres. The first point may appear trivial but in practice many drivers do not themselves notice under-inflation. A visual inspection is not considered to be a very accurate means of estimating tyre pressure except in extreme cases of under-inflation, as Figure 1.1 shows. In addition to this property of the tyre, driver assistance technology, such as power

assisted steering and electronic stability programs (ESP), mask the effects of the under-inflated tyre(s) through their normal action to maintain vehicle dynamics and handling properties.

Nowadays, mandates for TPMS legislation are increasing globally (GIA 2013). TPMS offers an average of 2% improved fuel economy (Clark and Dodge 1979) and is seen as one of several fuel efficiency improvements that European car makers are undertaking to achieve the new levels for average fleet CO_2 emissions, the Corporate Average Fuel Economy (CAFE) legislation (Greenhouse Gas Emissions Standards and Fuel Efficiency Standards for Medium and Heavy-Duty Engines and Vehicles 2011). Safety is generally regarded as an important benefit of TPMS, but the desire for CO_2 reduction has been a stronger influence in the European market due to the acceptance of climate change in general. This is reflected in the legislation associated with fossil fuel consuming activities, particularly personal vehicles. The situation in the USA is different in that the claims of climate change caused by human activity is generally viewed with more scepticism amongst the population at large. Considerations for CO_2 were not a factor in the development of the Transportation Recall Enhancement, Accountability and Documentation (TREAD) Act (Transportation Recall Enhancement, Accountability, and Documentation (TREAD) Act 2000), which is aimed at improving safety rather than reducing CO_2.

Following the lead of US and European TPMS mandates, Asia represents the next large vehicle market with incipient TPMS legislation. Japan, Korea, China and India are all currently in the process of adopting similar legislation. Korea has already confirmed its intention with legislation, two months behind the European timeline for full implementation. Japan, China and India are expected to follow, most likely within a year or two of these dates, with conservative estimates of Japan in 2017, China in 2018 and India in 2019 (Pucar 2011b).

After the TREAD Act was passed, many companies responded to the new market opportunity by releasing TPMS products that use an obvious means of getting tyre pressure and temperature data across a vehicle's rotating wheel-chassis boundary — battery-powered radio transmitter wheel modules.

The introduction of run-flat tyres and emergency spare tyres by several tyre and vehicle manufacturers has motivated the need to make at least some basic TPMS mandatory when using run flat tyres. With run flat tyres, the driver is more likely not to notice that a tyre is running flat (particularly a rear tyre, see Figure 1.1), hence the so-called 'run flat warning systems' were introduced. These are most often first generation, purely roll-radius based

indirect systems (based on measurements from the ABS wheel speed sensor), which ensure that run-flat tyres are not used beyond their limitations, usually 80 km/h and 80 km driving distance. Research into indirect solutions has also advanced. Indirect systems are able to detect under-inflation through combined use of roll radius and spectrum analysis and hence individual four-wheel monitoring has become feasible (Pucar 2012). This has allowed vehicles equipped with indirect systems to be homologated for the European and US market with respect to ECE-R 64 (Regulation No. 64 - Rev.1 - Temporary Use Spare Unit, Run Flat Tyres, Run Flat-System and Tyre Pressure Monitoring System 2010) and FMVSS 138 (US DoT 2005) regulations.

1.2. Aim and objectives

The single underlying aim of this research is to solve the problem of assessing tyre pressure without the requirement of inserting a sensor in the air space of a vehicle tyre. Aside from the obvious imperatives of a thorough literature search and assessment of developments in the field, there are several key objectives that have been established in the planning phase that represent milestones and aspirational targets for the research.

1.2.1. Assess the feasibility of tyre pressure estimation

It is hypothesised that it is possible to detect tyre pressure loss from a drivers' perspective due to the adverse effect low tyre pressure has on vehicle ride and handling. This is most readily assessed via analysis of the spectral characteristics of the chassis and/or axle assemblies. Since the target test vehicle does not feature air suspension (with suspension displacement sensors) or active suspension (with suspension accelerometers), the test will require instrumentation in order to capture the appropriate time series data.

1.2.2. Simulation of suspension & road, estimation of parameters

Some means of simulating the suspension and tyre pressure changes will vastly accelerate the development and assessment of the fault detection processes. This step necessarily involves the creation of a computerised model of the suspension and some way to automate the detection process, enabling Monte Carlo testing for various scenarios and permutations of vehicle properties such as fault-free and faulty, rapid/slow faults, vehicle speed and road conditions. These conditions may have an effect on the difficulty of detecting faults. Some means of generating realistic road surfaces or use of a pre-recorded measurement is an important aspect of the simulation environment.

1.2.3. Quarter car model

Since many of the algorithms rest on a model of the suspension, it is imperative that this area is considered carefully. The model (or models) should adequately explain the dynamics of the quarter car for the purposes of fault or change detection. The model should allow the necessary means of measuring and controlling the states and/or parameters, in order to assess the vehicle condition or simulate particular fault conditions.

1.2.4. Robustness and reliability

In common with many other model-based fault detection approaches, robustness and reliability are key issues. The intent of this thesis is to show how diversification of approach is the key to overcoming this obstacle. Model-based techniques should benefit from some *a priori* information such as clues about the vehicle state derived from velocity, gear position, steering angle and many other sources. Measurement-based approaches such as ABS wheel angular velocity comparison at the data level (numeric angular velocity) and signal level (spectral analysis) mitigate for shortcomings due to the nature of the input, which is unknown.

1.2.5. Unknown road input

Despite recent advances in camera based vision systems that have some ability to assess the road condition, it will be assumed that the diagnostic will act 'blindly' i.e. with no special information about the road surface, other than that which exists on the data-bus, usually some kind of suspension or chassis displacement measurement.

1.2.6. Regulatory requirements

Some consideration of the testing requirements for the major vehicle jurisdictions is helpful for setting realistic detection thresholds and gauging success.

1.2.7. Testing and validation

It is essential that the algorithms are tested on a vehicle in order that the algorithms may be properly assessed. Vehicle testing in controlled conditions also generates data which may later be used for refinement of models, fault scenarios and the simulation in general.

1.2.8. System identification of quarter car suspension

It is possible and highly advantageous to perform a static test of a vehicle suspension. This may be achieved on a so-called 'four-post rig' – a hydraulically actuated road simulator which allows complete control of the 'road' surface via automatic control whilst simultaneously

offering the possibility of making high resolution time-series measurements of input (‘road’) and output displacements (vehicle). A data set generated in this way would present the possibility of making a system identification of the suspension system with the afore-mentioned advantages.

1.3. Background reading – Firestone and Ford tyre controversy

The origins of TPMS legislation stems from vehicle accidents in the events surrounding the Firestone/Ford affair relating to vehicle products produced throughout the 1990s. As a result a milestone event in the evolution of TPMS technology occurred during the autumn of 2000. The Clinton administration signed into law the TREAD Act which mandated the fitment of a pressure measurement system to all vehicles, the first of such legislation globally. The driver for this legislation was the so-called Firestone and Ford tyre controversy (Greenwald 2001, Csere 2001, US DoT 2005).

1.3.1. Initial investigations

The US National Highway Traffic Safety Administration (NHTSA) initiated an investigation of allegations that Ford vehicle products equipped with Firestone tyres were involved in a higher than normal incidence of vehicle crashes, many of them fatal. The vehicles effected were primarily Ford Explorers, Mercury Mountaineers, and Mazda Navajos. Upon an internal enquiry Ford discovered that certain models of Firestone tyres (ATX, ATX II, and Wilderness AT) had above average failure rates in the field and there was some traceability leading back to those manufactured at Firestone's Decatur, Illinois plant.

The public advocacy group Public Citizen mounted an investigation and accused Ford and Firestone of systematically concealing the problem, before the Transportation Subcommittee United States Senate Committee on Appropriations on September 6, 2000, despite serious concerns about the safety of these vehicles. Representation from the Centre for Auto Safety reported before the Senate Committee on Commerce, Science and Transportation in Washington D.C., September 20, 2000 "Emerging Information shows that both Ford and Firestone had early knowledge of tread separation in Firestone Tyres fitted to Ford Explorer vehicles but at no point informed the NHTSA of their findings" (Corona and Komendanchik 2008).

1.3.2. Analysis of root cause

During standard critical manoeuvre testing, Ford test and design verification documents indicated that concerns were raised by the ride and handling development engineers regarding the vehicle stability during the testing phase of the prototypes. Fundamental design changes were recommended to mitigate the vehicles propensity to roll over in extreme cornering manoeuvres. Likely due to the economic implications, few of these recommendations were incorporated into the final design, critical vehicle dynamics attributes such as the suspension and track width were not changed.

In order to mitigate the handling issues Ford reacted by reducing the recommended tyre pressure to 26 psi and hence modifying the handling characteristics of the vehicle. The tyres were able to support a maximum pressure of 35 psi although the correct inflation pressure depends mostly on the vehicle mass and vehicle dynamics which is why it is set by the vehicle producer and not the tyre manufacturer. The failures in the field were exclusively attributed to the phenomenon of tread separation — the tread portion of the tyre separates from the carcass to reveal the supporting structure. If the vehicle is not immediately stopped total tyre failure is imminent. The problems are compounded critically at high speed owing to the fact that the driver has a substantially reduced time to react before total loss of control occurs due to lack of traction and/or blow-out. These crashes often involved vehicle roll over and severe damage to the vehicle structure and hence occupants. According to estimates at least 250 deaths and greater than 3,000 serious injuries were the result of these catastrophic tyre failures although not all of the incidents involved Ford products. Estimates in the range of 120 of the deaths can be attributed to the defective Ford vehicles.

Ford and Firestone have both blamed the other for the failures, which has led to the severing of relations between the two companies. Firestone has claimed that they have found no faults in design nor manufacture, and that failures have been caused by Ford's recommended tyre pressure being too low and the Explorer's design. Ford, meanwhile, point out that Goodyear tyres to the same specification have a spotless safety record when installed on the Explorer, although an additional liner was included into the Goodyear design after recommendations to that effect were made by Ford. Firestone included an additional liner in its product and this was then also used to replace tyres on Ford Explorers. It is well accepted within the tyre manufacturing industry that use of a ‘belt edge layer’ or as referred above as an additional liner, virtually eliminates belt edge separation. As a rubber tyre moves on the road, it generates

significant heat. As steel belts heat up, they expand and tend to pull away or separate from rubber. The use of nylon belt edges has been in use since radial tyres were first developed in the 1970s. Nylon, when heated, actually constricts in size; thus maintaining the belt edge integrity. Therefore an economic motivation exists for Firestone to achieve cost savings by eliminating this additional layer.

Some outside observers have speculated about the blame worthiness of both parties; Firestone's tyres being prone to tread separation and failure, and the Sport Utility Vehicles (SUV) being especially prone to rolling over if a tyre fails at speed compared to other vehicles. A subsequent NHTSA investigation of real-world accident data showed that the SUVs in question were no more likely to roll over than any other SUV, after a tread separation.

A product recall was announced, allowing Ford Explorer (popularly dubbed Ford Exploder) owners to change the affected tyres for others. Many of the recalled tyres had been manufactured during a strike period at Firestone. A large number of lawsuits have been filed against both Ford and Firestone, some unsuccessful, some settled out of court, and a few successful. Lawyers for the plaintiffs have argued that both Ford and Firestone knew of the dangers but did not address the problem, and that specifically Ford knew that the Explorer was highly prone to rollovers. To this date Ford denies these allegations.

A roll over test of a first-generation Explorer was conducted by Car and Driver magazine (Csere 2001). The vehicle was fitted with a roll cage and device that could remotely control the tyre pressure such that a blow-out condition could be simulated (rapid and total loss of pressure). The vehicle was driven through a series of critical manoeuvres (such as heavy cornering, slalom type manoeuvres) in order to recreate the condition of roll over. The vehicle passed these tests. Since it has been determined that the majority of fatal crashes involving the Ford Explorer were due to tread separation and not sudden pressure loss, this result merely demonstrates the vehicles stability in the low tyre pressure scenario. How the vehicle reacts to a tread separation event is not known due to the difficulty of creating a representative test scenario.

John T. Lampe (Chairman & CEO of Bridgestone/Firestone) announced in a 2001 letter to Jacques Nasser (Ford Motor Company Chief Executive) that Bridgestone/Firestone would no longer enter into new contracts with Ford Motor Company, effectively ending a 100-year supply relationship.

1.4. Legislation

In the United States, the United States Department of Transportation released the statute FMVSS No. 138, which requires an installation of a TPMS to all new passenger cars, multipurpose passenger vehicles, trucks, and buses that have a gross vehicle weight rating (GVWR) of 4,536 kg (10,000 lbs.) or less, except those vehicles with dual wheels on an axle, as of 2007. In the European Union, starting November 1, 2012, all new models of passenger cars were required to be equipped with a TPMS, with even tighter specifications that were defined by the United Nations Economic Commission for Europe (UNECE) Vehicle Regulations (Regulation No. 64). From November 1, 2014, all new passenger cars sold in the European Union must be equipped with TPMS. On July 13, 2010, the South Korean Ministry of Land, Transport and Maritime Affairs announced a pending partial-revision to the Korea Motor Vehicle Safety Standards (KMVSS), specifying that "TPMS shall be installed to passenger vehicles and vehicles of GVWR 3.5 tons or less, ... [effective] on January 1, 2013 for new models and on June 30, 2014 for existing models". Japan is expected to adopt European Union legislation approximately one year after European Union implementation. Further countries to make TPMS mandatory include Russia, Indonesia, the Philippines, Israel, Malaysia and Turkey.

1.4.1. Regulatory requirements

Since it is not possible to list the regulatory requirements for each individual jurisdiction, this section will be an abbreviated description of the requirements for the EU area, although requirements for USA vehicles are similar (e.g. deflation threshold being 25% of OEM recommended pressure). In order to offer a vehicle equipped with a TPMS in the EU market the OEM must satisfy regulation ECE-R 64 (Regulation No. 64 - Rev.1 - Temporary Use Spare Unit, Run Flat Tyres, Run Flat-System and Tyre Pressure Monitoring System 2010). Annex 5 of the regulation is a vehicle test which the regulator uses to assess conformity. There is a prescription for the ambient conditions, vehicle weight, and speed and measurement accuracy. Two tests are made: puncture and diffusion. A puncture is defined as (normal pressure -20%) in one tyre. The diffusion test simulates normal air loss due to micro leakages of the valves, wheel-rim contact area and propagation of air through the tyre rubber. Diffusion pressure is defined as (normal pressure -20%) in all road wheels.

1.4.1.1. Vehicle conditioning

The test procedure starts with inflation of the tyres to OEM recommended pressure, P_{rec}, and a 'soak' period where the vehicle is conditioned such that external disturbances do not effect the measurements and vehicle condition. The vehicle is driven for 20mins and the pressure, P_{warm}, is recorded. The reason for this soak period is to account for the additional pressure generated in the tyre by driving and thereby heating the tyre (typically a 3% increase has been recorded during testing).

1.4.1.2. Puncture test

The first test is a simulated puncture where one tyre is reduced in pressure by ($P_{warm} - 20\%$), to obtain P_{test}. The vehicle is then driven for 10mins or until the dashboard tell-tale lamp illuminates. The test is repeated for all tyres. The test is aborted after 10mins.

1.4.1.3. Diffusion test

All tyres are reduced in pressure by ($P_{warm} - 20\%$), to obtain P_{test}. The vehicle is driven for >20mins and <40 mins and stopped and ignition key removed for >1 min and <3mins. Driving resumes for 60mins or until the dashboard tell-tale lamp illuminates. The vehicle and engine is stopped and ignition set to 'run'. The tell-tale lamp must illuminate and remain on. The vehicle tyres are then inflated to P_{rec} and the TPMS system is reset (so that the TPMS is calibrated to the new tyre pressure). The tell-tale lamp must now be off (driving the vehicle may be necessary).

1.5. Benefits of TPMS

The dynamic properties of a pneumatic tyre are dependent on its inflation pressure. Vehicle performance properties such as braking distance and lateral stability require the inflation pressures to be maintained as specified by the vehicle manufacturer. Under-inflation is a significant factor in thermal and mechanical overload caused by overheating potentially leading to sudden destruction of the tyre itself. Additionally, fuel efficiency and tyre wear are severely affected by under-inflation. In addition to loss of pressure due to punctures, tyres also lose pressure by diffusion. In over the period of a year pressure in a tyre can reduce from between 20 to 60 kPa (3 to 9 psi), approximately 10% or even more of its initial pressure (Evans et al. 2009).

Fuel usage: For every 10% of under-inflation on each tyre on a vehicle, a 1% reduction in fuel economy will occur (Evans et al. 2009). The Department of Transportation of the USA has estimated that under inflated tyres waste 7,600,000 m^3 of fuel each year.

Extended tyre life: Under inflated tyres are the significant cause of tyre failure and contribute to tyre disintegration, heat build-up, ply separation and sidewall/casing breakdowns (Evans et al. 2009). In the case of a coaxially mounted wheel pair, a difference of 0.69 bar causes drag in the lower inflated tyre of equivalent energy required to move the vehicle 4 metres per 1.6 km. Operating a tyre, even briefly, on inadequate pressure breaks down the casing and prevents the ability to re-tread. However, not all catastrophic tyre failures are caused by under-inflation. Structural damage of the tyre is often accumulated over a long period of time in service by trauma such as striking curb stones or potholes which can lead to rapid tyre failures, not necessarily immediately after the damage was inflicted. This type of damage cannot be detected by any TPMS system.

Reduced operational downtime and maintenance: Since maintenance of correct pressure extends the life of a tyre, costs in this area are reduced due to increased service life of the tyre and reduced operational down-time due to maintenance (Singh et al. 2009).

Improved safety: Under-inflated tyres lead to tread separation and tyre failure, it is estimated that this phenomena lead to 192,277 accidents between July 3, 2005 – December 31, 2007 in the US alone (US DoT 2008, Choi 2012). Further, tyres properly inflated add greater stability, handling and braking efficiencies and provide greater safety for the driver, the vehicle, the loads and others on the road.

Environmental effects: Under-inflated tyres, as estimated by the Department of Transportation, release over 26 billion kg of unnecessary carbon-monoxide pollutants into the atmosphere each year in the United States alone (TRB 2006).

The European Union reports that an average under-inflation of 40 kPa produces an increase of fuel consumption of 2% and a decrease of tyre life of 25%. The European Union concludes that tyre under-inflation today is responsible for over 20 million litres of unnecessarily-burned fuel, dumping over 2 million tonnes of CO_2 into the atmosphere, and for 200 million tyres being prematurely wasted worldwide.

Having established the requirement for TPMS on vehicles worldwide this naturally prompts the requirement for research into effective alternative forms of TPMS owing to the high cost

and relatively low reliability of direct measurement systems. In this thesis an investigation of alternative forms of indirect tyre pressure estimation forms the basis of the research conducted

1.6. Outline of approach and thesis structure

The approach is based on theoretical study, simulation and analysis of experimental data and critical appraisal of methods/algorithms developed. The thesis structure is as follows: Chapter 2 provides a critical appraisal of the current literature in the field of TPMS, with particular attention to the indirect methods that have been developed. Chapter 3 describes the data acquisition process, methods and tools. Chapter 4 describes the theory behind suspension models and develops the quarter car model used for this work with preliminary considerations highlighting some of the issues of stiff systems. Chapter 5 provides a brief review of model parameter estimation in the context of the quarter car model with a comparison of discrete-time and continuous-time model parameter estimation as well as details of the development each of the proposed tyre pressure change detection methods. Chapter 6 concludes the research and suggests opportunities for further work. A list of the references quoted is provided and Appendix 2 provides details and specifications of the tools and equipment used for the experimentation and data acquisition.

1.7. Contributions of the Author

The main outcomes and contributions of this work are considered, by the author, to be (in order of significance) as follows:

1.7.1. Tyre pressure diagnosis via wheel angular velocity comparator

This piece of work is original in the sense that the method does not appear in the literature. A method was independently developed to acquire, interpret and process the Controller Area Network (CAN) data such that it is in a useful form for analysis and is effective at detecting specific modes of tyre pressure loss – validated on a vehicle. This was achieved with basic tools and available open source software/freeware, rather than state of the art data acquisition (Data Acquisition) DAQ equipment.

1.7.2. Model-based tyre pressure diagnosis via application of an unknown input observer and a parameter estimation scheme

The continuous-time, model-based tyre pressure change detector is enhanced by the addition of an unknown input observer (UIO) that simultaneously reconstructs the road profile input and provides a fault diagnostic in the form of a phase portrait.

1.7.3. Model-based tyre pressure diagnosis via an enhanced filter configured to estimate input and suspension state

In this work a Kalman filter configured for state estimation is enhanced by inclusion of the input state in the estimation scheme. The continuous-time, model-based tyre pressure change detector is enhanced by the addition of the Kalman state estimate of the road profile and gives an estimate of the tyre sidewall height, which is a function of the tyre pressure.

1.7.4. Model-based tyre pressure diagnosis via cautious least squares

Cautious least squares (CLS) is used as a fault detector by the addition of a parameter reset counter. Analysis of the fault counter provides some insight into the tyre condition. Two estimators are trialled and compared, namely recursive least squares (RLS) and a Kalman filter.

1.7.5. Investigation of the effects of sampling interval on discrete-time models and estimation thereof, with the corresponding continuous-time model and estimation of parameters

In the context of tyre pressure monitoring, this piece of work highlights the properties of suspension systems and the interaction of two dynamic modes, namely wheel hop frequency and that of the vehicle body frequency. The two modes interact with the result being regarded as a stiff system. The advantages and limitations of the discrete-time and continuous-time approaches provides the reader with a valuable insight.

Note that in the case of 1.7.1 - 1.7.5 the work reported in each case is original in the sense that the method does not appear in the literature. Each of the methods is effective at detecting specific modes of tyre pressure loss, which are detailed in the description of the method. In each case the method has been validated using data acquired from a vehicle in a test facility.

1.8. Publications of the author

Ersanilli, V.E., Reeve, P.J., Burnham, K.J., 2009. A Continuous-Time Model-Based Tyre Fault Detection Algorithm Utilising a Kalman State Estimator Approach. In *IAR Workshop on Advanced Control and Diagnosis*. Zielona Góra.

Ersanilli, V.E. & Burnham, K.J., 2014. A survey of vehicle tyre pressure detection methods and related legislation. In *UKACC International Conference on Control*. Loughborough.

Ersanilli, V.E. & Burnham, K.J., 2012. Comparison of Continuous-Time Vehicle Model Estimators as Candidates for Suspension System Fault Detection. In *International Conference on Systems Engineering*. Coventry.

Ersanilli, V.E., Burnham, K.J. & King, P.J., 2009. A Continuous-Time Model-Based Tyre Fault Detection Algorithm Utilising an Unknown Input Observer. In *International Conference on Systems Engineering*. Coventry.

Ersanilli, V.E., Burnham, K.J. & King, P.J., 2008. Comparison of Continuous-Time and Discrete-Time Vehicle Models as Candidates for Suspension System Fault Detection. In *IAR Workshop on Advanced Control and Diagnosis*. Coventry.

Chapter 2.

Literature survey on tyre pressure monitoring

The approaches to the solution of the tyre pressure measurement problem can be divided by the mode of measuring or detecting the pressure namely – direct or indirect. Directly sampling the tyre pressure involves placing a sensor in contact with the air space of the tyre while indirect methods typically use vehicle sensor data to infer the condition of the tyre, without actually having to measure the pressure.

Direct measurement solutions are problematic because they usually require a sensor to be placed in the tyre air space. This means that the task of supplying the sensor with power is curtailed to the use of batteries (VisiTyre 2001), inductive (Hill and Turner 1992) or kinetic energy scavenging solutions (Wang, Y. et al. 2012) and it also means that the pressure data must be obtained over a wireless link. The mass of the sensor will form an eccentric load on the axle and hence some provision to limit the weight of the sensor and counteract the force is required (this is usually achieved by the conventional tyre balancing method of applying weights opposite to the additional mass).

Indirect measurement approaches usually attempt to offer the advantage of reduced component count in the measurement system by using sensor data that already exists on the vehicle data network to perform a diagnosis (Carlson & Gerdes, 2005; Craighead, 1997; Ersanilli & Burnham, 2014; Isermann & Wesemeier, 2009; Mayer, 1995; Persson, Gustafsson, & Drevö, 2002; Ryan & Bevly, 2012; Umeno, Asano, & Iwama, 1994). Some approaches combine many sources of data in a manner sometimes referred to as data-fusion (Persson et al. 2001a). This reduces the system to an algorithm that resides in one of the ECU on-board the vehicle. Typically a model-based approach is employed (Ersanilli et al. 2009b), with data coming from sources such as accelerometers, suspension height and wheel speed sensors.

To the best knowledge of the author at the commencement of this research study, TPMS fitted by OEM were exclusively direct measurement systems. The evolving landscape in this regard has changed and there is at least one supplier, at the time of writing, of indirect measurement systems to a major OEM, Nira Dynamics AB (Pucar 2011a), which complies with the US FMVSS 138 (US DoT 2007) and EU ECE-R 64 (Regulation No. 64 - Rev.1 - Temporary Use Spare Unit, Run Flat Tyres, Run Flat-System and Tyre Pressure Monitoring System 2010)

regulations, albeit with some exceptions for FMVSS 138 regulation (Harris, C. H. 2011). This is partly due to the way the US and EU regulations have been worded, making it problematic for an indirect solution to be achieved, and partially because of complexity of implementing indirect systems that can detect tyre pressure within the allotted time with sufficient accuracy without causing false alarms. Figure 2.1 shows various relationships between the main approaches to tyre pressure detection.

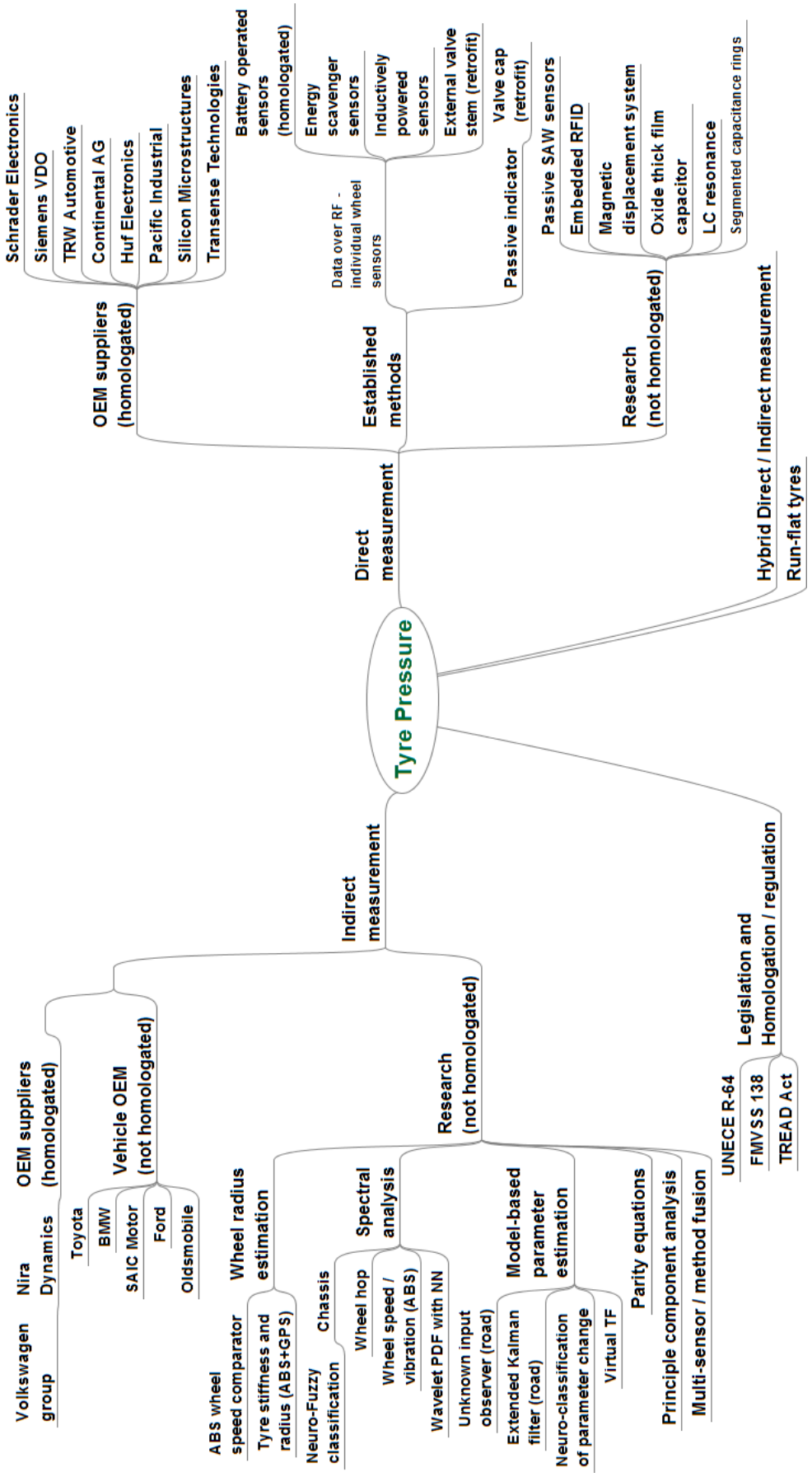

Figure 2.1 The tyre pressure monitoring landscape

2.1. Direct measurement

With reference to Figure 2.1 a number of direct measurement approaches are now described.

2.1.1. In-tyre TPMS

Direct pressure measurement approaches, specifically in-tyre measurement, are currently the preferred method for the vehicle OEM (GIA 2013). The reasons for this may be that direct measurement approaches are considered to be more reliable than an inferred scheme although, to the best knowledge of the author, no research exists that demonstrates this is true. Direct measurement solutions generally have the advantage of providing an actual measurement of the tyre pressure in a given wheel, which is useful information for the driver and may also factor into the electronic stability program (ESP) in order to predict the vehicle dynamics. It could also be argued that the automotive industry as a whole is generally considered to be relatively conservative (in common with many other engineering disciplines, such as rail, process and civil, for example), and are reluctant to adopt unproven technology, particularly in areas of safety critical systems, such as tyre and braking systems. Due to the inherent dangers of automotive transport, OEM are also vulnerable to litigation which compels careful consideration of vehicle design in safety critical areas. Another argument for direct TPMS could be made on the basis of their perceived superior reliability and hence reduced warranty repair costs and associated negative customer sentiment (Federal Motor Vehicle Safety Standards; Tire Pressure Monitoring Systems; Controls and Displays 2000). This is due to the fact that model-based methods are not well understood or used outside of research institutions such as universities and engineers within an OEM may not understand or trust this type of technology (Forssel 2009).

The systems implemented by an OEM generally consist of a remote pressure sensor (in each wheel), and a central processing ECU. Depending on the sensor activation method, some systems incorporate a low frequency activator (in each wheel arch) per sensor so that the data transmissions can be requested by the ECU and the sensor is subsequently allowed to ‘sleep’ on a reduced power setting, to preserve battery power. Figure 2.2 illustrates a direct pressure measurement system.

The sensor module must be small in both size and weight to minimise the effect of centrifugal forces. The module is designed to operate between −40 °C and 120 °C. For example, a tyre pressure sensor manufactured by Hella Inc., shown in Figure 2.3(a), consists of a sensor, transmitter, antenna, and control unit as well as a long-life battery to supply energy. This pack

has a valve stem, which is inserted from inside the tyre through a hole on the wheel rim as shown in Figure 2.3(b). The aluminium cap of the valve stem acts as an antenna, while the nickel valve core helps prevent corrosion. Most TPMS sensors feature a pressure transducer manufactured with semiconductor technology, which provides low energy consumption. The sensor is designed together with an analogue-to-digital converter and non-volatile memory to store tyre pressure data. In advanced models, a temperature sensor is also embedded with the pressure sensor. To control the functions of the sensor and transmitter, a microcontroller is fitted on the sensor module. A software routine is loaded in the flash memory of the microcontroller to define its operation. Optimal utilisation of battery energy is crucial since it cannot be replaced easily. The radio frequency transmission stage typically expends five times more energy than the sensing stage (Freescale 2009, Löhndorf et al. 2007a). Various energy-management techniques are used to save battery energy. In some models, when the vehicle is parked, the sensor transmits the signals once an hour, while other models are equipped with angular velocity detectors that shut down the transmission. More sophisticated sensor modules contain a low-frequency receiver integrated circuit, which waits in standby mode and wakes up the sensor once it detects a trigger from the vehicle's main processor. This technique is called pressure on demand (Atmel 2008). In the sensor module circuit shown in Figure 2.3(a), each sensor is coded differently so that the receiver can distinguish between tyres. If one of the tyres is replaced or if the tyres are interchanged, the sensor or sensors must be reset (Velupillai and Güvenç 2007b)

Once pressure data is obtained from the sensors it is not simply a matter of outputting the signal to an indicator for the driver to observe. The data must be processed to give an accurate indication of the pressure; this is because as the vehicle traverses the road, shocks from the road surface will deform the tyre causing the pressure to fluctuate. An averaged value is calculated from the stream of sampled measurements, which is then transmitted via the vehicle network to the instrument panel. It is possible to retro-fit these type of systems (Schrader 2014), although the vast majority of systems in use are OEM fitted during series production (GIA 2013).

This item has been removed due to 3rd Party Copyright. The unabridged version of the thesis can be viewed in the Lanchester Library Coventry University.

Figure 2.2 A direct pressure measurement system. Sensors in each tyre measure pressure and report this to an ECU which processes the data and communicates with the instrument panel over the vehicle network to inform the driver (Velupillai and Güvenç 2007b)

This item has been removed due to 3rd Party Copyright. The unabridged version of the thesis can be viewed in the Lanchester Library Coventry University.

Figure 2.3 (a) Sensor module and (b) when installed on the rim, inside the tyre. The valve stem acts as an antenna for the built-in transmitter (Velupillai and Güvenç 2007b)

2.1.2. Non-intrusive direct measurement

A branch of direct measurement techniques that do not rely on battery power is discussed in this section. The rationale for the inclusion of this sub-category is that these approaches attempt to overcome the same problem of supplying power to a device in the tyre, in the same way that indirect measurement approaches do. An extension of this concept is the energy scavenging approach, which is essentially identical to the conventional direct TPMS approach, with four tyre mounted pressure sensors, but without the requirement for a conventional battery. The electrical power is harvested from conversion of the road disturbance input and rotational energy of the wheel.

2.1.2.1. Tyre valve cap system

The tyre cap system is a low cost after-market solution for vehicles that do not have an OEM fitted TPMS. There are two types tyre cap system, a multi coloured indicator type (Figure 2.4) and flashing lamp type (Figure 2.5). The multi coloured indicator is encapsulated in the valve cap and indicates critical (yellow), low (red) and normal (green) pressure. The flashing lamp type activates once a pressure threshold has been transgressed.

This type of system is very inexpensive and simple to implement but vulnerable to tampering and is not visible to the driver whilst the vehicle is in motion. It is aimed at avoiding the low pressure tyre condition rather than warning the driving of an imminent fault whilst on a journey.

An extension of this type of system, namely FOBO Tire, is under development. A tyre valve cap pressure transducer (Figure 2.6) is linked to a microprocessor with a Bluetooth transmitter which can be connected to a suitable Bluetooth equipped device, such as a smartphone (Figure 2.7).

Figure 2.4 Multi-coloured cap

Figure 2.5 Flashing cap

Figure 2.6 FOBO Bluetooth pressure sensor

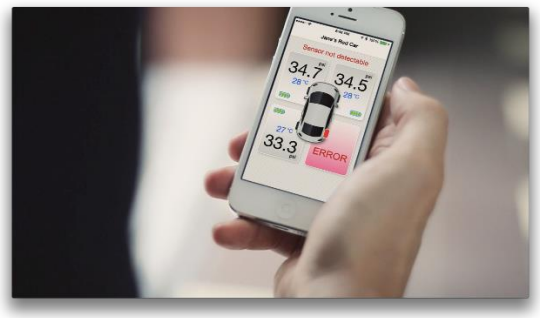

Figure 2.7 FOBO Smartphone application

2.1.3. Intrusive direct measurement not requiring an in-wheel battery

This subset of direct measurement approaches remains reliant on a direct sensing element in some area of the wheel-tyre assembly with the distinction that the approaches attempt to solve the problems of the in-wheel battery requirement (which necessitates tyre removal in order to service the component) and ability to retro-fit (in some cases). This is generally achieved by some novel application of electromechanical techniques in order to determine tyre pressure change via some abstracted property of the wheel-tyre system.

2.1.3.1. Magnetic displacement system

The magnetic displacement system is intended as a series production vehicle solution that is integrated into the vehicle systems during the design phase of the vehicle, similar to direct TPMS. In this system a wheel-mounted mechanism produces a displacement as a function of tyre pressure. This displacement is used to vary the separation of a pair of permanent magnets. The position of these magnets is sensed from the vehicle chassis by means of a Hall probe (Figure 2.8). The Hall probe reading then forms the basis of a pressure indication that can be fed back to a data processing ECU and then the instrument panel. This is achieved via the Hall effect, whereby a potential difference is set up transverse to a current in the conductor and a magnetic field perpendicular to the current. This approach is currently a research project and has no practical applications to date.

The benefit of this system is that it is a direct measurement system and hence potentially more accurate (although this has yet to been demonstrated for mass manufacturing) but without the requirement for a remote battery operated device and so would not incur a service penalty in the event of battery failure. The system could be expensive in terms of components (Figure

2.9), depending on the sensor costs, in addition four Hall probes are required and an ECU, making it a comparatively expensive solution for mass manufacturing (Hill and Turner 1992).

This item has been removed due to 3rd Party Copyright.
The unabridged version of the thesis can be viewed in the
Lanchester Library Coventry University.

Figure 2.8 The stationary mounted Hall probe of the magnetic displacement system (Hill and Turner 1992)

This item has been removed due to 3rd Party Copyright. The
unabridged version of the thesis can be viewed in the Lanchester
Library Coventry University.

Figure 2.9 The wheel mounted pressure transducer of the magnetic displacement system (Hill and Turner 1992)

2.1.3.2. Electronic article surveillance techniques

Electronic article surveillance is intended as a series production vehicle solution that is integrated into the vehicle systems during the design phase of the vehicle, similar to direct TPMS. This is an alternative direct sensing approach that does not require in-tyre power source. In Electronic Article Surveillance (EAS) or 'Shop Security' systems a common method for detecting the removal of an unauthorised item uses a small passive inductive-capacitance resonant circuit, as shown in Figure 2.10, attached to the item with radio frequency transmitting and receiving systems located at exits. If the item bearing the LC circuit or 'tag' is brought into the area between the transmit and receive antennas the presence of the tag will register with the receiver and an alarm will sound.

This method of detection is normally based upon the use of a frequency modulated transmitter and antenna able to continuously sweep across a frequency range covering the resonant

frequency of the tag. As the system relies upon the response of a highly resonant LC circuit it can be made very sensitive to changes in the circuit properties.

If a tag is located in the area close to the antenna, as depicted in Figure 2.10, the transmit burst will energise the tag, which is loosely coupled to the transmit and receive antennas. When the frequency of the burst corresponds closely to the natural resonant frequency of the tag, the tag will absorb energy from the radio frequency field.

This item has been removed due to 3rd Party Copyright. The unabridged version of the thesis can be viewed in the Lanchester Library Coventry University.

Figure 2.10 Structure and Equivalent Circuit of EAS Passive LC Tag (Smith, D. 1997)

In order to use this system for tyre monitoring applications two main problems need to be addressed. Firstly the resonant frequency of the passive LC circuit must be made to change in response to variations in tyre pressure and it must prove possible to detect this change. This can be achieved by varying either the capacitance or inductance of the circuit. Secondly it must be possible to design and manufacture the LC circuit in such a manner as to be easily incorporated with the tyre or valve. One possible method of achieving both could be to incorporate the LC circuit as part of the tyre sidewall structure. If the tyre sidewall changes shape due to partial deflation this will cause a change of shape of the wire loop forming the circuit inductance. Such a change would give rise to a change of inductance and hence a change of resonant frequency (Smith, 1997). The problem with this type of solution is the requirement for the sensor to be installed in the tyre itself. This approach has never been shown to be reliable in practice and as such no tyres currently exist which incorporate sensors for on-board analysis of tyre pressure although research continues in this area (Rodríguez-Madrid et al. 2012, Tuononen 2009, Li, L. et al. 2005)

2.1.3.3. ‘Intelligent tyre’ - passive surface acoustic wave system

The term ‘intelligent tyre’ describes tyres equipped with sensor systems to monitor thermal and mechanical parameters while driving. Information about temperature, tyre pressure and tread wear can be obtained and used for control or diagnostic purposes.

In this system the friction coefficient is measured by evaluating the mechanical strain in the tyre surface contacting the road—utilising the deformation of the tread elements (Figure 2.11

and Figure 2.12). The system employs a monitoring method using passive radio activated surface acoustic wave (SAW) sensors. During the road contact, the local stress within the tread depends on the tyre pressure, the load and the mechanical parameters of the wheel suspension system. Numerous theoretical and experimental investigations have been conducted and published on this subject (Pohl et al. 1999, 1997, Dixon et al. 2007, Rodríguez-Madrid et al. 2012, Zhang, X. and Wang, F. Y. 2009, Li, L. et al. 2005, Matsuzaki and Todoroki 2006).

This item has been removed due to 3rd Party Copyright. The unabridged version of the thesis can be viewed in the Lanchester Library Coventry University.

Figure 2.11 Cross section of a SAW sensor mounted on the inside of a tyre (Pohl et al. 1999)

This item has been removed due to 3rd Party Copyright. The unabridged version of the thesis can be viewed in the Lanchester Library Coventry University.

Figure 2.12 SAW sensor mounted on the inside of a tyre (Pohl et al. 1999)

The main benefit of this system is that while it is a direct measurement scheme, it does not require battery power. However, the relationship between tyre flex and pressure is not a linear one, especially considering that the exact mass of the vehicle cannot be known to the system (passengers and cargo). A significant shortcoming with this type of solution is the requirement for the sensor to be installed in the tyre itself. This approach has never been shown to be reliable in practice and as such no tyres currently exist which incorporate sensors for on-board analysis

of tyre pressure although research continues in this area, see references relating to article surveillance techniques (Smith, 1997).

Intelligent tyre concepts are in various stages of development by Goodyear Dunlop and Continental Automotive. Dunlop has proposed a battery free design embedded in the rubber which reports on tyre pressure, temperature and the tyre identification details to onboard vehicle systems. It is proposed (Burt 2014) that this information will lead to improvements such as reduced stopping distance under ABS operation, enhanced cornering response, improved yaw stability and optimised stability control systems. Continental Automotive have proposed similar embedded tyre technology (Continental 2015) but there is no evidence that either company have succeeded in series production implementation.

2.1.3.4. Energy harvesting for tyre pressure monitoring systems

This area of research is not solely devoted to the application of tyre pressure monitoring although it is attractive because it addresses one of the major obstacles in the direct sensing approach by obviating the requirement for a specialist long life battery installed in the wheel (in order to supply the sensing circuit). In the study (Löhndorf et al. 2007), a MEMS based electrostatic vibration energy harvester is simulated and shown to deliver 10μW average power to supply a TPMS. There are no known applications for this technology amongst the vehicle producers at the present time, indicating that this area of research is still in its infancy but is considered to be feasible considering the significant energy dissipation in the average vehicle wheel, during a drive cycle (Hu et al. 2011, Kubba and Jiang 2014).

2.2. Indirect measurement

With reference to Figure 2.1, a number of developments in indirect measurement are now described.

2.2.1. Wheel rotation observer-based approaches

This approach could be argued to be the original indirect method that spawned the research into indirect and data fusion methods generally. This particular method is still in use in some jurisdictions and it is a useful component of any data fusion approach, as will be discussed in Section 5.7.

The premise upon which this method is founded is that the tyre radii are a function of the load (vehicle mass) and tyre pressure, with the major contribution attributed to the tyre pressure (Pacejka 2006a). These properties have a marked effect on the angular velocity of the wheel. Vehicles equipped with an antilock braking system (ABS) automatically provide the angular velocity, ω, of each tyre to a central processor. A straightforward algorithm based on monitoring of the inflation measure β defined by

$$\beta = \left| \frac{(\omega_{LF} + \omega_{RR}) - (\omega_{RF} + \omega_{LR})}{\omega_a} \right| \tag{2.1}$$

$$\omega_a = \frac{\omega_{LF} + \omega_{RR} + \omega_{RF} + \omega_{LR}}{4} \tag{2.2}$$

is used to predict tyre under inflation, where ω_{LF}, ω_{RF}, ω_{LR}, ω_{RR} denote left front, right front, left rear, and right rear wheel angular velocities, and ω_a is the average angular velocity. The tyre inflation measure β is close to zero for normal tyre pressure. Owing to the existing availability of the wheel velocities, only software is needed to implement this indirect TPMS (Velupillai and Güvenç 2007b). There are significant contributions to research in this area, particularly in the early periods, around the time of the Ford-Firestone incidents of 1997 (Mayer 1994, Beeson and Ishihara 1998, Atherton 1992, Walker, J. C. and Rehal 1993, Nakajima 1998), see Figure 2.13.

There are, however, several shortcomings associated with the above type of indirect TPMS. The system does not report the actual pressure of each tyre and only operates when the vehicle is in motion. The system does not warn when two tyres are equally underinflated on the same side or same axle or when all four tyre pressures are equally low (which is the normal mode of gradual decline in pressure due to leakage). The finest resolution of the system is typically a

pressure drop of more than 25% and systems may generate false alarms when the vehicle is driving on a sustained curve or during tyre slip on low friction surfaces such as ice and wet leaves. This type of indirect system remains in use but it is confined to jurisdictions other than EU and US (and others) due to incompatibility with UNECE (2010); US DoT (2005).

This item has been removed due to 3rd Party Copyright. The unabridged version of the thesis can be viewed in the Lanchester Library Coventry University.

Figure 2.13 Wheel angular and vehicle velocities. Tyre pressure changes result in changes in wheel angular velocity. Wheel rotational speeds are measured in all vehicles by the ABS sensors (Velupillai and Güvenç 2007a)

2.2.2. Tyre pressure estimation via ABS signal processing

This technique first appeared in the literature in 1994 with a paper by Toyota (Umeno et al. 1994). It appears that in this period Toyota was conducting research into tyre modelling and estimation generally, as papers have been published on estimation of tyre-road friction and pressure estimation until 2002 by Umeno (2002). The method relies upon analysis of the ABS wheel speed signal at the electrical level, rather than the processed samples that are broadcast on the vehicle data bus, as in the wheel rotation observer approaches.

2.2.3. Tyre pressure monitoring with wavelet-transform

This technique relies upon analysis of the frequency spectrum of the ABS wheel speed signal by directly sampling the signal at the electrical level, rather than conditioned signal that is broadcast by the ABS ECU. The approach differs from the observation of absolute differences between individual wheel speeds in that, due to the mass-spring-damper properties of the wheel system, there is a frequency component of the signal that is dependent on the tyre pressure. The property of interest in this work is the eigen frequency which is dependent on the physical properties of the system (in this case the tyre), a hypothesis is proposed such that any change in the physical constants, such as tyre pressure, mass or damping, will have a measureable

effect on the eigen frequency. Since mass and damping can reasonably be assumed to be constant, it is proposed that the frequency shift is due to tyre spring rate, which is a linear function of tyre pressure (Heißing and Ersoy 2011). The novelty of this work is the application of wavelet transformations (in the place of examining the frequency spectrum via a Fourier transform), in an effort to reduce computational time and builds on the ABS wheel speed analysis work of Gustafsson et al. (2001).

2.2.4. Tyre radii estimation using a marginalized particle filter and Bayesian parameter estimation

This approach utilises individual wheel angular velocity measurements and absolute vehicle position from a global positioning system (GPS) to estimate tyre radius. The radii deviation from its nominal value is modelled as a Gaussian random variable and included as noise components in a simple vehicle motion model. The novelty lies in a Bayesian approach to estimate online both state vector and the parameters representing the process noise statistics using a marginalised particle filter (Lundquist et al. 2014). This solution, which builds on the work of (Gustafsson et al. 2001), is appealing due to the high level of estimation accuracy of the tyre radii and hence tyre deflation, tested according to UNECE (2010). An important caveat is that this approach relies upon ABS wheel speed data in order to operate which is not simple to retrofit. In common with other indirect approaches, this technique does not provide actual pressure measurements and only works when the vehicle is in motion,

2.2.5. Diffusion deflation detection using wheel angular velocity signals

This work attempts to overcome the problem of four tyre deflation (usually associated with normal diffusion of the tyres) and tyre deflation of tyres which share an axle, which are the limitations that prevent simple wheel angular velocity observer approaches (Nakajima 1998) being ratified by the regulators of the major vehicle markets (Regulation No. 64 - Rev.1 - Temporary Use Spare Unit, Run Flat Tyres, Run Flat-System and Tyre Pressure Monitoring System 2010, US DoT 2005). The premise of this method posits that the radius of a vehicle tyre is dependent on the relationship between the load and the tyre pressure (Figure 2.14). The researchers have shown that the tyre rolling radius rate of change in the deflated condition (140 kPa) is smaller than that in the normally inflated condition (200kPa) over a wide range of tyre aspect ratio (70% to 50%), as shown in Figure 2.15 and Figure 2.16.

This item has been removed due to 3rd Party Copyright. The unabridged version of the thesis can be viewed in the Lanchester Library Coventry University.

Figure 2.14 Load sensitivity of tyre rolling radius (Yanase 2005)

The author Yanase (2005) claims that due to the load shift which occurs during cornering and acceleration/deceleration, detection of 4-tyre diffusion deflation is possible by comparing the tyre rolling radius change rate under cornering or acceleration/deceleration between a normally inflated tyre and a deflated tyre. Figure 2.15 shows the rolling radius change in the normally inflated condition under cornering and Figure 2.16 is of a vehicle with tyres in the 40% deflated condition. The slope of the line represents the load sensitivity of the tyre in each condition. The data set is continuously processed during the drive cycles and the slope is calculated after each sample. When the slope transgresses a threshold it is deemed that the average tyre pressure has changed. In this way four tyre diffusion may be detected (Yanase 2005).

This item has been removed due to 3rd Party Copyright. The unabridged version of the thesis can be viewed in the Lanchester Library Coventry University.

Figure 2.15 Angular velocity difference during cornering due to load shift (Normally inflated condition) (Yanase 2005)

This item has been removed due to 3rd Party Copyright. The unabridged version of the thesis can be viewed in the Lanchester Library Coventry University.

Figure 2.16 Angular velocity difference during cornering due to load shift (40% deflation condition) (Yanase 2005)

This approach is attractive in the sense that is common to most indirect approaches: no additional sensors are required (assuming wheel angular velocity is known, i.e. an ABS is equipped). However it relies upon the fact that the vehicle is in motion and the vehicle state is suitably excited in order to make the analysis. The author does not state whether the level of vehicle excitation due to the regulation prescription is sufficient to elicit a diagnosis using this approach. There is no evidence that this particular approach has been adopted by vehicle OEM which suggests that in practice it is not able to meet (Regulation No. 64 - Rev.1 - Temporary Use Spare Unit, Run Flat Tyres, Run Flat-System and Tyre Pressure Monitoring System 2010, US DoT 2005).

2.2.6. Model based detection of tyre deflation by estimation of a virtual transfer function

In this research a method for monitoring the tyre pressures is developed using chassis acceleration signals. The authors (Halfmann et al. 1997b) develop the concept of a 'virtual transfer function' which describes the relationship between the front and rear wheels on a given side of the vehicle (bicycle model)

$$|G(s)| = \frac{|\ddot{z}_{BR}(s)|}{|\ddot{z}_{BF}(s)|} \tag{2.3}$$

where z is the vertical displacement of the chassis and BF, BR represent the front and rear wheels. Analysing the chassis in this way (Figure 2.17) is an attempt to mitigate the effect of the unknown input, i.e. the road surface excitation that is present during driving. By classifying the frequency spectrum of the virtual transfer function between the body acceleration at the front and rear wheel on one side of the vehicle, characteristic features are generated.

This item has been removed due to 3rd Party Copyright. The unabridged version of the thesis can be viewed in the Lanchester Library Coventry University.

Figure 2.17 Comparison between the power spectral density of the left front wheel and the left rear wheel at an engine angular velocity of 2000 rpm (Halfmann et al. 1997b)

This item has been removed due to 3rd Party Copyright. The unabridged version of the thesis can be viewed in the Lanchester Library Coventry University.

Figure 2.18 The generated symptom space and the associated classes of tyre pressure (RF=right front wheel, RR=right rear wheel) with symptom S_1 on the x-axis and S_2 on the y-axis (Halfmann et al. 1997b)

The first symptom is generated by assessing the characteristic frequency response of the tyre oscillation in the fault-free condition. There is a relationship between spectral amplitude of the virtual transfer function $G(s)$ and tyre pressure quotient $\mathrm{P_{front}}/\mathrm{P_{rear}}$. A change in the first symptom S_1 can be interpreted physically because its value depends directly on the fault-free vertical oscillation of the tyre, which is strongly influenced by tyre pressure.

Figure 2.18 shows the filtered symptoms of the right-hand-side track, with five classes of tyre pressure. The relative location of the first characteristic feature reflects the change in the value of the pressure quotient between the rear and the front wheel on the same side: With a decreasing pressure quotient value, S_1 tends to decrease in value. A second symptom S_2 which cannot be interpreted physically, covers the remainder of the frequency range under consideration, to the upper frequency limit of 25 Hz

To diagnose the tyre pressure, a neuro-fuzzy classification of the characteristics is applied which allows the authors the advantages of automatic learning (from the neural network component) that is enhanced and constrained by the addition of expert knowledge (from the fuzzy logic component) (Halfmann et al. 1997a).

The advantages of this type of system are that it does not require knowledge of the road input to make a diagnosis (which is a significant obstacle for model-based approaches) and does not require wheel angular velocity information, unlike many indirect solutions. However, accelerometers in all four corners are required and depending on the required accuracy this may add significant cost to a vehicle. Accelerometers are increasingly being deployed for the purposes of active suspension control and hence this approach may be more suitable in this setting. There is no evidence that this particular approach has been adopted by a vehicle OEM. This likely due to the limitation that four wheel diffusion cannot be detected using this approach, which suggests that it is not able to meet UNECE (2010; US DoT (2005) regulation requirements.

2.2.7. Model-based parameter estimation

The model-based approach (Ersanilli and Burnham, Keith J. 2012) attempts to model the vehicle suspension, typically a quarter car representation and use a signal such as chassis acceleration, suspension deflection or axle acceleration with the input from the road to estimate the parameters of a transfer function model (Figure 2.19). Since the parameters of the transfer function relate back to the physical constants, such as tyre spring, it is possible to make a

diagnosis of the condition of the suspension based on the parameter deviations. Figure 2.19 illustrates the approach whereby a multiple model is used to overcome the non-linearity of the damper.

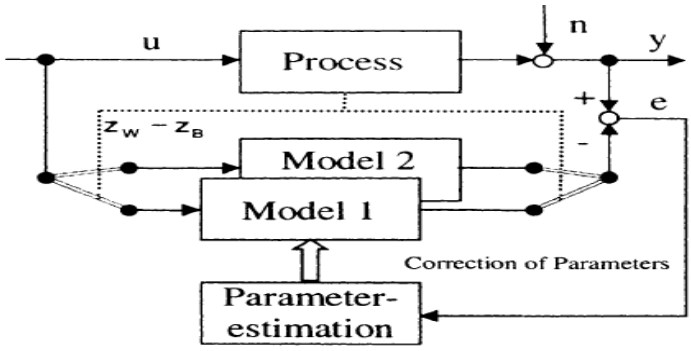

Figure 2.19 A multiple model parameter estimation scheme to alleviate non-linearities in the damper

In this type of fault detector, the parameters will be changing in patterns according to what is changing in the system. For automatic fault detection, the estimated parameters have to be mapped to the different faults, which is a classification task. Neural networks, especially feed forward perceptron networks, have proven to be well suited to such tasks. A multilayer perceptron network, with two hidden layers and sigmoid functions as activation functions in all layers can be used, see Figure 2.20 (Borner , Straky, Weispfenning and Isermann, 2002).

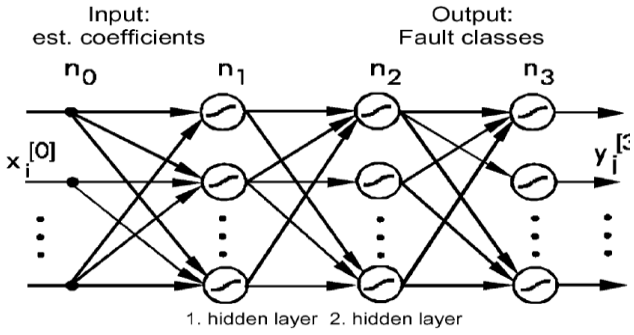

Figure 2.20 Multilayer perceptron network

One of the problems with the parameter estimation approach is that the system would never know the input and so this needs to be reconstructed or estimated from what is known about the system. The suspension constants and the output are known, using these two it is possible to estimate the input. However, this will always be an estimate and this causes problems for

the parameter estimation. In addition to this problem, the non-linear nature of vehicle suspension will cause parameter deviations even in the absence of a fault and so this needs to be addressed before a correct diagnosis can be made.

2.2.8. A study on radial directional natural frequency and damping ratio in a vehicle tyre

An interesting approach is to make an attempt to form a connection between the radial directional natural frequency, damping ratio and tyre pressure in various vehicle tyres. The radial direction modal parameters of tyres subjected to different levels of inflation pressure have been determined by using a frequency response function method. To obtain the theoretical natural frequency and mode shape, the plane vibration of a tyre has been modelled as though it were that of a circular beam. By using the Tielking method that is based on Hamilton's principle, theoretical results have been determined by considering the angular velocity, tangential and radial stiffness, radial directional velocity and tension force which is due to tyre inflation pressure. The results show that experimental conditions can be considered as the parameters that shift the natural frequency and damping ratio (Kim et al. 2007)

2.3. Concluding remarks – Literature survey

What has been shown here is not an exhaustive list of tyre pressure detection approaches. Rather, it is meant to identify the range of approaches that exist without delving into every single deviation of each method within a category. There are many patents in the area of tyre pressure measurement, particularly the direct approach but most of these techniques are very similar and meant as devices to protect intellectual property, not advance the frontiers of science and engineering.

Currently, Nira Dynamics is the only supplier of indirect tyre pressure sensing systems deployed in large scale manufacturing of vehicles. The reasons for this are partly due to US law but may also indicate a lack of imagination amongst the OEM and component manufacturers, since there are more cost effective alternatives. Implementing a model-based alternative would require significant investment into the development and testing of an algorithm but this cost would be limited to the development rather than multiplied by the number of vehicles produced, as a direct sensing approach does, with its additional hardware.

Direct sensing from the valve cap is not considered to be a robust solution due to the exposed nature of the device and the limited functionality. The aftermarket solution offered by FOBO challenges the space that conventional TPMS occupies with direct and potentially highly accurate real-time measurement that also wirelessly integrates with a smartphone, enhancing its popular appeal. However, it remains to be seen if this type of approach is viable in the long-term. As with all tyre valve cap/stem sensors, they are exposed and vulnerable to thieves.

Of the indirect approaches, the model based techniques offer the benefits of reduced hardware complexity and insightful diagnosis that need not be confined to just tyre fault detection, the entire suspension system can be diagnosed by the parameter estimation approach. The weakness of these solutions is that it would be difficult to detect small changes in pressure over time (natural leakage) as the dynamics of the tyre are heavily filtered through the suspension system, which is not an impediment for a direct approach. The most significant challenge for the model-based implementations is the unknown road input, particularly in the face of model uncertainty. Most of the indirect approaches hinge on how this problem is handled.

A multifaceted approach is more likely to succeed against the background of unknown input and modelling uncertainty. In general the indirect approaches have a limited area of operation, that is not effective at detecting tyre pressure change in the range of acceptable operation, as

determined by the regulations (Directive 98/69/EC of the European Parliament and of the Council 1998, US DoT 2005). As technology develops and proliferates, so do the number of automatic controllers and their associated sensors. In modern vehicles properties such as, chassis and axle acceleration, wheel angular velocity, steering angle, and virtually every piece of sensor data is broadcast on the network to support the distributed functionality (Navet et al. 2005). This implies the possibility of implementing a hybrid approach utilising a variety of indirect techniques without requirement for costly additional sensors and their associated warranty and maintenance burden. Reducing piece-cost and warranty claims are particularly appealing properties to manufacturers of mass produced products.

Chapter 3.

Data acquisition

3.1. Introduction to experimental work

Having conducted a review of the literature on TPMS and observed the breadth of TPMS approaches, as well as the similarities and common shortfalls of many proposals, this Chapter considers the feasibility of some of the more promising approaches.

As a starting point a number of actual vehicle test scenarios were conducted and an attempt made to analyse the data gathered from experimental trials. Some of the questions initially posed were as follows

1. From an analysis of wheel natural frequency from vertical acceleration, when subjected to multi-surface tests conducted with different tyre pressures, does the natural frequency shift due to load/surface?
2. From an analysis of chassis natural frequency from turret vertical acceleration, when subjected to multi-surface tests conducted with different tyre pressures, does the natural frequency shift due to load/surface.

In total, three sets of tests were conducted on three vehicles, namely a Volvo V40 when driven on the public highway, a Jaguar X-Type using the Crest road simulator and a Ford C-Max for wheel angular velocity signal message acquisition. The data sheet/specifications of these vehicles are given in Appendix 1. Specifications and operating descriptions of the data acquisition equipment, i.e. the MEPHM, ELM327 CAN Microprocessor, PCL TG1 tyre pressure gauge, USB Instruments DS1M12, ELMConfig, FORScan and Controller Area Network (CAN) is given in Appendix 2.

3.1.1. Spectral analysis of Volvo V40 suspension

According to Wong (2001) the input excitation to the road wheels of a vehicle is a function of vehicle velocity and road surface type. For a given velocity there will be a variable amount of displacement of the suspension dependent on the roughness of the road surface being traversed. In order to objectively test two different vehicle states the same road and same velocity must be used so a series of tests were devised to obtain Power Spectral Density (PSD) responses

from different vehicle states with identical roads and speeds. The testing method evolved as the results were analysed, with the final test schedule detailed in Table 3.1.

Some of the tests are circuits that were driven at the same average velocity; the only difference between them being the tyre pressure. This is especially true for Motorway Circuit 1 (‘circuit’ is used in the sense that the same stretch of road was used for all the tests of that name), the conditions allowed a constant velocity and lane to be used. The remaining tests do not have identical companions (in terms of the tyre pressure/road/velocity relationship) although they were selected so that the same road types and speeds could be compared for different tyre pressures. It is useful to keep in mind that the objective of the testing is to find differences in the chassis acceleration due to tyre pressure, not differences in chassis acceleration to other disturbances such as road type. The drives were time consuming so it was not possible to test every scenario and configuration of Fast Fourier Transform (FFT) averaging.

All the tests were performed on a public road so the urban drives are not identical in duration due to traffic conditions. Ideally, no data should be logged when the vehicle is at rest but the test set up did not allow this level of integration and it should be considered when viewing the results. Logging when stationary will cause the averaging to be offset because samples will be recorded when there is no road excitation. The nominal condition for the Volvo tyre pressure is 32psi, the other conditions are considered to be faulty. The vehicle was loaded with a single occupant, the driver, for all tests.

	FFT Averaging		Tyre Pressure			Velocity			
	FFT no averaging	FFT 8 times averaging	32 psi	28 psi	20psi	80mph	70mph	40mph	30mph
Urban circuit 1		•	•						•
Urban circuit 1		•		•					•
Urban circuit 1		•			•				•
Motorway circuit 1		•	•				•		
Motorway circuit 1		•			•		•		
Rough road circuit 1		•	•					•	•
Rough road circuit 1		•		•				•	•
Urban driving 1		•		•				•	•
Urban driving 2		•		•				•	•
Urban driving 3		•	•					•	•
Urban driving 4	•		•					•	•
Motorway driving	•		•			•			
Motorway driving	•			•		•			
Extra-Urban driving		•	•					•	•

Table 3.1 Vehicle tyre pressure vs. chassis acceleration testing schedule

3.1.1.1. Micro Electronic Prognostic Health Monitor: Chassis acceleration tests

The results of the testing work and the software modifications generously carried out by Steve Booth of BAE made a case for the use of the Micro-Electronic Prognostic Health Monitor (MEPHM) as a tool to test the concept of detecting tyre pressure changes from chassis acceleration measurements. The data collected could also be used in the modelling activity to compare responses and eventually recreate the road surface.

3.1.1.2. Installation of the Micro Electronic Prognostic Health Monitor

In order to isolate the MEPHM from vibration that was not associated to chassis displacement due to road input, a very rigid piece of chassis had to be located. Some of the most rigid parts of the chassis exist around the suspension load bearing portions of the chassis, called turrets. The suspension strut is bolted to this part of the chassis and a suitable location for the MEPHM was found on the left hand turret (Figure 3.1) in the engine bay (Figure 3.2).

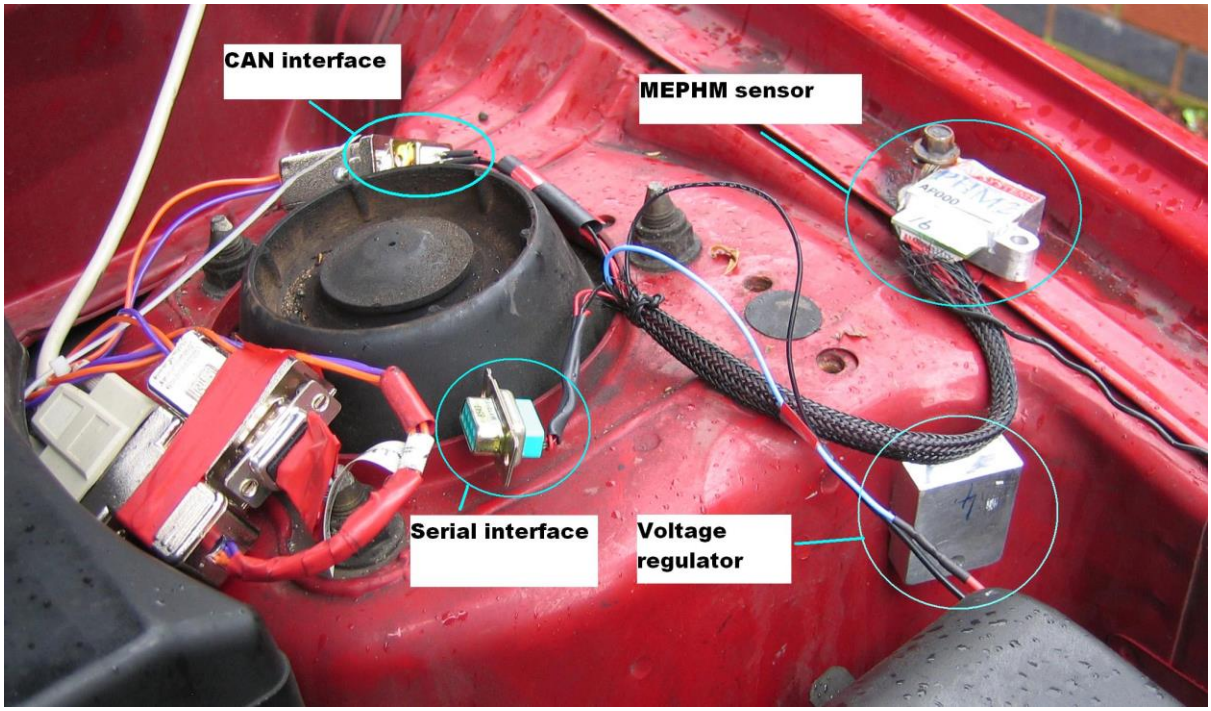

Figure 3.1 MEPHM mounted to a Volvo V40 front suspension turret

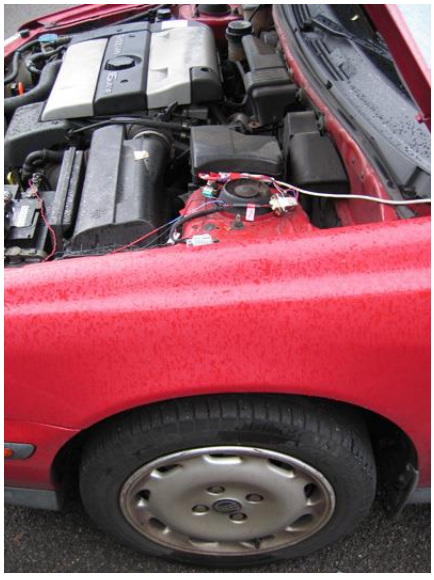

Figure 3.2 MEPHM mounted to a Volvo V40 front suspension turret, side view

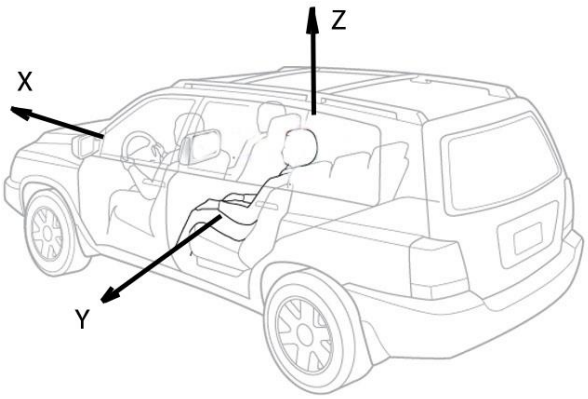

Figure 3.3 Orientation of the MEPHM accelerometer axes with respect to the chassis of the Volvo V40 test vehicle

Selection of the front left hand turret means that portion of chassis will be most affected by tyre pressure changes of the front left tyre and hence allows a degree of isolation from the other tyres than a central location would afford.

3.1.1.3. Urban road test

Urban Circuit 1 was the first test. The tyre pressure was checked and observed to be 32psi. The route was arbitrarily chosen and the drive lasted approximately 20 minutes, including stops at junctions. This equates to 51 sample batches of 1024 which means a total of 52,224 samples were processed for the 3 axes. This may appear to be a large number of samples but with the FFT averaging set to 8 times the actual amount of time that the Digital Signal Controller (DSC) was sampling the chassis acceleration was only 8.67 seconds out of the 20 minutes drive time.

The second run of the Urban Circuit 1 test was the same route with the front left tyre deflated to 20psi. This is over a 30% reduction in tyre pressure but the vehicle did not exhibit any undue handling deficiencies for the sedate 30mph drive. The Volvo V40 is equipped with power steering so there was no noticeable heaviness in the steering action. The only noticeable difference was under heavy cornering, such as a roundabout where a small amount of tyre scrubbing could be heard.

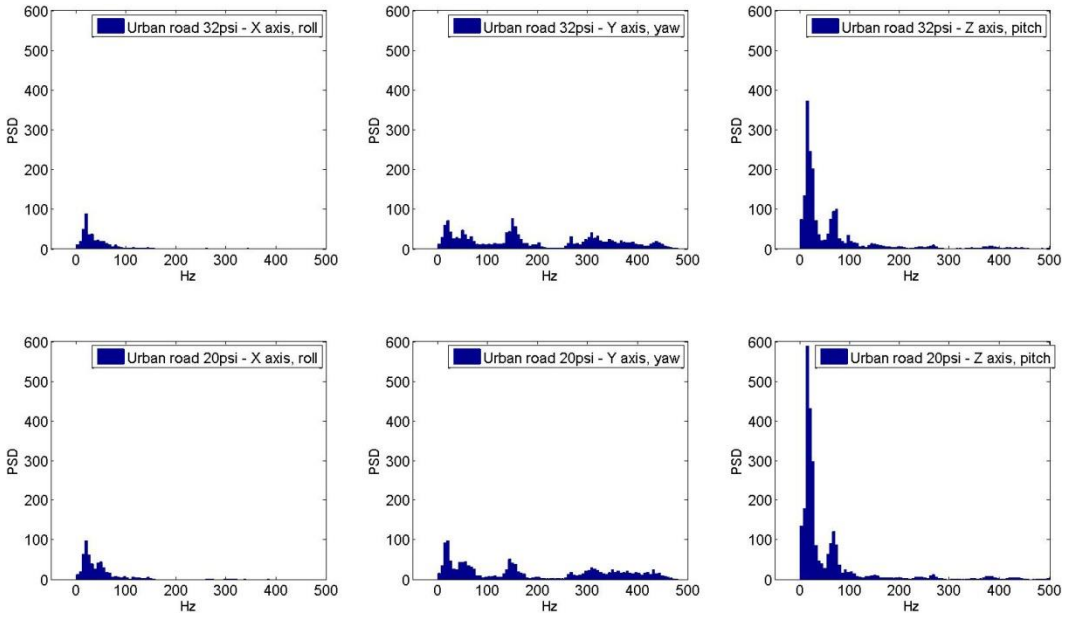

Figure 3.4 PSD results for 2 drives of Urban Circuit 1 – upper plots 32psi, lower plots 20psi, X,Y and Z accelerometer axes

Once the two data sets were acquired they were processed in Excel and a MATLAB script was created to analyse the results. The first part of the script takes every measurement and averages them for the particular axis and then plots the results for the two drives. The following is the calculation for the X axis

$$\frac{X_i}{N} \tag{3.1}$$

where N is the total number of samples in a batch of data and i of X_i denotes the value of the PSD in bins $i \ldots m$

The Y axis represents latitudinal plane (left to right) and the Z axis represents the vertical plane, or bounce (Figure 3.3). The upper portion of Figure 3.4 are the normalised X,Y and Z axis results for the nominal tyre pressure (32psi) drive and the lower portion is for the LH front tyre pressure 20psi. The X axis represents longitudinal plane of the chassis (front to rear of the car),

The plots are very similar with the majority of the excitation in the Z axis, as expected. There is very little activity in the X axis; most of this is probably due to deceleration and acceleration of the vehicle. Acceleration in the Y axis is most likely due to the cornering force in the lower frequencies and any imbalances in the rotating parts such as the wheels and brake rotors, in the higher frequencies the vibration is most likely to be caused by components in the engine bay.

The MEPHM could not be mounted perfectly square to horizontal and so there will be a small amount of interaction between the axes.

The second part of the script analyses the differences between the two drives. This was achieved by taking the bin-wise squared differences of the two normalised data sets, for each axis. The following is the calculation for the X axis

$$\left[\frac{X_{i1}}{N_1} - \frac{X_{i2}}{N_2}\right]^2 \tag{3.2}$$

where X_{i1} are samples for a given frequency bin for the first drive and X_{i2} are the corresponding samples for the second drive.

The results of this calculation are shown in Figure 3.5

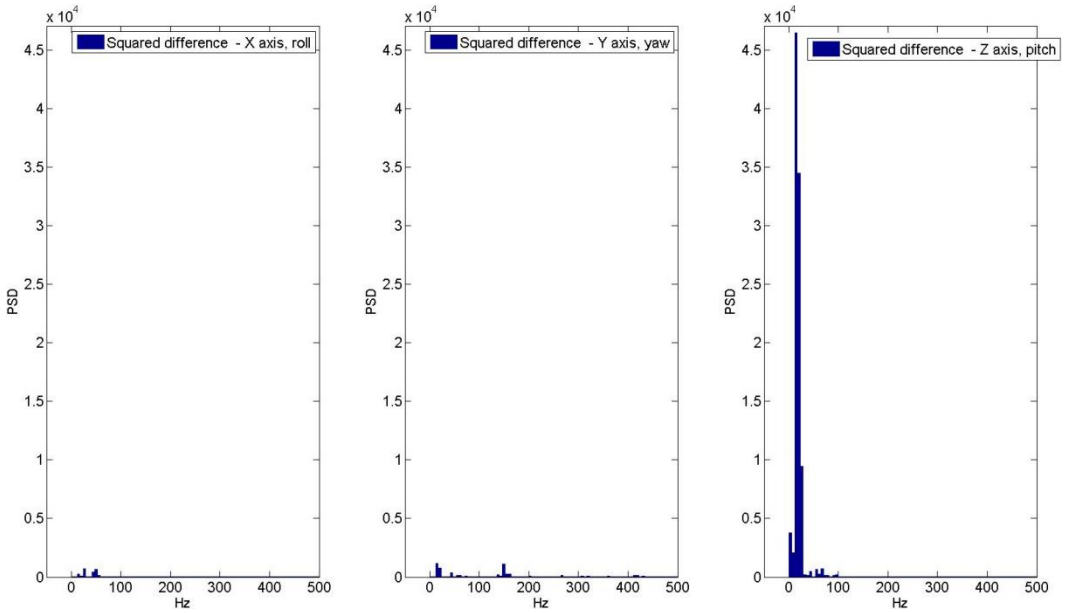

Figure 3.5 Squared bin-wise differences of the two normalised PSD results for Urban Circuit 1 – 32psi vs. 20psi, X,Y and Z accelerometer axes

Figure 3.5 makes an argument for the concept of tyre pressure detection from chassis acceleration. The squared differencing computation indicates that virtually all the difference between the two test drives lies in the Z axis, which is the prime axis to be affected by tyre pressure. Common vibration components such as engine vibration and rotating parts that were not affected by the tyre pressure change have effectively cancelled each other out in the other two axes (X and Y). Thus it is the difference between the two that manifest a faulty condition. To put this result into perspective, tyre pressure reduction of 30% is a gross amount and a

casual inspection of the vehicle would reveal this fact. A more realistic reduction which would not be easily visible or perceptible from the handling dynamics would be a reduction of around 10% but this figure remains relatively arbitrary quantity whose significance and effect on vehicle performance would depend on other factors such as road conditions and added vehicle mass. This type of tyre pressure reduction would impact the fuel economy of the vehicle (TRB 2006).

The tyre was inflated to 29psi for the third drive and the same circuit and average velocity was observed.

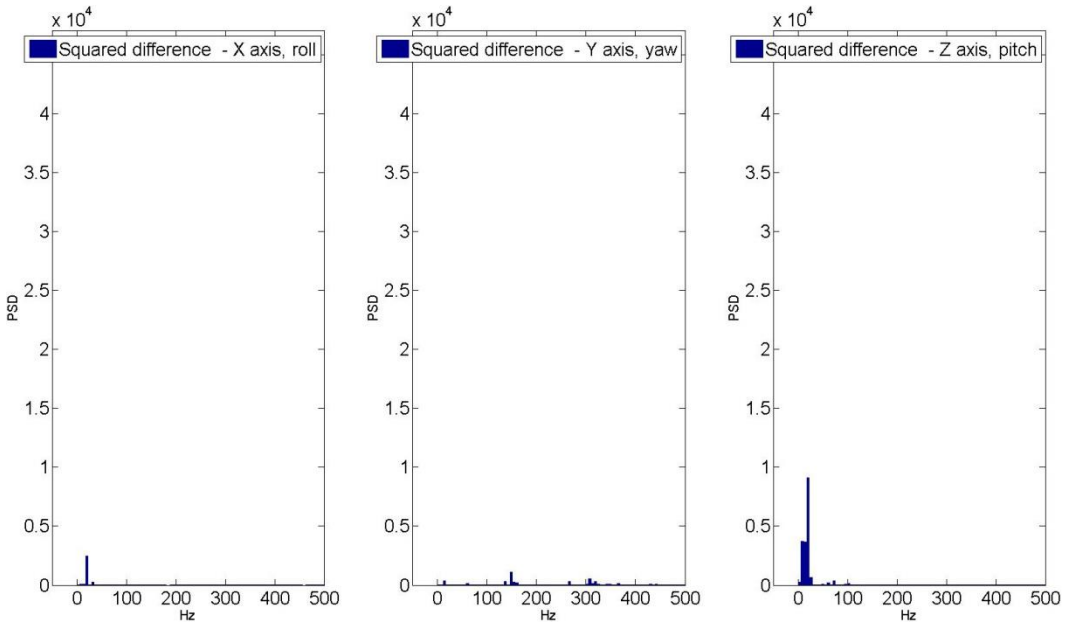

Figure 3.6 Squared bin-wise differences of the two normalised PSD results for Urban Circuit 1 – 32psi vs. 29psi, X,Y and Z accelerometer axes

Figure 3.6 shows a much smaller difference but the difference is still present. The vehicle dynamics were perceived to be identical during the drive which is exactly the condition that the system is intended to find i.e. a tyre pressure difference that is imperceptible to the user but is causing excess wear to the tyre and degraded fuel economy.

3.1.1.4. Motorway test 1

The next test was a high speed motorway drive, another typical driving scenario and one which poses somewhat of a challenge since there will be far less vertical displacement and much more noise, due to the greater angular velocity of the road wheels and higher engine RPM. This test was carried out at 20psi and 32psi on a very good road surface. The data represents virtually identical routes as it was possible to use the same lane and maintain the same velocity of 70mph for the tests.

Figure 3.7 shows, as expected, a lot more activity in the higher frequencies. However, the degree of difference in the Y axis was not expected. Up to this point it was assumed that all the information would be contained in the vertical plane but the squared difference plot of Figure 3.8 shows that there is very little difference between the tyre pressures in the vertical plane for a motorway drive. In actual fact there is less vibration in the Y axis for the tyre that is deflated. This result makes a case for a dual axis accelerometer to be employed in a practical system, especially considering the challenges a smooth road surface would pose to a detection algorithm.

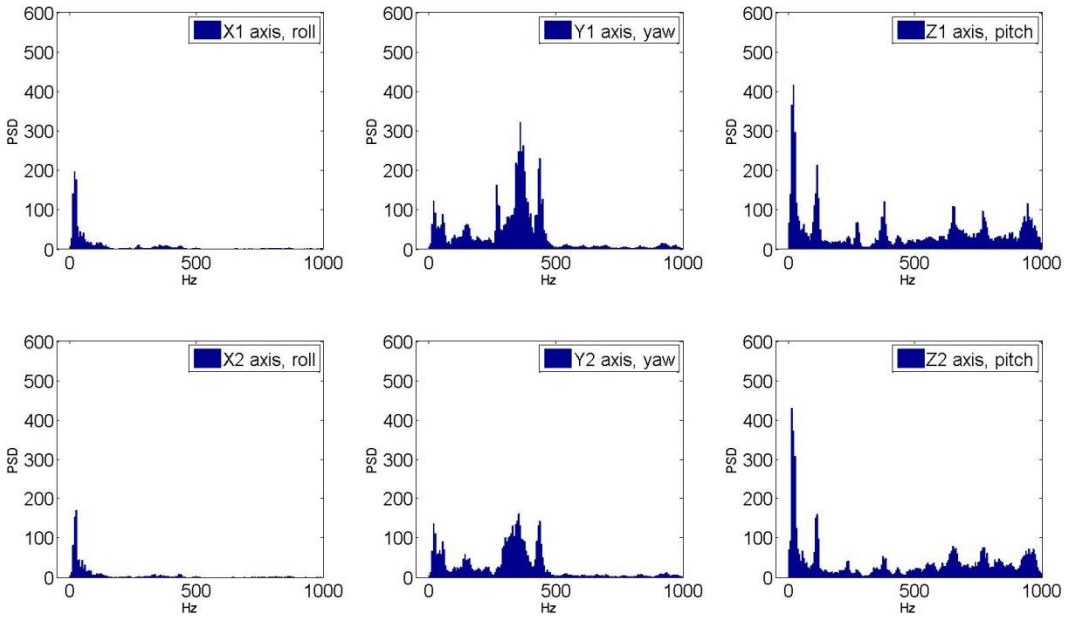

Figure 3.7 PSD results for 2 drives of Motorway Circuit 1 – upper plots 32psi, lower plots 20psi, X,Y and Z accelerometer axes

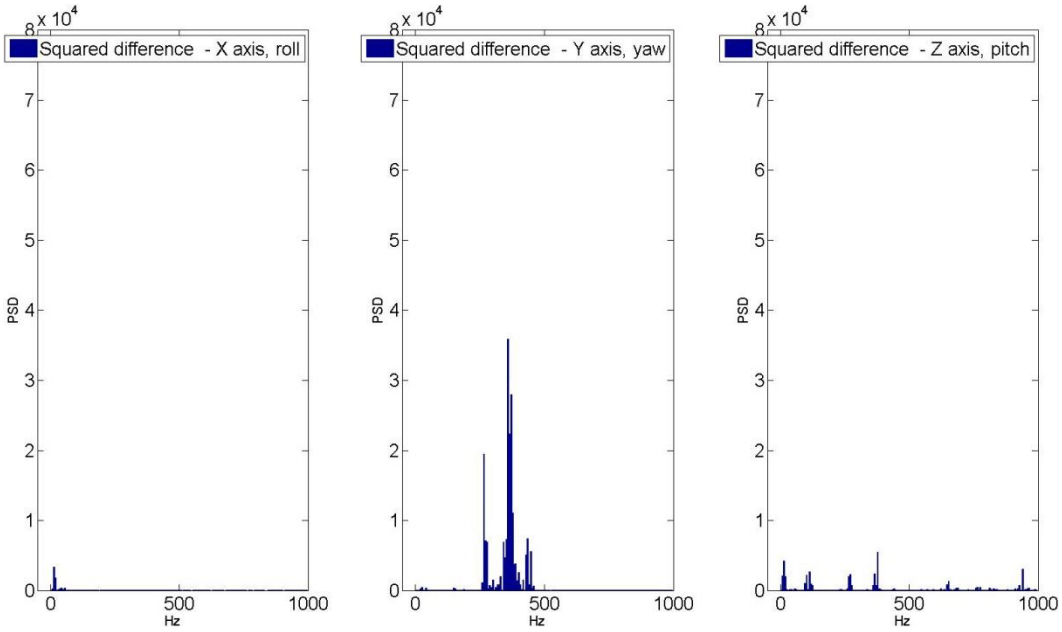

Figure 3.8 Squared bin-wise differences of the two normalised PSD results for Motorway Circuit 1 – 32psi vs. 20psi, X,Y and Z accelerometer axes

3.1.1.5. Motorway test 2

Another motorway test was undertaken and this is the only test to compare two independent routes at two different tyre pressures. The FFT averaging was switched off for this test so there is much more data but the accuracy may be a little compromised, to ameliorate this effect the test was run for a longer period of 40 minutes. This time the MEPHM obtained 128 sample batches, corresponding to 131,072 samples.

For the measurements in the Y axis, the situation is now reversed (compared to the previous motorway test), more vibration was recorded for the lower tyre pressure, see Figures 3.8 and 3.9. This highlights the problems associated with different road surfaces (the velocity was also greater, 80mph) even though they are of the same general type.

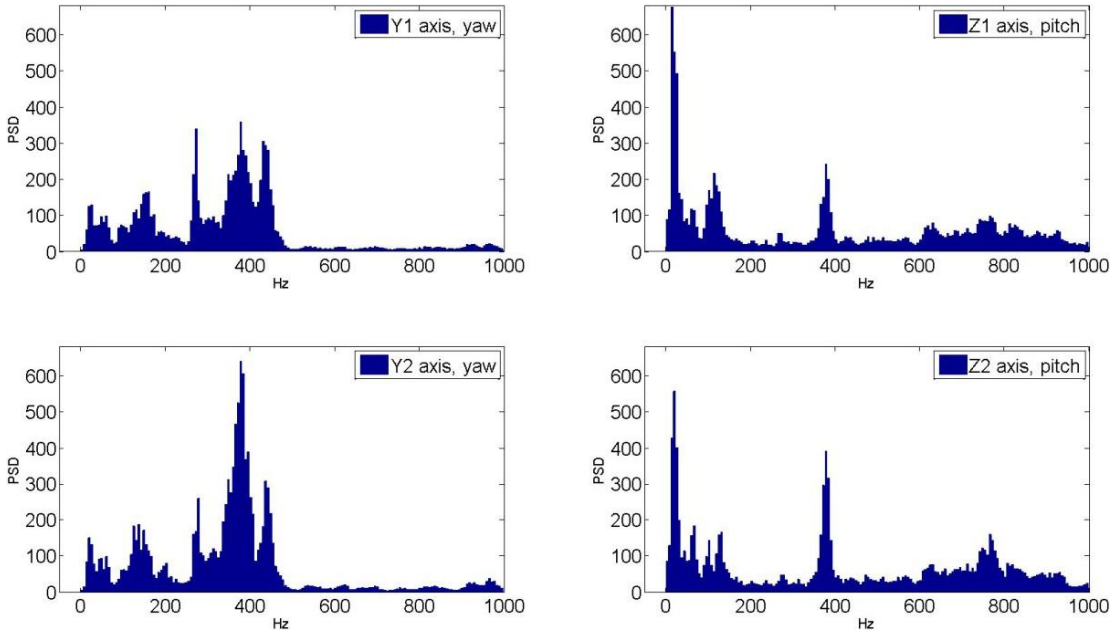

Figure 3.9 PSD results for Motorway individual routes – upper plot 32psi, lower plot 28psi, Y and Z accelerometer axes

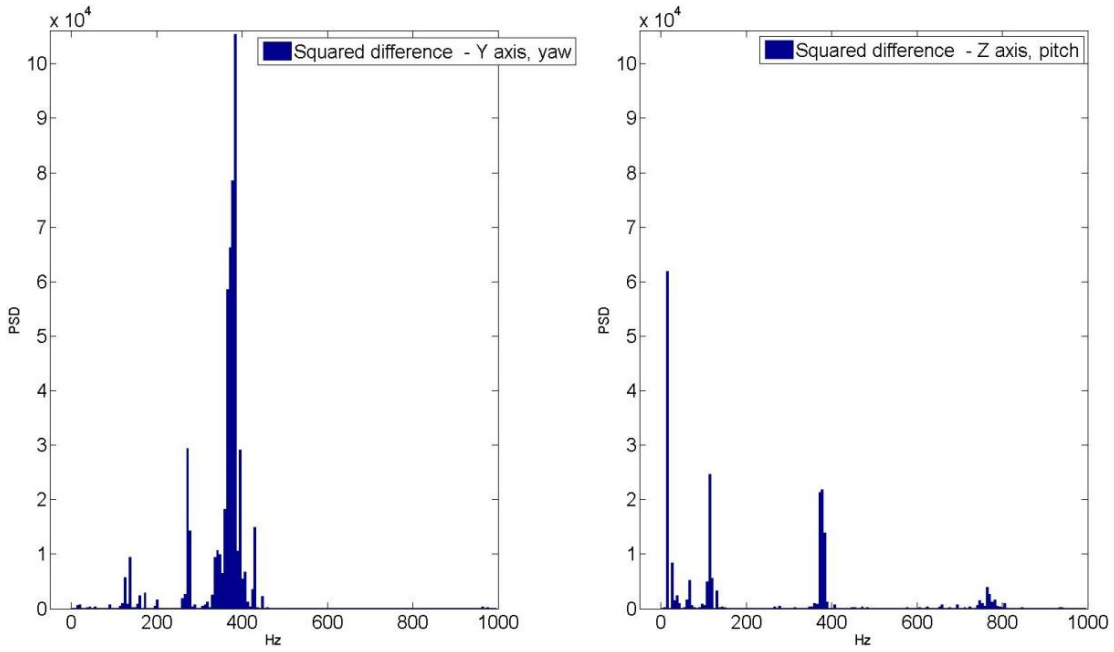

Figure 3.10 Squared bin-wise differences of the two normalised PSD results for Motorway individual routes – 32psi vs. 28psi, Y and Z accelerometer axes

3.1.1.6. Rough road test

The final test was a rough road circuit for 32 and 28psi tyre pressures. The road surface is a mixture of pot holes approximately 10-70mm deep with some cobbled areas.

As expected, this drive produced the largest acceleration measurements (Figure 3.11 and Figure 3.12), approximately 3 times greater than any other response. It also produced the largest bin-wise squared difference of all the plots but this is partially due to the magnitude of the normalised responses. The result is the opposite of the first urban circuit test, where the lower pressure tyre recorded greater acceleration, which is a more intuitive result since a fully inflated tyre has less compliance than an underinflated tyre and hence would deflect the suspension to a greater extent when subjected to violent input excitation.

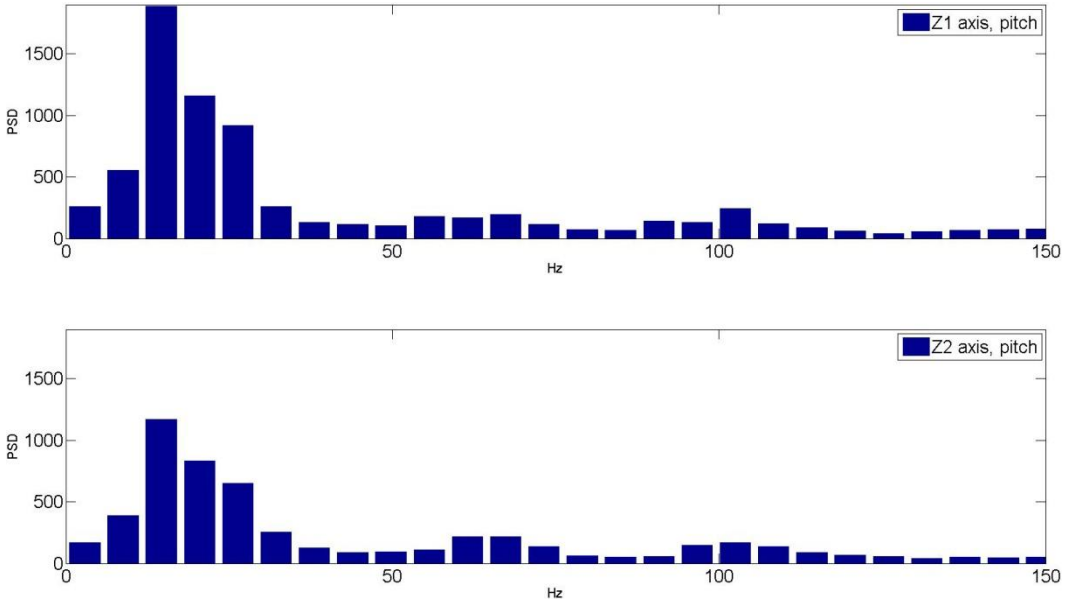

Figure 3.11 PSD results for rough road – upper plot 32psi, lower plot 28psi, Z accelerometer axis, 2.9 to 150Hz

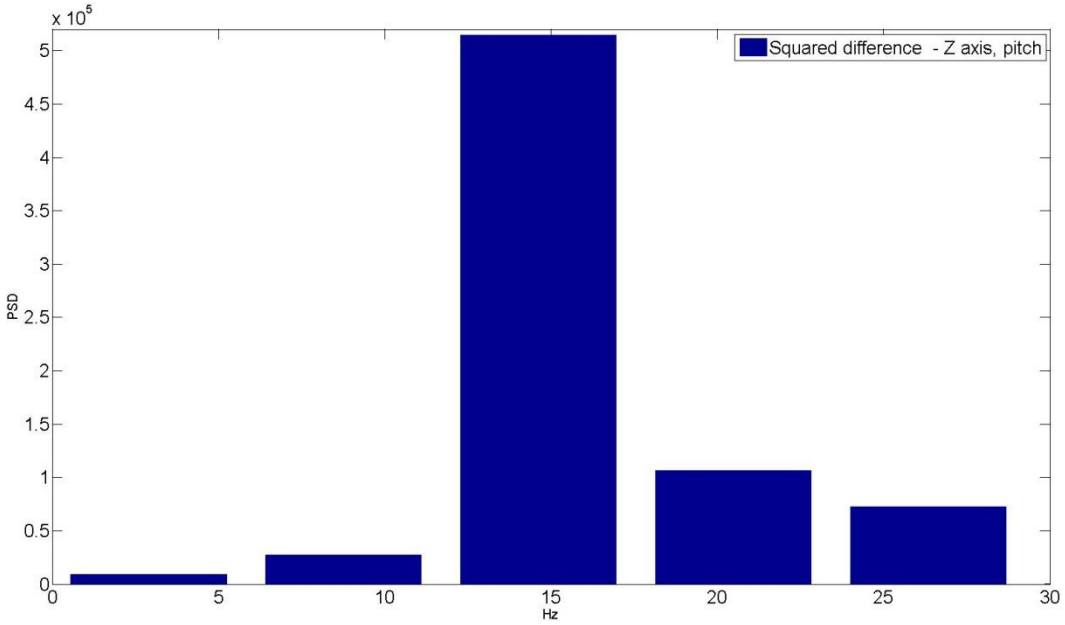

Figure 3.12 Squared bin-wise differences of the two normalised PSD results for rough road – 32psi vs. 28psi, Z accelerometer axis, 2.9 to 30Hz

3.1.1.7. Conclusions – Initial chassis acceleration testing

Despite every effort taken to eliminate misleading results and set up the experiments that isolated the tyre pressure as the only difference between the tests on the same surfaces it was not possible to make them perfectly objective. Traffic conditions did not allow a constant velocity and the logging device was not integrated with the vehicle velocity to prevent logging during periods when the vehicle was not moving. While the same tyre pressure gauge was used for all the tests, the experiment would benefit from a more accurate device.

The problem of measuring acceleration with no *a priori* knowledge of the road surface is that drastic road surface changes from smooth to rough and vice versa could appear to be tyre pressure changes to an insufficiently tuned algorithm. While it is technically not possible to know the road surface in advance, there are many improvements that could be made to the measuring and logging system (modern image recognition technology could alleviate this in the near future) (Mercedes-Benz 2013).

A modern vehicle uses a network to distribute the sensor data amongst the onboard ECUs so it is possible for any network connected ECU to be supplied with the vehicle velocity, gear position, engine angular velocity, GPS location and many other pieces of data. Armed with this information, an algorithm can be encoded with some information about the road surface. For

instance, if the vehicle is in top gear and cruising at 70mph, in all likelihood the vehicle is on a motorway. The driving style of the driver can be categorised by the throttle pedal position and brake fluid pressure. Data may be stored for a GPS position so there is a log of road conditions in the past. A fully equipped sensing system with an accelerometer on each corner of the vehicle would be able to compare data from tyres on the same side of the car, perturbation at the front of the car is likely to affect the rear after a short time delay, if the vibrations begin to differ then this is cause to suspect a change is occurring in the suspension. When the vehicle stops and doors open and close and the vehicle resumes progress, it indicates that passengers or cargo has been loaded/unloaded.

In summary there is potential to use the existing MEPHM sensor for the purpose of detecting tyre pressure changes but it would need to be integrated with the vehicle network in order that any proposed fault detection algorithm has access to the vehicle sensor and controller data, which has not been possible to date.

The next Chapter considers the suspension system in isolation and develops fault detection strategies which are the bases for model based approaches.

3.1.2. Suspension system data gathering using Jaguar X-Type on the Crest road simulator

The objective of this series of tests was to acquire time series data of road position, axle position, suspension deflection and chassis position of a car in motion. When this experimented was conducted in 2010, acquiring road profile data whilst driving was not a realistic prospect. Many alternative methods were considered, such as measuring a road profile with Lidar (light-radar) sensing technology and driving an instrumented vehicle over a precise course.

The Crest facility (Figure 3.13), generically referred to as a 'four poster rig', is composed of four hydraulically actuated posts. The vehicle is driven onto the rig and secured with strapping. At this point the vehicle may be equipped with instruments to record the displacements. Suspension height sensors were selected for this task (they are usually deployed on air suspension vehicles). The input is sampled automatically by the controller at 200Hz. The DAQ was set to 500Hz in order that no potentially useful dynamics or effects were missed, although from a theoretical point of view no features of great significance exists beyond 20Hz, with respect to suspension and tyre dynamics (wheel hope for the X-Type is around 13Hz).

In some ways, the Crest facility is superior as a testing and data acquisition platform. It allows the user almost total control and knowledge of the road surface, combined with the convenience of being in a room, with all the associated benefits that brings. The main limitation of this equipment, with respect to analysis of the tyre pressure, is that the wheels do not rotate. This means a portion of the suspension dynamics is not present, as it would be driving on a normal road. Since the objective of the test was analysis of the dynamics in the vertical plane, this limitation was not considered to be of great significance.

For the testing it was decided that a range of road surfaces would be simulated, including urban driving, A-road (medium speed), motorway cruising and 'third world road' which is used for accelerated aging durability tests. In order that the suspension did not approach its extent of travel (and become significantly non-linear), the deflection of the input actuation was limited to 300mm. This means the average height is 150mm.

Figure 3.13 Jaguar X-Type on the Crest road simulator

3.1.3. Wheel speed signal and message acquisition of Ford C-Max

Wheel angular velocity for the candidate vehicle (Ford C-Max) is produced by the ABS/ESP ECU in the form of four 15-bit hexadecimal numbers (one for each wheel). These signals are contained in a single 8-byte CAN data frame under the CAN identifier (ID) 0x4B0. From experimentation it is possible to determine that a 100 offset is applied to the signal, the precise reason for this is not known, possibly to assist in the removal of implausible values by the receiver nodes in the case of data corruption (values less than 100 would be discarded). Alternatively, a 100 offset would allow the ABS to register up to $100km/h$ vehicle velocity in reverse gear, with values less than 100 interpreted as 'vehicle moving backwards'. This explanation would avoid the requirement for a signed variable, which would be redundant for the vast majority of the time during drive cycles. These decisions are made during the development of the vehicle distributed functionality control systems and are the result of cooperation by the CAN engineers and the individual sub-system engineers, with the goal of making the CAN as compact and robust as possible, not clarity and transparency for the designers of third party network analysers or applications.

3.1.3.1. Network analyser considerations

An obvious choice for research into CAN is the Vector suite of network analysis software and hardware. Vector are a dominant constituent of this space and their tools are widely deployed in vehicle OEM. They are, however, extremely costly which motivates the consideration of other solutions. There has been a substantial increase in the number of software solutions, in large part due to the proliferation of low cost CAN data acquisition integrated circuits, such as the ELM327. Due to the proprietary nature of a particular CAN implementation, as outlined above, these tools are often restricted to a particular vehicle brand or group.

3.1.3.2. FORScan

FORScan is a multifunction piece of software designed to assist diagnosis of electrical faults, compatible with Ford, Mazda, Lincoln and Mercury. Within this software is a data logging facility that allows the user to specify OBD sanctioned parameters and create a time series measurement file in CSV format. The creators of the software have avoided the problem of unknown message ID, format and location by restricting the available parameters to the OBD sub-set. In many cases this results in reduction of the parameter resolution and increased sampling interval. These constraints are attributed to the retrieval mechanism (the OBD

protocol and ECU diagnostic function/interface) which has low network priority. See the CAN section of Appendix 2 for more details.

While FORScan remains a useful diagnostic tool, it constrains the user to a hundredth of the resolution for wheel angular velocity and steering angle measurement. The sampling interval via the diagnostic interface ($\sim 50ms$) is up to three times greater than the signal available on the vehicle network. Due to the low priority of diagnostic messages (in the range 0x7xx), they are necessarily susceptible to intermittent fulfilment when the data-bus load increases.

3.1.3.3. ELMConfig

ELMConfig is alternative piece of software that interfaces with the CAN via the ELM327 microprocessor. As the name suggests, its main purpose if configuration of the electronically controlled systems present on a vehicle. In addition to the configuration functions, a CAN data logging function allows the user to capture any or all CAN data frames that are broadcast by the vehicle controllers. Due to the baud rate of a high speed CAN and the limited internal memory of the ELM327 PIC, it is not possible to log all frames indefinitely, a buffer over-run occurs after approximately 2 seconds (in the case of data logging of the Ford C-Max HS-CAN). This constraint is mitigated by a filter-mask configuration, whereby only specific sets of messages are logged and committed to the log file, the remainder are immediately discarded. See Appendix 2 for details on how this is achieved.

3.1.4. Determining the nature of signals on the CAN

Conducting targeted experiments whilst logging CAN data reveals the nature of the signal when

- Vehicle is stationary
- Cruising at constant velocity
- Manually rotating individual wheels.

In the case of message 0x4B0 with vehicle stationary, regardless of the engine angular velocity, the message contents remain fixed at

{time stamp} 4B0 27 10 27 10 27 10 27 10

Following the time-stamp, the first three digits are the CAN identifier (transmitter) and the remaining eight fields contain the wheel angular velocity data in hexadecimal format (Table 3.2). When the vehicle is in motion, the data bytes are updated at ~$14ms$ intervals.

	CAN identifier	Data bytes for CAN data frame 0x4B0 (stationary vehicle)							
Data byte		1	2	3	4	5	6	7	8
CAN data frame	**4B0**	**27**	**10**	**27**	**10**	**27**	**10**	**27**	**10**

Table 3.2 CAN frame 0x4B0 wheel speed data

In order to interpret the wheel speed signals some assumptions must be made. The maximum velocity of this particular vehicle is $\sim 200 km/h$. Assuming that ability to record the velocity in reverse up to $100 km/h$ is required, without implementing a signed variable, it would necessitate a velocity range of $300 km/h$. In order to achieve a minimum range of $300 km/h$, a 9-bit binary value is required since $2^8 = 256$ (possible permutations) is not quite enough and $2^9 = 512$ allows some margin.

However, this assumes a $1 km/h$ resolution, which may not be adequate for optimal performance of the ABS-ESP. It is likely (from the testing evidence) that the designers of this ABS-ESP system implemented $0.01 km/h$ resolution.

With four individual signals at $0.01 km/h$ resolution, each one would be ~15 bits in length which renders $2^{15} = 32768$ permutations. This leads to a wheel angular velocity range of $327.68 km/h$. Considering the offset of 100 (broadcast at $0 km/h$ actual vehicle velocity) this implies a forward velocity range of $0 - 227.68 km/h$ which is consistent with the vehicle properties.

Assuming that the wheel speed signals are broadcast simultaneously, this implies that they occupy approximately 8 bytes per sample, which corresponds to an entire CAN data frame.

This interpretation (Table 3.3) has been verified by logging data at a particular cruising velocity (registered on the vehicle speedometer) and comparing the cruising velocity with the data log. It has also been independently verified via the velocity estimation function within a smartphone-based satellite navigation application (Nokia E72).

	Wheel speed signals (CAN frame 0x4B0)							
Data byte	1	2	3	4	5	6	7	8
Hexadecimal value	27	10	27	10	27	10	27	10
Decimal value	**100**		**100**		**100**		**100**	
Wheel position	**Front Left**		**Front Right**		**Rear Left**		**Rear Right**	

Table 3.3 Interpreted values for CAN data frame 0x4B0 (wheel speeds)

3.2. Concluding remarks

This chapter has discussed the data acquisition undertaken for three vehicles which provide the data for validation of the tyre pressure detection algorithms, which are developed in Chapter 5 following a preliminary investigation and modelling a suspension system in Chapter 4. Test requirements and subsequent data acquisition is further discussed and clarified in Sections 1.2, Conclusions 6.3 and Appendix 2.

Chapter 4.

Modelling the suspension components

In this chapter a procedure for modelling the car suspension system is described. The elementary components of a suspension are introduced in Section 4.1. Some of the methods of modelling the suspension are assessed in Section 4.5.

In common with other model-based fault detection schemes (Isermann and Wesemeier 2009, Carlson and Gerdes 2005, Persson et al. 2001a), the general modelling requirements for an indirect tyre pressure measurement system are

- **High fidelity.** A natural consequence of the model-based approach is the requirement for an accurate model in order to estimate the small deviations in physical constants that accompany tyre pressure change
- **Ability to tolerate noise and uncertainty.** Due to the fact that the road, the primary input to the suspension system, is completely unknown the model must have some means of acquiring an estimate of the road profile or be modelled in such a way that the road profile information is not required
- **Online model.** The objective of the algorithm is to detect changes in the suspension system and this requirement necessitates an online model which is updated at regular intervals via input from the vehicle sensors

Practical constraints, such as model complexity and computer hardware are not considered, although this would be a consideration for any embedded system designer. The model should describe the properties of the suspension system and simultaneously be as simple as possible. As models become more complex this increases the computational load and problems associated with converging to a solution without being constrained to unrealistically small sampling intervals. In contrast, a simplistic model will not describe the system in sufficiently accurate detail to make a reliable diagnosis of tyre pressure. It is convenient to model physical systems in terms of transfer functions, as they relate to physical properties and the parameters can be updated online by means of parameters estimation techniques such as least squares regression. However, transfer functions can only describe the linear portion of the response.

While the linear response usually constitutes the majority, a significant proportion is not linear and this will prevent an accurate diagnosis.

4.1. Vehicle Suspension Overview

The term suspension describes the arrangement of springs, dampers and linkages that connect the road wheels to the chassis (Figure 4.1). A road vehicle does not necessarily have to be suspended but suspended vehicles exhibit superior road holding and comfort characteristics. The suspension acts in two ways, to isolate the occupants and cargo from an unevenness of the surface the vehicle is traversing and to maintain the optimum contact of wheel and road. The design and set up of a suspension system is often a trade-off between these two characteristics. For example, a racing car has very stiff suspension which is well adapted for taking corners at high velocity but it is uncomfortable for long duration drives and uneven surfaces. On the other hand, an off-road vehicle may have very soft suspension to isolate the occupants of the vehicle from the extreme terrain but such a vehicle may be unstable at high velocity.

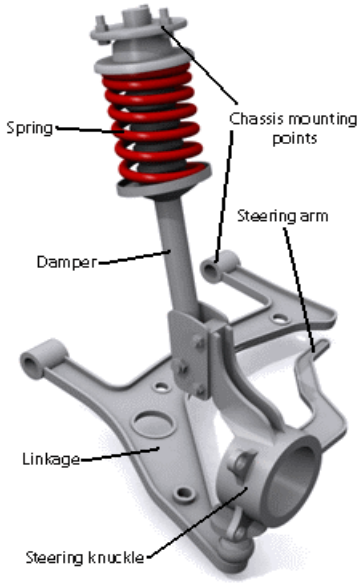

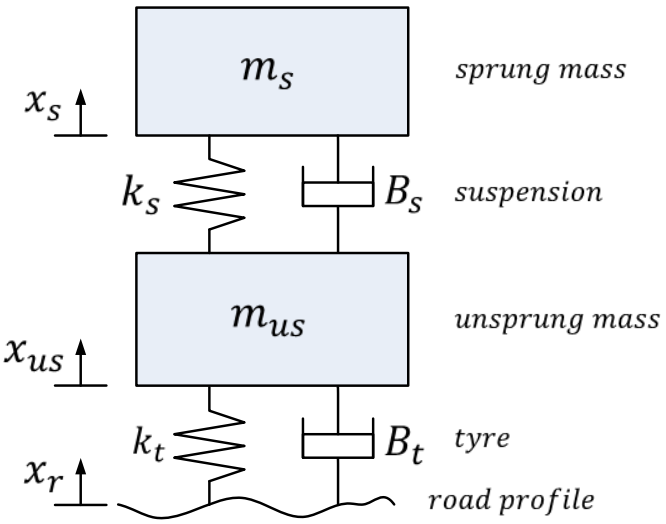

Figure 4.1 McPherson strut suspension **Figure 4.2 Quarter car suspension**

4.1.1. Tyre and Wheel

Although its contribution to many of the fundamental vehicle properties is easily overlooked, the tyre is considered a critical component of a vehicle due to the fact that this component must transmit the force required to accelerate and change the direction of the vehicle, under a wide range of temperatures and road surfaces for many years at a time, with minimal failures.

Pneumatic tyres are used to provide a spring effect for most of the un-sprung mass, rubber tyres include some damping properties which can be controlled by the compounds used during manufacture but the amount of damping that can be included in the tyres is limited by considerations of fuel economy, wear and ride performance.

The tyre spring rate can be assumed to be a linear spring in the vertical direction (Gillespie 1992) and the tyre stiffness k_t (Figure 4.2) is dependent on the flexibility of its sidewalls (Rajamani 2006)

Tyre pressure is crucial to the performance of the vehicle; underinflated tyres have higher rolling resistance, causing reduced fuel economy and deteriorated handling characteristics. Under inflation also makes the tyre more prone to punctures. Over inflation of tyres does not pose problems in terms of handling, it can even improve matters on wet surfaces but continued use may lead to uneven wear in the central part of the tyre.

The main failure modes of tyres are punctures and explosive decompression (often referred to as 'blow out'). Continued use of an underinflated tyre can cause heat build-up and destroy the internal parts of the tyre causing a catastrophic failure.

4.1.2. Spring

The principal function of the spring k_s (Figure 4.2) is to isolate the occupants, cargo and vehicle components from shocks induced by the vehicles motion over the road surface. Springs are mounted to the chassis and the un-sprung mass in the same way the damper is attached.

The spring rate defines the handling characteristics to a great extent. Low stiffness results in a smooth ride but at the expense of road holding in corners and under heavy braking or acceleration. Stiff springs increase the general road holding and cornering velocity that can be achieved but reduce the comfort of the ride. Spring stiffness selection is a compromise between these characteristics.

Most modern vehicles are equipped with helical springs which can be viewed as linear over their operating range. However, the springs are not anchored directly to the chassis or suspension; there is some interface material which introduces a non-linear element to the system.

The suspension must have some mechanism to prevent the wheel coming into contact with the chassis or components of the suspension from 'clashing' at the extremes of the suspension range. This is achieved with bump and rebound stops. The term 'bump' refers to the compression of the suspension and 'rebound' to the extension of the suspension. Bump and rebound stops are made from some elastic material which adds to the spring force at the limits of travel causing the suspension to stop its extension or compression in a more controlled manner than steel on steel contact. This property introduces a large non-linear effect (which is accurately modelled as a bilinear effect, i.e. there is an additive multiplicative effect stemming from input and output) into the system but can be assumed to be zero for normal driving conditions as a vehicle only hits its bump stops during extreme manoeuvres.

Assuming no non-linearities discussed above the spring constant is defined $k_s = F/\Delta x$ where F is the force compressing or extending the spring expressed in N/m and x is the displacement.

4.1.3 Damper

The suspension dampers regulate the spring motion to prevent oscillations in the sprung portion of the vehicle mass, without these the vehicle would be unstable, especially at high velocity. This is because an unregulated spring will rebound after compression, causing wheel hop (the wheel losing contact with the road surface). The vehicle would lose traction and skid. The damper must be less stiff than would optimally damp the wheel hop. The wheels will oscillate after each perturbation from the road surface before coming to rest. They also contribute to the drive quality of the vehicle by damping the oscillations of the passenger compartment (Gillespie 1992).

Dampers are mounted to the chassis and the un-sprung mass in the same manner as the spring. They feature a piston in a chamber which is filled with a viscous fluid (and may also be gas charged) which is forced through an orifice during extension or contraction, this regulates the spring action due to the road surface.

Dampers expand at a different rate to the contraction, this is a design feature that allows the suspension to extend rapidly when the wheel rolls down a pot hole and resist compression when the wheel hits a bump (Gillespie 1992). This behaviour is non-linear which complicates attempts to model the damper but for simplicity the damper can be assumed to be linear.

Damper force $F_D = B\Delta\,\dot{x}$ where B=Ns/m is the damper constant and $\Delta\dot{x}$ is the velocity of the damper piston (B_s – Figure 4.2).

4.2. Sprung and Un-Sprung Mass

In a vehicle with a suspension, the un-sprung mass is the mass of the suspension (denoted m_{us} 2, wheels and other components directly connected to them, rather than supported by the suspension springs. The mass of the body and other components supported by the suspension is the sprung mass. Un-sprung mass includes the mass of components such as the brakes, wheel axles, wheel bearings, tyres, and a portion of the weight of drive shafts, springs, shock absorbers, and suspension links that attach the suspension to the chassis.

The un-sprung weight of a wheel is part of a compromise between a wheels terrain following ability and its vibration isolation. Surface imperfections in the road cause tyre distortion which induces a force on the un-sprung weight. The un-sprung weight then reacts to this force causing compression of the suspension spring. The degree of suspension deflection is inversely proportional to the mass - a lighter wheel has less inertia and will react more rapidly than a wheel with greater mass, this allows the lighter wheel to better track the terrain of an imperfect road surface. The lighter wheel will therefore transmit less vibration into the cabin. Obviously, the weight of a wheel cannot be reduced beyond the point that it is not able to carry the load placed upon it without destruction occurring. There is a relationship between the mass of the wheel and the mass of the vehicle, if the mass of the wheels becomes too great a proportion of the total vehicle, deterioration in ride quality will result (Gillespie 1992). Large un-sprung mass degrades wheel control under hard acceleration or braking. Large forces exerted on the suspension combined with large un-sprung mass can lead to wheel hop, reducing traction and steering control (Gillespie 1992).

4.3. Suspension Fundamental Frequencies

At the most basic level, all road vehicles share the same ‘ride isolation’ properties common to a sprung mass supported by primary suspension systems at each wheel. The dynamic behaviour of this system is the first level of isolation from the roughness of the road. The essential dynamics can be represented by a quarter car model, as shown in Figure 4.2 (Gillespie 1992).

The effective stiffness of the suspension and the springs in series is called the ‘ride rate’ determined as follows

$$RR = \frac{K_s K_t}{K_s + K_t} \qquad (4.1)$$

where

RR = Ride rate

K_s = suspension stiffness

K_t = Tyre stiffness

In the absence of damping, the bounce natural frequency at each corner of the vehicle can be determined from

$$\omega_n = \sqrt{\frac{RR}{m_s}} \qquad (rads/sec) \qquad (4.2)$$

When damping is present, as it is in suspension, the resonance occurs at the damped natural frequency

$$\omega_d = \omega_n\sqrt{1-\zeta_s^2} \qquad (rads/sec) \qquad (4.3)$$

where ζ_s is the damping ratio

$$\zeta_s = \frac{\mathrm{B_s}}{\sqrt{4\mathrm{K_s}m_\mathrm{s}}} \qquad (4.4)$$

where $\mathrm{B_s}$is the suspension damping coefficient

For good ride the suspension damping ratio on modern passenger cars usually lies between 0.2 and 0.4. Owing to the way damping influences the damped frequency in (4.3) i.e. under the square root, it is usually quite close to the natural frequency.

Taking the parameters of the Volvo V40

RR = 13953

ω_n = 6.31 rads/sec

ζ_s = 0.24

ω_d = 6.02 rads/sec

6.02 rads/sec is approximately equal to 0.96 Hz, the chassis natural frequency

Consequently, the modes of the system are represented by frequencies of 10Hz and 1Hz which has ramifications for the model and estimator which will be described in section 5.2.3.

4.4. Modelling the Suspension

The so-called quarter car suspension model will be used for the fault detection simulation (Figure 4.2). This is a basic model of one corner of the vehicle with parameters detailed in Table 4.1

Parameter	**Value/Unit**	**Description**
m_s	350 kg	Sprung mass
k_s	15,000 N/m	Suspension spring
B_s	1100 Ns/m	Damper
m_{us}	45 kg	Un-sprung mass
k_t	200,000 N/m	Tyre
x_s	m	Displacement of the chassis
x_{us}	m	Displacement of the un-sprung mass
x_r	m	Road input displacement

Table 4.1 Quarter car suspension typical parameter values

The model assumes two degrees of freedom; in reality a suspension system would have many more degrees of freedom as all the components have some form of elasticity and will deform in use. However, the model utilised is sufficiently detailed to demonstrate a fault detection scheme. The damper, suspension spring and tyre spring are assumed to be linear over their operating ranges. No account is taken of any compliance in the mountings of the components. There is no maximum travel of the suspension as the bump and rebound stops have not been modelled. The model of the tyre assumes no damping characteristic.

Many of these simplifications and assumptions will limit the analysis hereafter. However, a more detailed modelling approach has been identified as an area of future work.

Newton's second law states: the force on an object is proportional to the time rate of change of its linear momentum

$$F = \frac{d(mv)}{dt} \qquad (4.5)$$

Momentum mv is the product of mass and velocity. Force and momentum are vector quantities and the resultant force is found from all the forces present by vector addition.

Using this property, the suspension system of Figure 4.2 can be expressed as

$$m_s\ddot{x}_s + B_s(\dot{x}_s - \dot{x}_{us}) + k_s(x_s - x_{us}) = 0 \qquad (4.6a)$$

$$m_{us}\ddot{x}_{us} + k_t(x_{us} - x_r) - B_{us}(\dot{x}_s - \dot{x}_{us}) - k_s(x_s - x_{us}) = 0 \qquad (4.6b)$$

where x_r, x_{us} and x_s are the road input displacement, the unsprung mass displacement and the body displacement, respectively.

4.4.1. State Space Implementation

State space representation is a convenient way of modelling systems, especially since they can be expressed in vector matrix form and transferred into MATLAB directly. MATLAB functions can then be used to calculate transfer functions in discrete or continuous time. Utilising state space representations also simplifies the calculation of multi input, multi output systems so that refinements to include disturbances to the model can be included, for example.

The general form of a state space representation is

$$\dot{\boldsymbol{x}} = \boldsymbol{A}\boldsymbol{x}(t) + \boldsymbol{B}u(t) \quad \text{and} \quad \boldsymbol{y} = \boldsymbol{c}\boldsymbol{x}(t) \qquad (4.7)$$

For the system of Eqn 4.7, the states are set as the position and rate of change of position of the sprung mass, x_{s} ; and the un-sprung mass, x_{us} ; and the input to the system is x_{r}

$$x_1 = x_s \quad x_2 = \dot{x}_s \quad x_3 = x_{us} \quad x_4 = \dot{x}_{us} \qquad (4.8)$$

where

$$\dot{x}_1 = x_2 \qquad (4.9a)$$

$$\dot{x}_2 = -\frac{1}{m_s}[B_s(x_2 - x_4) + k_s(x_1 - x_3)] \qquad (4.9b)$$

$$\dot{x}_3 = x_4 \qquad (4.9c)$$

$$\dot{x}_4 = \frac{1}{m_{us}}[B_s(x_2 - x_4) + k_s(x_1 - x_3) - k_t(x_3 - u)] \qquad (4.9d)$$

State Space vector matrix form

$$\begin{bmatrix}\dot{x}_1\\ \dot{x}_2\\ \dot{x}_3\\ \dot{x}_4\end{bmatrix} = \begin{bmatrix}0 & 1 & 0 & 0\\ \frac{-k_S}{m_S} & \frac{-k_S}{m_S} & \frac{k_S}{m_S} & \frac{k_S}{m_S}\\ 0 & 0 & 0 & 1\\ \frac{k_S}{m_{us}} & \frac{B_S}{m_{us}} & \frac{-k_t-k_S}{m_{us}} & \frac{-B_S}{m_{us}}\end{bmatrix}\begin{bmatrix}x_1\\ x_2\\ x_3\\ x_4\end{bmatrix} + \begin{bmatrix}0\\ 0\\ 0\\ \frac{k_t}{m_{us}}\end{bmatrix} u \qquad (4.10)$$

$$\begin{bmatrix}y_1\\ y_2\\ y_3\\ y_4\end{bmatrix} = \begin{bmatrix}1 & 0 & -1 & 0\\ \frac{-k_S}{m_S} & \frac{-B_S}{m_S} & \frac{k_S}{m_S} & \frac{B_S}{m_S}\\ 0 & 0 & 0 & 0\\ 0 & 0 & 0 & 0\end{bmatrix}\begin{bmatrix}x_1\\ x_2\\ x_3\\ x_4\end{bmatrix} \qquad (4.11)$$

C is the output matrix; the first row represents the suspension deflection which is the difference between x_{s} and x_{us} ; the second row represents chassis acceleration $\ddot{x}_s$; the third and fourth rows are not populated but other outputs of the system can be included, such as tyre force, chassis displacement relative to the road and the un-sprung mass displacement relative to the road. Vertical acceleration is the output of interest for this system as it is the measured variable on the vehicle

$$\ddot{x}_s = -\frac{1}{m_s}[B_s(x_2 - x_4) + k_s(x_1 - x_3)] \qquad (4.12)$$

The other outputs will not be considered with the exception of suspension deflection as this has an impact on the sampling frequency used in discrete models and to a lesser extent in continuous models.

The outputs of the system can be expressed in terms of their transfer functions by applying

$$G(s) = c^T(sI - A)B \qquad (4.13)$$

where c^{T} is a particular row of the output matrix C

For suspension deflection this leads to

$$\frac{-2222s^2}{s^4 + 27.59s^3 + 2598.4s^2 + 6984s + 95238}. \qquad (4.14)$$

For chassis acceleration this leads to

$$\frac{6984s^3 + 95238s^2}{s^4 + 27.59s^3 + 2598.4s^2 + 6984s + 95238}. \qquad (4.15)$$

4.4.2. Discrete and Continuous Models

Two different approaches will be applied to the task of modelling the system, namely discrete and continuous time models.

When obtaining a discrete time transfer function from the frequency domain model (4.15), a conversion takes place. The continuous-time (CT) transfer function is converted with a sampling interval factored into the resulting expression and the result is a transfer function with at least one additional zero. The coefficients of the transfer function no longer bear any resemblance to the continuous transfer function. Local changes to a particular parameter that occur in the continuous case may be distributed amongst the parameters of the discrete transfer function. This leads to a level of abstraction that is not beneficial for the purposes of fault detection and isolation. For instance, ideally, a change in tyre pressure affects a certain parameter or set of parameters in the continuous model. If this change is then spread across all the parameters, it may become problematic to differentiate tyre stiffness changes from main suspension stiffness changes.

Modelling in continuous time requires no conversion of the transfer function, the parameters are estimated directly and in the event of a vehicle fault, the link to the change in the actual vehicle parameters is more direct. For most physical systems it is easier to construct models with physical insight in continuous time than in discrete time, simply because most laws of physics (Newton's law of motion, relationships in electrical circuits, for example) are expressed in continuous time. Another benefit of estimating a continuous time model is that the estimation is less dependent on the sampling interval. The sampling interval is set to capture the fastest mode in the system or whatever the sampling ECU is capable of obtaining.

4.4.3. Sampling Interval

The sampling interval for the models is an important consideration. The procedure of sampling the data that are produced by the system is inherent in computer based data acquisition systems. It is unavoidable that sampling as such leads to information losses, and it is important to select the sampling instances so that these losses are insignificant. Suppose a signal $s(t)$ is sampled with sampling interval T:

$$s_k = s(kT), \qquad k = 1,2, \dots$$

If $\omega_s = \frac{2\pi}{T}$ is the sampling frequency, then $\omega_N = \omega_s/2$ is the Nyquist frequency which is the minimum frequency a sinusoid can be sampled to be distinguishable from a sinusoid of lower frequency (Ljung 2006).

In practice, the sampling interval should be at least one tenth of the time constant of the fastest mode of the system (Franklin et al. 1997) to capture the dynamics of the system in sufficient detail. To determine the sampling interval of the suspension system it is assumed that the suspension deflection which is associated with the tyre displacement will be the fastest mode. The roots of 4.15 are calculated to be.

$$p_{1,2} = -12.588 \pm 48.386\text{i} \qquad p_{2,3} = -1.2052 \pm 6.0538\text{i}$$

The time constant associated with the fastest mode is thus calculated to be 1/12.588 = 0.0794s, and an ideal sampling frequency of 126Hz. However this sampling interval is far too short for the low frequency mode. Indeed herein lies the problem since a lower frequency will be too slow for the fast mode. This is issue is considered in more detail in Section 5.3, where a comparison is made between discrete time and continuous time models.

These are theoretical limits, and meant as a guide only. As it is a simple matter to change the sampling frequency in a simulation, some experimentation is required to find the optimum value.

From the testing with the MEPHM it is clear that the majority of the response from the chassis at low speeds exists in the 3 – 32Hz region, centred on the 14.6Hz bin (see Figure 3.5). This is the characteristic frequency of the wheel hop, usually in the region of ~10Hz for good ride and handling. Insufficient resolution of the frequency binning prevents a more accurate measurement.

The frequency of the un-sprung mass is greater than that of the sprung mass (usually around 1Hz), there will be some trade off when attempting to capture the dynamics of both components. A sampling frequency that is fast enough to capture the dynamics of the un-sprung mass may be too fast for the sprung mass to give enough difference between the samples. A sampling frequency that is slow enough for the sprung mass frequency may not capture enough information on the un-sprung mass frequency. If they were much further apart the slower response could be ignored; if they were closer together, a common sampling interval could be satisfactory for both modes. This property of the suspension will have a negative effect on any

attempt to estimate the parameters of a model using discrete methods, especially when implemented to realise model based fault detection. The effect of sampling in the estimation of discrete-time and continuous-time models is explored in greater detail in Section 5.3.

4.5. Spectral analysis of vehicle suspension

The main appeal of spectral approaches for the purpose of tyre pressure analysis is that exact knowledge of the input is not required. Instead the input becomes the vibration that is measured (usually by accelerometers) at the unsprung mass (axle, rotor, wheel assembly) and the sprung mass (chassis). Another advantage is that precise knowledge of the vehicle model is not required. A model of the suspension is built from data obtained during drive cycles under the normal and faulty conditions. A very large data set can be built over the life of the vehicle, which motivates the usage of machine learning approaches (Halfmann et al. 1997a). The following examples of suspension spectral analysis are used to determine the properties of the candidate test vehicles but were not used directly in any of the fault detection methods.

Consider a vehicle model with seven degrees of freedom (Figure 4.3). The tyres are modelled as spring elements, as are the suspension pieces between the axles and the body. The front and rear axles are included as rigid bars, and the body mass is supported by the suspension springs. Since the model has seven degrees of freedom, it also has seven eigenvalues that can be associated with specific types of response. For instance, the lowest natural frequency mode is associated with 'heave' or the chassis natural frequency, it corresponds to purely up-and-down motions of the body. Although the physical mode (heave) does not purely correspond to vertical up-and-down motions (there is some contribution to pitch and roll), the approximation found by neglecting everything but the vertical motions is satisfactory. The roll mode corresponds to rotations about the longitudinal axis of the car. Pitching refers to rotations about a lateral axis through the car perpendicular to the normal forward motion. These low frequency modes are rigid body modes because they reflect motions of the chassis itself, oscillating on its suspension. The remaining modes are higher frequency modes that involve motions of smaller subsystems within the vehicle, primarily associated with the unsprung mass.

Owing to the fact that the unsprung masses are decoupled from the chassis, they experience their own, higher frequency modes. One of these is called wheel hop, which occurs when the front or back wheels oscillate in unison. If a set of wheels is moving in an antisymmetric way (one up and the other down), the mode is called tramp. Phenomena such as tramp and roll dynamics motivate the use of the quarter car model, in order to reduce the modes and hence complexity in the system.

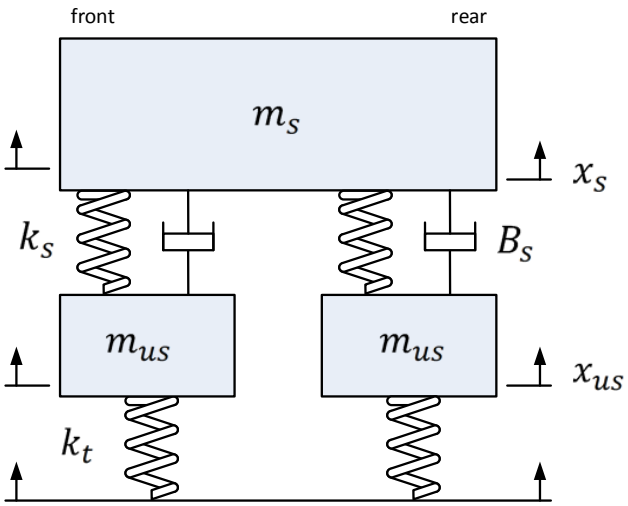

Figure 4.3 Simplified vehicle model

Parameters	Values
Tyre stiffness	184 kN/m
Front suspension stiffness	18.7 kN/m
Rear suspension stiffness	26.1 kN/m
Vehicle mass	1065 kg
Total unsprung mass	175 kg
Front unsprung mass	73 kg
Rear unsprung mass	102 kg
Rear axle	52 kg
Body roll inertia	190 kg m^2
Body pitch inertia	1080 kg
Rear axle rotational inertia	8 kg m^2
Wheelbase	2.42 m
Front wheels to CG	0.46m
Front track	1.38 m
Rear track	1.35 m

Table 4.2 Parameters for compact vehicle

The various physical parameters of the vehicle model are given in Table 4.2. In order to analyse the system and determine the modal frequencies and their distributions, a white box model from the equations of motion would be a valid approach. However a similar result can be achieved with a simpler approach allowing rapid assessment of various vehicle types.

Consider the heave mode in the ideal case of purely vertical oscillation. Disregarding the unsprung mass, they may approximated by two springs in series. Thus the equivalent spring at each front corner of the car is equal to

$$k_f' = \frac{k_{ft}k_{fs}}{k_{ft} + k_{fs}} = 16{,}975\ N/m \tag{4.14}$$

and

$$k_r' = \frac{k_{rt}k_{rs}}{k_{rt} + k_{rs}} = 22{,}858\ N/m \tag{4.15}$$

where subscripts f and r refer to front and rear springs, respectively, and subscripts t and s refer to the tyre and suspension springs, respectively. Defining ω as the bounce mode, it follows that

$$1065\ddot{x}_{us} + 2(16{,}975 + 22{,}858)x_{us} = 0 \tag{4.16}$$

where x_{us} denotes the displacement of the unsprung mass, leading to

$$\omega_n = \sqrt{\frac{79{,}666}{1065}} = 8.65\ rad/s = 1.38\ Hz \tag{4.17}$$

The moment of inertia for the sprung mass about the longitudinal axis is $190\ kg\ m^2$. In order to estimate the roll mode an estimate of angular stiffness is made. When the chassis rolls, the springs on one side are extended and the opposite springs are compressed. The equivalent torsional spring for each spring is equal to $k_{eq}l^2$, where l is the distance from the roll centre to the spring and k_{eq} corresponds to the k_f' and k_r' defined. Note that the distances from the roll centre to the equivalent spring is given by the front and rear track data in Table 4.2. The equation of motion for the roll mode is therefore given by

$$190\ddot{x}_r + 2\left(16{,}975\left(\frac{1.38}{2}\right)^2 + 22{,}858\left(\frac{1.35}{2}\right)^2\right)x_r = 0 \tag{4.18}$$

The natural frequency is

$$\omega_n = \sqrt{\frac{39{,}598}{190}} = 14.0\ rad/s = 2.22\ Hz \tag{4.19}$$

The remaining mode of significance to the vehicle dynamics is front-wheel hop. This can be approximated by inspection of the physical constants, a relatively large sprung mass of 890 kg is coupled to a relatively small unsprung mass, 73 kg by the suspension springs, each with stiffness equal to 18,700 N/m. The unsprung mass is coupled to the road via the tyre springs, each having stiffness equal to 184,000 N/m. Disregarding the sprung mass and suspension springs, consider the unsprung mass supported by the tyre springs

$$73\ddot{x}_h + 2(184{,}000)x_h = 0 \qquad (4.20)$$

This simplified model leads to a natural frequency estimate of 11.3 Hz. Note the difference between the heave frequency of the chassis and the wheel hop. The distance between these major modes in the suspension is maintained by automotive designers in order to preserve the ride and handling of the vehicle. Consider the sprung mass of the chassis, that is attached to the suspension springs, the natural frequency of this sub system approximates to

$$\omega_n = \sqrt{\frac{37{,}400}{890}} = 6.48\ rad/s = 1.03\ Hz \qquad (4.21)$$

The approximation may be improved by constraining the position of the sprung mass and including both sets of springs, associated with the sprung and unsprung masses:

$$73\ddot{x}_h + 2(184{,}000 + 18{,}700)x_h = 0 \qquad (4.22)$$

which leads to a natural frequency

$$\omega_n = \sqrt{\frac{405{,}400}{73}} = 74.5\ rad/s = 11.86\ Hz \qquad (4.23)$$

This simplified analysis depends upon the existence of distinct and identifiable modes of vibration in the system (Tongue 2002). This is invariably the case for any modern passenger vehicle, due to ride and handling considerations. A vehicle design that does not obey this principle would be unmarketable. However, the analysis relies upon idealised conditions and constraints, such as the pure heave mode, which will be unlikely to occur in real data sets, taken from candidate vehicles. The particular road surface may induce fractions of the various modes simultaneously, making identification problematic, particularly in the case of series production vehicles where sensors may be sparse and of relatively low quality.

4.6. Concluding remarks

This Chapter has considered the problems associated with modelling a vehicle suspension system for the purpose (in Chapter 5) of developing algorithms for detecting tyre pressure changes via model-based indirect approaches. The outcome is a base model which is considered to be sufficient for detecting pressure changes in tyres.

Chapter 5.

Condition monitoring and fault detection methods

5.1. Outline of the chapter

Section 5.2 of this chapter provides a description of a recursive least squares (RLS) parameter estimation scheme in discrete-time. Section 5.2.2 shows the corresponding scheme in continuous-time. Section 5.3 compares the two approaches and there is a discussion about the relative merits of the two approaches. Section 5.4 incorporates the concept of cautious least squares (CLS) into the RLS and Kalman estimators. Section 5.5 details an alternative approach to the unknown input problem by the application of an enhanced filter (EKF) which estimates states, including the input, of the vehicle-road system. Section 5.6 develops the continuous-time approach to include an unknown input observer (UIO), which attempts to solve the problem of the unknown road surface input and includes some change detection methods. Section 5.7 introduces a wheel angular velocity observer method from the first principles of CAN data acquisition and interpretation to key indicators of change detection in the variables.

5.1.1. Introduction

In this chapter the methods for detecting tyre pressure change are presented. The concept of inference based schemes is demonstrated to warrant further investigation by the results of chassis acceleration testing during driving, described in Chapter 0. The first step for development of an inference-based tyre pressure detection method could be to obtain a model of sufficient fidelity in order to describe the dynamics of the suspension and hence enable detection of changes that are occurring in the suspension components by comparison of the model states, parameter variations and other indicators, such as a phase portrait. Transfer function models of the suspension have been created for the purpose of change detection and this research has been presented in Chapter 0. In order that changes in the suspension may be detected it is necessary to obtain an estimate of the transfer function parameters and internal states, depending on the particular approach.

Sections 5.2-5.6 are concerned with parameter estimation schemes configured to detect changes in tyre stiffness. These approaches assume that the road profile is a known quantity (to varying degrees), which is technically possible (Rankin et al. 2009; Ray 2008; Manduchi et al. 2005) although not currently a realistic proposition for mass produced vehicles. However,

this is beginning to change, with the development of laser terrain estimation systems and stereo camera techniques, see (Oniga & Nedevschi 2010) for methods using stereo cameras and image processing techniques and (Yuan et al. 2008), utilising laser based implementations, commonly referred to as light detection and ranging (LIDAR) or laser detection and ranging (LADAR). Mercedes-Benz has deployed terrain estimation using stereo cameras and image recognition for an active suspension system (known as Magic Body Control) of the 2013 Mercedes-Benz S-Class (code name W222). In a promotional press release the road profile generation is described by (Daimler 2013): "The 'eyes' for the ROAD SURFACE SCAN function are provided by a stereo camera fitted behind the windscreen, which scans the road up to 15 m ahead of the vehicle and delivers a precise image of the road contours. Based on the camera pictures and driving status information, the control unit constantly calculates the best control strategy for overcoming unevenness such as prolonged bumps."

Anecdotal reports of the suspension performance suggest that the system is only effective in a limited set of driving scenarios, primarily low speed navigation of 'road hump' traffic calming features, and that the system has diminishing effectiveness in low-light conditions and on other types of road irregularities, such as pot holes or features that do not readily resolve into high contrast images. The evidence currently available suggests that terrain estimation, in the sense of practical automotive application, is in its infancy stage of development but remains an enticing possibility for model-based control and diagnostics.

5.1.2. Definitions and approaches to condition monitoring and fault detection

Condition monitoring has been defined as "a continuous real-time task of determining the conditions of a physical system by recording information, recognising and indicating anomalies in the behaviour" (Simani et al. 2003). A monitoring system, configured to detect faults and diagnose their nature, is called a fault diagnosis system. Its operation can be divided into three areas.

1. Detect that a fault has occurred (fault detection)
2. Locate the fault in the system (fault isolation)
3. Characterise the fault (fault identification) - estimation of the magnitude, type or nature of the fault

Correct and timely detection are indispensable properties. The location of the fault may also be an essential property, depending on the physical size and access to the system in question. It is common practice amongst maintenance technicians, in the pursuit of the location of a fault, to test areas of the system that are easily accessible first in order to glean some information. This approach is generally motivated by the time-consuming nature of diagnosing a complex and often physically inaccessible system. Depending on the nature of the system, the requirement for characterisation may or may not be necessary. Electrical faults commonly feature a binary magnitude i.e. they are either present or not (and may be intermittent). Mechanical faults are more likely to change in magnitude, as tolerance builds in coupled mechanisms, such a system deteriorates in a gradual way. Fault diagnosis is generally considered to be Fault Detection and Isolation (FDI). FDI approaches can be grouped in two sub-divisions: measurement-based and model-based.

5.1.3. Measurement-based approach

Conventional measurement-based (analytical or model-free) approaches to fault detection are abundant in practical applications. There are many examples of model-free diagnostics and the methods are well developed and robust. The main drawback of this class of fault detection approaches is the additional cost of additional hardware and the associated maintenance and space requirements (Isermann & Ballé, 1997; Isermann, 1997).

In the analytical redundancy scheme of Figure 5.1 Illustrates the concepts of hardware and analytical redundancy (Simani 2003), the resulting difference generated from the comparison

of different variables is called a residual or symptom signal. The residual should be zero when the system is in normal operation and non-zero when a fault has occurred. This property of the residual is used to determine whether or not faults have occurred (Chen & Patton, 1999)

This item has been removed due to 3rd Party Copyright.
The unabridged version of the thesis can be viewed in the
Lanchester Library Coventry University.

Figure 5.1 Illustrates the concepts of hardware and analytical redundancy (Simani 2003)

Threshold detection

A normal range of operation is defined either by the designer or via empirical testing and measurement. Measurements made during system operation can be compared against the normal range and an alarm or mitigation strategy is triggered. A major problem with this method is that in the presence of noise, disturbances or input variation, false alarms may be triggered (Chen & Patton, 1999).

Redundant sensors

Commonly used in the aviation industry, equipping aircraft with redundant sensors is an effective means of improving safety. This approach is particularly effective if the sensing techniques are divergent, such that effects due to prevailing conditions or common faults (due to mass production) are minimised. The avionics of most commercial aircraft now feature multi-redundant self-monitoring systems with segregation and purposeful dissimilarities between related / redundant software and hardware; these systems require complex redundancy negotiation and consensus voting strategies to operate (Eubank et al. 2010).

Spectral analysis

Analysis of the frequency spectrum is a widely used technique, with notable examples in the field of rotating machinery and bearings (Chen, Jinglong et al. 2012). Frequency domain methods are typically applied when the effects of faults as well as disturbances have frequency characteristics which differ from each other and thus the frequency spectra serve as criterion to distinguish the faults (Simani et al. 2003).

5.1.4. Model-based approach

In a model-based FDI scheme, some model of the system is used as a mechanism to compare the state of the system in question with a predicted state(s), derived from the model and the measured state(s). The difference between the measured and estimated state is defined the 'residual'. The appeal of this class of fault detection methods is the ability to predict failure before the event rather than merely reacting to a threshold transgression swiftly followed by a total failure. The model may also allow the monitoring of internal states that are impossible to actually measure. Another advantage of the model-based approach is that no additional hardware components are required in order to realise a FDI algorithm. A model-based FDI algorithm can be implemented via software on a process control computer. In many cases, the measurements necessary to control the process are also sufficient for the FDI algorithm so that no additional sensors have to be installed (Basseville & Nikiforov, 1993; Chen & Patton, 1999; Simani et al., 2003).

The system in Figure 5.2 is composed of actuators, plant and sensors. The alarm is triggered when a disparity is detected between the output state, $y(t)$, and the estimated output state ($\hat{y}(t)$).

This item has been removed due to 3rd Party Copyright. The unabridged version of the thesis can be viewed in the Lanchester Library Coventry University.

Figure 5.2 Fault Detection and Identification Methods based on Analytical Redundancy (Simani 2003)

Model-based FDI methods can be categorised in three top level groups:

- Output observers
    - State estimation
    - Filtering
- Parity equations
- Identification and parameter estimation

These types of approach have been extensively covered in the literature (Basseville & Nikiforov, 1993; Chen & Patton, 1999; Gertler & Singer, 1990; Simani et al., 2003).

Output observers generate residuals from time-invariant parametric models. Parity equations may employ time-invariant parametric or non-parametric models. Parameter estimation techniques generate the residual via adaptive non-parametric or parametric models.

An important consideration that should guide the selection of a particular approach is the likely type of fault that is to be diagnosed. Each method has a 'zone of operation' such that it is more or less suitable to a particular application. Consider the case where only the output, $y(t)$, of a system can be measured, this constrains the choice of fault detection scheme to frequency domain methods. This is typically seen in situations where an input is not necessarily under control of the system, as in the previous example by (Chen, Jinglong et al. 2012). Typical signal model-based methods of fault detection are:

- Band-pass filters
- Spectral analysis
- Maximum entropy spectral estimation

Faults are characterised by their distributions and analysis of the 'tails' or outliers, which usually also involves distinguishing normal faulty behaviour from noise. Analysis of the number of standard deviations from the mean and variance is commonly used (Hodge and Austin 2004). Deviation from normal behaviour must then be identified and classified.

5.1.5. Modelling issues in fault detection and isolation: uncertainty, disturbances and non-linearity

Since the premise of model-based FDI is the model itself, it is often incorrectly assumed that adequate knowledge of its properties exists, in order to proceed with the design of such a system. However, this is rarely the case. Fundamentally a mathematical model is a notional entity and there will likely always be some uncertainty in the model. This has been shown to be the case through the history of science. As an example of this, the theory upon which many models rely, is classical mechanics. Newton's theories stood from 1685 until the time of Einstein, when the theory was revised to include the phenomena of relativity. The eminent statistician, George Box, wrote "essentially, all models are wrong, but some are useful" (Box and Draper 1987).

The parameters of a model may vary as a function of time (time-varying model) or some other variable (state-dependent model) if these dependencies are not observable or are unpredictable (stochastic) there will be some disparity between the model states and the measured states of the system. Other sources of errors include additive disturbances to the system and noise, which may only be classified in terms of their probability. These uncertainties must be considered and accounted for ahead of any consideration for the faults themselves. Model-mismatches commonly manifest in the form of false positives if the decision threshold is close to the normal operational modes or the failure to detect a fault if the threshold is distant from the operational region (Chen & Patton, 1999). Sensitivity is a key area in FDI and it has been overcome by various techniques, including:

- Modelling and parameter estimation techniques that account and/or estimate noise, such as those devised by Box and Jenkins (Box et al. 2008)
- Simultaneous application of multiple FDI techniques to the same system, see (Isermann, 2006), amongst many others
- Unknown Input Observer (UIO)
- Parity relation
- Increasing the insensitivity to modelling uncertainty and the sensitivity to faults

The last point is often challenging to achieve in practice. Increasing fault sensitivity often leads to increased occurrence of false positives. It may be mitigated by careful examination of the fault definition and selecting the appropriate fault detection technique for the particular application (Gertler 1998).

5.2. Recursive least squares parameter estimation

In this section a method is developed for the estimation of the parameters of a discrete-time transfer function model of a quarter car suspension, introduced in Chapter 4. An objective for this work is an analysis of estimation under fault condition with respect to the sampling frequency. For this reason the majority of the estimation trials test the estimators ability to detect varying parameters rather than the fault-free condition. The discrete-time model has been selected primarily since observed data are always collected by sampling. This makes relating the observed data to the discrete-time models more straightforward. This is not such a significant concern in a simulation study as it is when the observed data is actually some real measurement taken during an experiment.

The estimation scheme for this task is recursive least squares (RLS) which is the online implementation of least squares. It is also possible to process the data *en bloc* by implementing a simpler least squares algorithm but since an attempt is being made to detect changes in the tyre as they happen, i.e. during the course of a drive cycle, RLS is more suitable. The estimate is continuously updated and can be filtered via a forgetting factor, which progressively diminishes the significance of older estimates and smooths the values, such that estimates that are corrupted by noise are not given undue significance.

RLS and least squares estimates in general are optimal in the sense that in a linear model where the errors have a mean of zero, are uncorrelated, and have equal variances, the best linear unbiased estimators of the coefficients is the least-squares estimators (Markov estimate). Despite the fact that real systems are rarely completely linear and measurement noise is rarely white, the least squares approach is a good starting point when estimating because it is a well understood method, extensively covered in the literature and a standard procedure for the analysis of data from the beginning of the 1800s (Golub and Van Loan 1996).

The discrete-time model is obtained from the continuous-time white box model derived in Chapter 4, via a Tustin transformation. The Tustin transformation is selected in order to preserve the dynamics at the frequencies of interest (~1Hz for chassis resonance and ~12Hz for wheel ‘hop’). Herein lies a fundamental constraint of the discrete-time approach – the system features two modes which are approximately ten times distant. Selecting a sampling interval for the transformation that is optimal for the chassis dynamics, it is sub-optimal for the wheel hop dynamics (sampling too slow). The situation is also problematic in reverse, Selecting the wheel hop frequency as the dynamics of interest. The phenomena reverses when selecting

a sampling interval for the estimation scheme (sampling too fast). This type of system is commonly referred to as 'stiff' in the literature (Young & Garnier, 2006) and is usually dealt with by compromising the dynamic description of both modes by selection of a sampling interval that occupies the middle ground between the two frequencies of interest.

The nominal suspension parameters are used to generate a transfer function in continuous-time from the model and this model is converted to its discrete-time equivalent via the Tustin transformation. This process is repeated for the suspension in its faulty state i.e. low tyre pressure

Faulty parameters are loaded and MATLAB computes two discrete transfer functions for the nominal and faulty states. The RLS algorithm is applied to the Box-Jenkins transfer function model

$$y(t_k) = \frac{B(z^{-1})}{A(z^{-1})}u(t_{k-1}) + \frac{D(z^{-1})}{C(z^{-1})}e(t_k) \qquad e(t_k) = N(0, \sigma^2) \tag{5.1}$$

where the white noise input $e(t_k)$ is independent and identically distributed with zero mean and value and variance σ^2. In this model, it is assumed that the data are sampled uniformly in time, at sampling interval of Δt units; $y(t_k)$ and $u(t_k)$ represent the sampled values of the output and input, respectively, at the time $t_k = k\Delta t$; δ is the number of sampling intervals in a pure time delay of $\delta\Delta$t time units affecting the input to the model; and z^{-1} is the backward shift operator, i.e. $z^{-r}y(t_k) = y(t_{k-r})$. This model can also be represented in the following decomposed form

$$y(t_k) = x(t_k) + \xi(t_k) \tag{5.2}$$

Here, the deterministic, noise-free output of the system, $x(t_k)$, is generated by the equation

$$x(t_k) = \frac{B(z^{-1})}{A(z^{-1})}u(t_{k-\delta}) \tag{5.3}$$

which is the transfer function part of the model, and the coloured noise $\xi(t_k)$, is generated by the equation

$$\xi(t_k) = \frac{D(z^{-1})}{C(z^{-1})}e(t_k) \tag{5.4}$$

which is the associated Auto Regressive Moving Average (ARMA) noise part of the model. In the equations (5.1) to (5.4), the polynomials are defined as

$$A(z^{-1}) = 1 + a_1 z^{-1} + \cdots + a_n z^{-n} \tag{5.5a}$$

$$B(z^{-1}) = b_0 + b_1 z^{-1} + \cdots + b_m z^{-m} \tag{5.5b}$$

$$C(z^{-1}) = 1 + c_1 z^{-1} + \cdots + c_p z^{-p} \tag{5.5c}$$

$$D(z^{-1}) = 1 + d_1 z^{-1} + \cdots + d_q z^{-q} \tag{5.5d}$$

(Young, P. C. 2004).

The system estimation equation is formulated as

$$y(t_k) = \phi^T(t_k)\theta + e(t_k) \tag{5.6a}$$

where

$$\phi^T(t_k) = [-y(t_{k-1}) \ldots - y(t_{k-n})\ u(t_{k-\delta}) \ldots u(t_{k-\delta-m})] \tag{5.6b}$$

$$\theta = [a_1 \ldots a_n\ b_0 \ldots b_m]^T \tag{5.6c}$$

The noise polynomial used is

$$\frac{1 + 0.5z^{-1}}{1 - 1.4z^{-1} + 0.7z^{-2}} \tag{5.7}$$

The simulations are run for 60,000 samples. At the theoretically ideal sampling rate of 126Hz this equates to a simulation run time of 8 minutes. As time progresses to sample 20,000 (approximately a quarter of the total time), θ starts to change from its nominal value to the system with a tyre fault. The change continues for 20,000 samples at which point the parameter vector θ settles to its new values and stays there for the remainder of the simulation. This behaviour is analogous to a vehicle with a slow puncture. The estimator and model feature a forgetting factor, denoted λ, and gain control over the additive noise, ξ, on $y(t_k)$. The forgetting factor allows the estimator to disregard past samples and is useful for a system that is changing, to prevent bias in the estimates of θ. The three variables are adjusted to obtain the most accurate estimates of θ. The memory length, denoted M, is approximated by

$$M = \frac{1}{1 - \lambda} \tag{5.8}$$

For a forgetting factor of $\lambda = 0.99$ the estimator makes use of approximately the last 100 samples.

The performance of the estimator is measured by taking the average of the θ estimates for the constant parameter regions i.e. before the fault begins and after it has finished and calculating the Euclidean norm (EN) between θ and its estimate, $\hat{\theta}$. Only the EN for the post fault is shown in Table 5.1 as this is the area of most interest.

The difference between the Euclidean norms of θ and $\hat{\theta}$ is given by

$$\|EN\| = \sqrt{\theta_1^2 + \cdots + \theta_n^2} - \sqrt{\hat{\theta}_1^2 + \cdots + \hat{\theta}_n^2} \qquad (5.9)$$

5.2.1. Estimation trials

Refer to Table 5.1 for the details of the simulation configurations. The initial trials tested the system without faults at the theoretically ideal sampling rate of 126Hz. The estimator makes very accurate predictions of θ as shown in Figure5.3 and the system is stable. A property of estimators generally is that a little noise is beneficial, especially in cases where there is low activity on the input(s). The configuration of the estimator that is depicted in Figure 5.5 produced an EN of 1.6117 and if the ARMA noise is added, the EN is reduced to 0.7552 (see Table 5.1 for details).

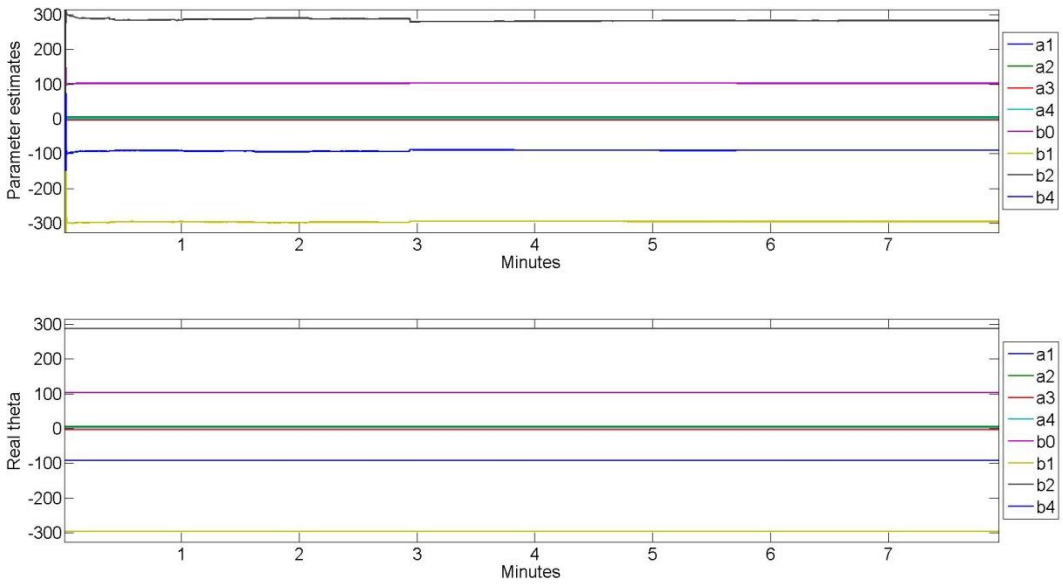

Figure 5.3 Upper plot, simulation configuration 2, parameter estimates for the nominal system (no faults) due to white noise input, SF=126Hz, λ=1, ξ=0, x axis samples 1 – 60,000 (8 minutes). Lower plot, actual θ values

The remainder of the tests were conducted with the gradual tyre deflation fault (reduction in the parameter k_t from 200,000 to 100,000) occurring in the system for various controlled sampling frequencies (SF), additive noise levels ξ, and forgetting factors λ. The fault should be identifiable as the estimator tracks the new values of θ. The true value of θ can be seen in the lower portion of all the plots for comparison.

Figures 5.4 and 5.5 demonstrate the effect of the forgetting factor. The estimates converge at a much faster rate (resulting in a smaller EN) with a forgetting of 0.99 than they do with no forgetting but the variance in the estimates is more pronounced for smaller values of λ. The system can operate at very low sampling frequencies; estimates were obtained for a rate of 5Hz but only with zero additive noise. Additive noise at extremely low sampling frequencies generally caused instability in the system and no estimates could sensibly be made. It was possible to sample at high frequencies, the highest of 450Hz resulting in a stable system. The ultimate limit of estimation stability depended on the forgetting factor and the noise level; if the noise was removed the system became unstable beyond 400Hz. The noise level also had a positive effect on the rate of convergence at the very high frequencies. A small amount of noise generally proved to be beneficial for the estimates in most cases. Removal of the forgetting factor causes degradation in the estimates, although it is impossible to test the asymptotic case, it is unlikely $\hat{\theta}$ would converge to θ.

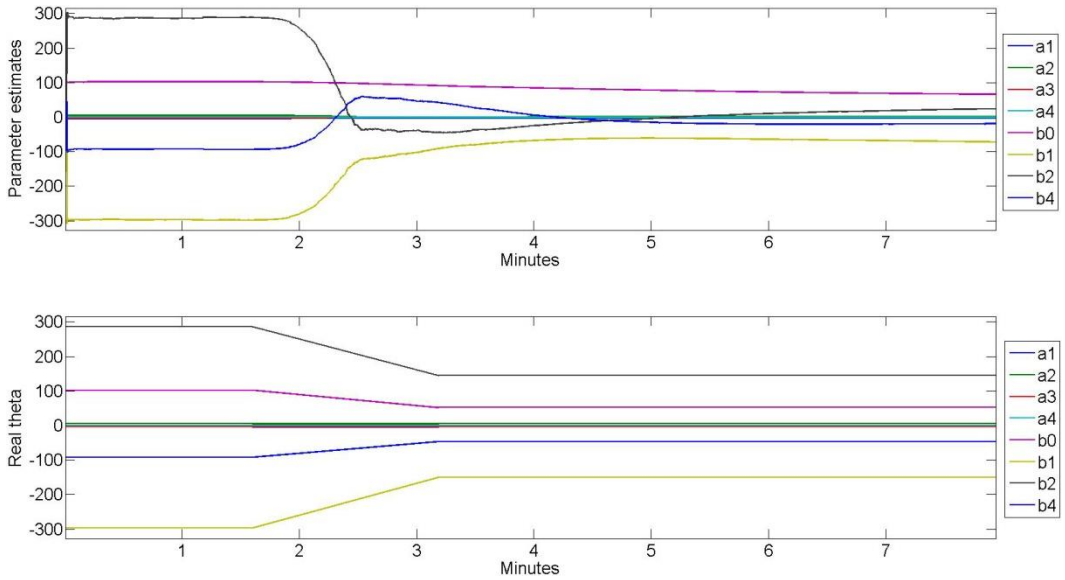

Figure 5.4 Upper plot, simulation configuration 3, parameter estimates for the faulty system with SF=126, λ=1, ξ=0.0025, Lower plot, actual θ values

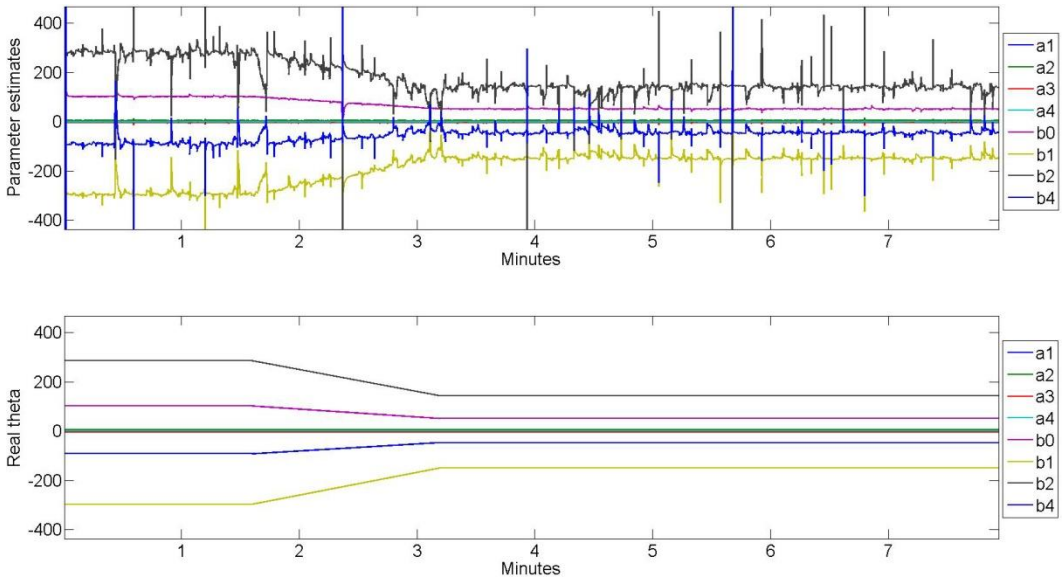

Figure 5.5 Upper plot, simulation configuration 12, parameter estimates for the faulty system with SF=126, λ=0.99, ξ=0.0025, Lower plot, actual θ values

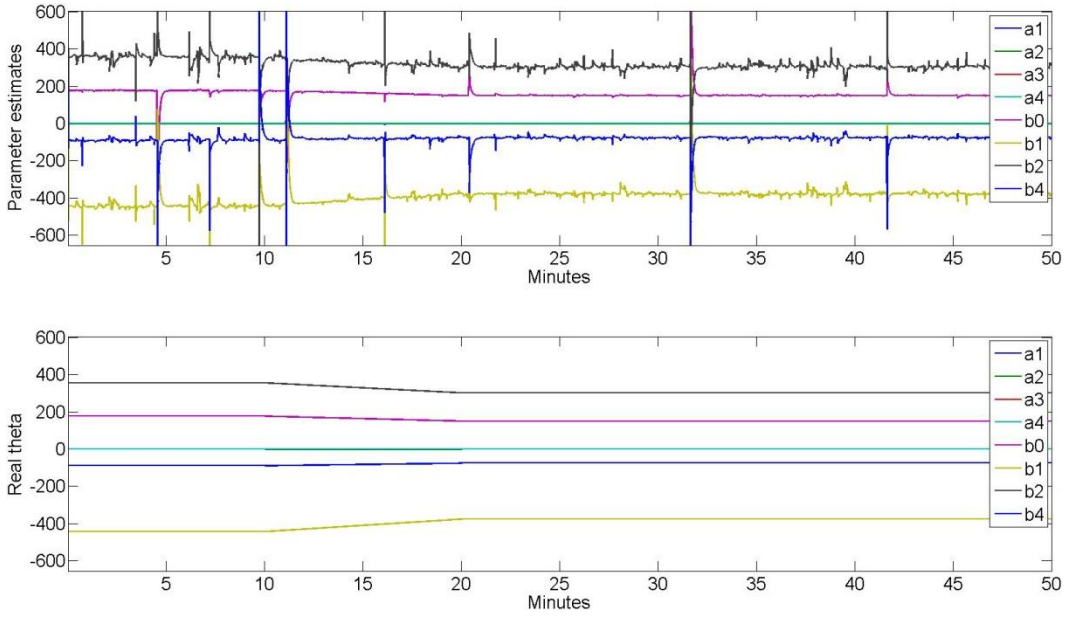

Figure 5.6 Upper plot, simulation configuration 6, parameter estimates for the faulty system with SF=20, λ=0.99, ξ=0.0025, Lower plot, actual θ values

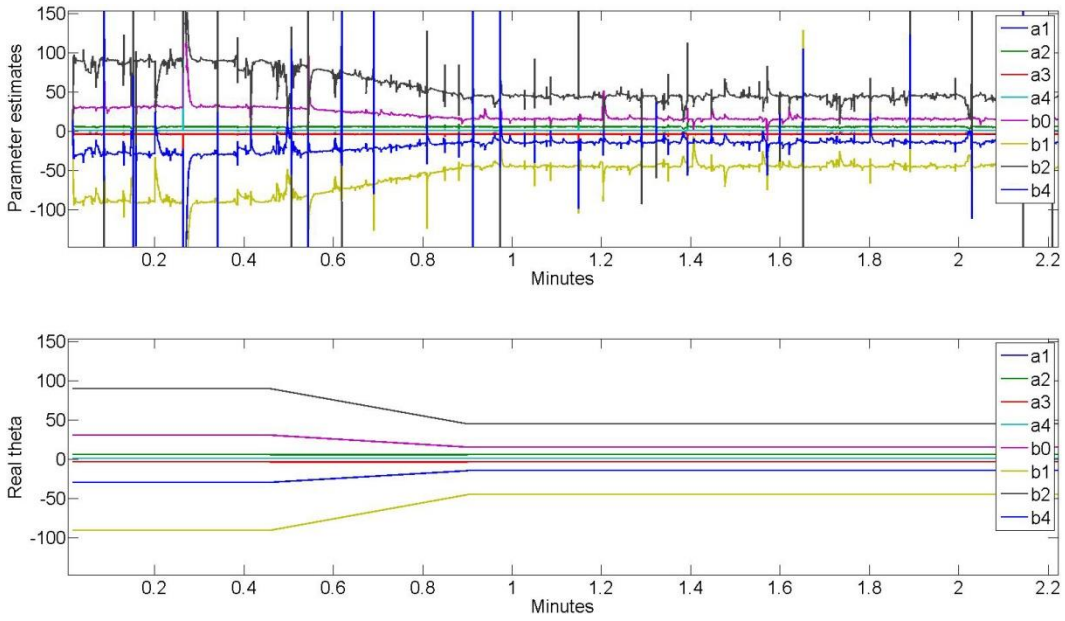

Figure 5.7 Upper plot, simulation configuration 16, parameter estimates for the faulty system with SF=450, λ=0.99, ξ=0.0025, Lower plot, actual θ values

Simulation property	Simulation configuration number							
	1	2	3	4	5	6	7	8
Sampling Frequency SF (Hz)	126	126	126	5	10	20	50	60
Noise gain ξ	0.0025	0	0.0025	0.0025	0.0025	0.0025	0.0025	0.0025
Forgetting λ	1	1	1	0.99	0.99	0.99	0.99	0.99
Simulation time (seconds)	476.191	476.191	476.191	12000	6000	3000	1200	1000
Euclidean norm *EN* (θ)	0.7552	1.6117	16.5919	9.4895	7.9388	1.7536	6.0749	11.9733
Fault type	No fault	No fault	Tyre deflated	Tyre deflated	Tyre deflated	Tyre deflated	Tyre deflated	Tyre deflated

Simulation property	Simulation configuration number							
	9	10	11	12	13	14	15	16
Sampling Frequency SF (Hz)	70	80	110	126	140	190	350	450
Noise gain ξ	0.0025	0.0025	0.0025	0.0025	0.0025	0.0025	0.0025	0.0025
Forgetting λ	0.99	0.99	0.99	0.99	0.99	0.99	0.99	0.99
Simulation time (seconds)	857.14	750	545.455	476.191	428.571	315.79	171.429	133.333
Euclidean norm *EN* (θ)	8.843	6.7706	9.0938	5.0005	4.1611	12.4373	3.5149	92.235
Fault type	Tyre deflated	Tyre deflated	Tyre deflated	Tyre deflated	Tyre deflated	Tyre deflated	Tyre deflated	Tyre deflated

Table 5.1 Estimation results for the discrete time system

Table 5.1 shows the effect of sampling interval and reinforces the notion put forward in Section 4.4.3 that sampling interval for discrete time estimation of vehicle suspension is a compromise between the wheel hop frequency and chassis frequency (see Section 4.5) of ~12Hz and ~1Hz, respectively. 450Hz sampling frequency produces particularly poor estimates, (sampling too fast for either mode) while 350Hz and 140Hz are substantially more accurate. This can be attributed to good estimates of the wheel hop. At the other end of the spectrum, a sampling frequency of 20Hz is likely capturing the dynamics of the chassis. This may not be the case for every type of input signal i.e. road surface. In the case of high excitation (e.g. rough roads), there may be too great a difference between the samples and degradation in the estimates may occur at low sampling frequencies. The variance in the estimates, which manifest as spikes in Figure 5.7, for example, can be attributed to the additive ARMA noise. This type of variance in the estimate becomes more pronounced as the noise amplitude increases and the forgetting factor decreases.

5.2.2. Estimating the continuous-time transfer function

In many ways, estimating a continuous model is a more direct approach to the problem of fault detection. The parameters of the transfer function are estimated directly and there is no conversion process, with no additional parameters to estimate as in the discrete method i.e. numerator terms. The sampling interval is no longer an issue; the system can be sampled as fast as the user desires i.e. fast enough to capture all the modes of the system; with no problems of instability or sensitivity. This part of the work differs from the discrete time model in that the continuous time model was built in Simulink although the estimation algorithm was executed in MATLAB script language.

This continuous time estimation scheme is based on the work of Young (1981). Although Young used instrumental variable techniques his method is equally applicable with RLS.

The RLS algorithm estimates a continuous time differential equation model based on discrete time sampled data measurements of the input and output variables

$$\frac{d^n x(t)}{dt^n} + \alpha_1 \frac{d^{n-1} x(t)}{dt^{n-1}} + \cdots + \alpha_n x(t) = \beta_0 \frac{d^m u(t-\tau)}{dt^m} + \cdots + \beta_m u(t-\tau) \qquad (5.10)$$

Here the pure time delay τ is assumed to be an integer number related to the sampling interval as in the discrete time case: i.e. $\tau=\delta\Delta t$ but this is not essential; in this continuous time

environment, fractional time delays can be introduced if required (Young & Garnier, 2006). In transfer function terms, the above differential equation takes the form

$$x(t) = \frac{B(s)}{A(s)}u(t-\tau) \tag{5.11}$$

with

$$B(s) = \beta_0 s^m + \beta_1 s^{m-1} + \cdots + \beta_m \tag{5.12}$$

$$A(s) = s^n + \alpha_1 s^{n-1} + \cdots + \alpha_n \tag{5.13}$$

where *s* is the differential operator. It is assumed that the input signal $\{u(t), t_1 < t < t_N\}$ is applied to the system and that this input and the output $x(t)$ are sampled at discrete times $t_1, \ldots, t_N$, not necessarily uniformly spaced.

In the case of uniformly sampled data (as in the vehicle suspension simulation) at a sampling interval Δt, the measured output $y(t_k)$, where $t_k = k\Delta t$, it is assumed to be corrupted by an additive measurement noise $\xi(t_k)$ (see Figure 5.1)

$$y(t_k) = x(t_k) + \xi(t_k) \tag{5.14}$$

where $x(t_k)$ is the deterministic, noise free output of the system and, as in the discrete time case, $\xi(t_k)$ is modelled as a discrete time ARMA process

$$\xi(t_k) = \frac{D(z^{-1})}{C(z^{-1})}e(t_k) \qquad e(t_k) = N(0, \sigma^2) \tag{5.15}$$

The estimation problem is to estimate the parameters of the continuous time transfer function model (5.11) from N sampled measurements of the input and output $Z^{\mathrm{N}} = \{u(t_k); y(t_k)\}_{k-1}^{N}$. The transfer function system estimation model at the k^{th} sampling instant is written in the following pseudo linear regression form

$$y_f^{(n)}(t_k) = \phi_f^T(t_k)\theta_c + e(t_k) \tag{5.16}$$

$$\phi_f^T(t_k) = \left[-y_f^{(n-1)}(t_k) \ldots - y_f^{(0)}(t_k)\ \ u_f^{(m)}(t_k - \tau) \ldots u_f^{(0)}(t_k - \tau)\right] \tag{5.17}$$

$$\theta_c = [\alpha_1 \ldots \alpha_n\ \beta_0 \ldots \beta_m]^T \tag{5.18}$$

where now the subscript f denotes hybrid filtering which involves a combination of continuous and discrete time filters. First the pre-filtered derivatives are obtained as the inputs to the integrators in the continuous time implementation of the initial pre-filter $1/A\,(s)$, as shown in Figure 5.8. These pre-filtered derivatives are then sampled at the sampling interval Δt. The pre-filters are loaded with the coefficients of the model polynomial (5.15). In the case of a practical implementation these parameters would be iteratively updated with the estimates of the model polynomial, $\hat{\theta}_c$ (Young & Garnier, 2006)

5.2.3. Estimation trials

Refer to Table 5.2 for the details of the simulation configurations.

The initial trials of the continuous time estimator were conducted using a simple transfer function block representing the suspension system (Figure 5.8) with no method of inducing faults and no additive noise so that potential causes of problems could be isolated during development of the scheme.

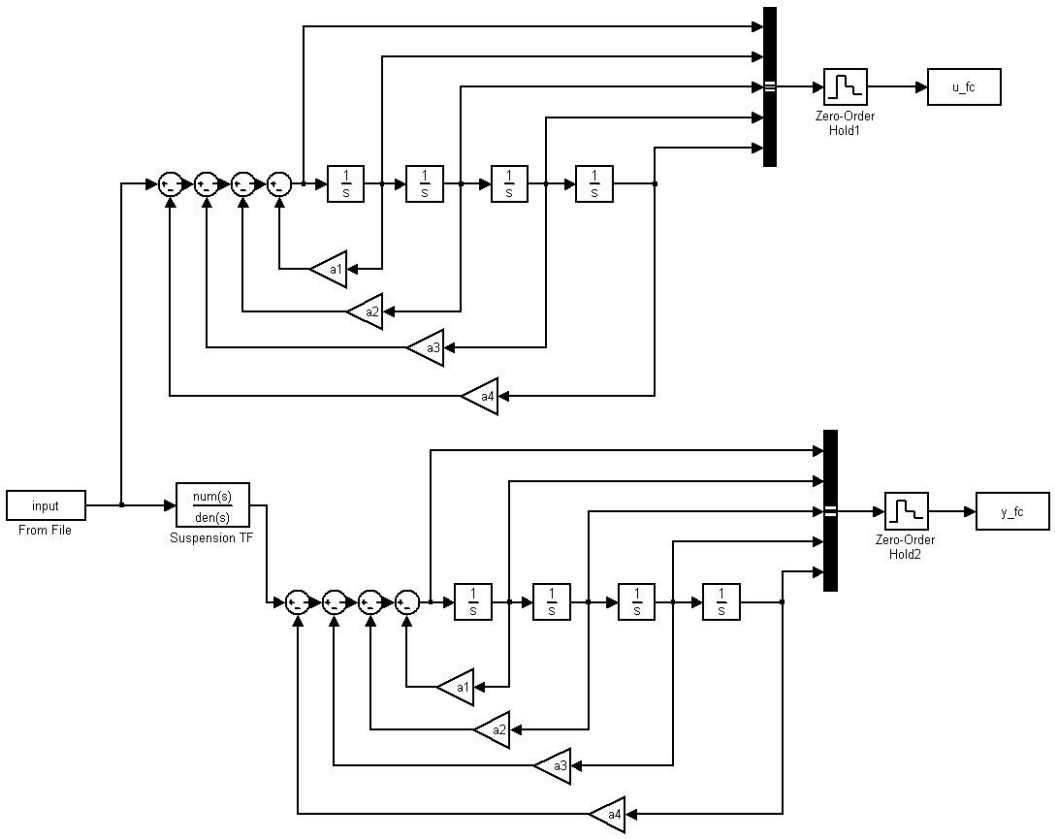

Figure 5.8 CT transfer function model and pre-filters

The input (road surface) to the system comes from a workspace vector populated with zero mean unity variance random numbers, on the left hand side of Figure 5.8. The input derivatives, u_{fc}, are filtered, sampled and stored as a matrix in the workspace. The suspension acts as a filter, attenuating the input (as would happen in a real vehicle suspension) and the output of the transfer function is chassis acceleration. This acceleration is filtered for the derivatives, y_{fc}, which are sampled and stored as a matrix in the workspace. The input and output measurements are computed by the RLS algorithm and an estimate of θ_c can be made.

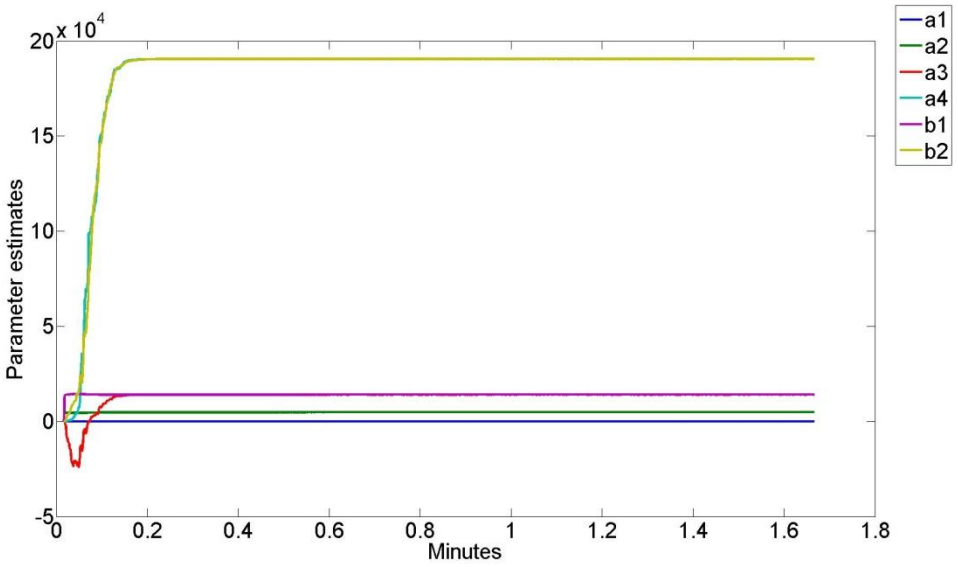

Figure 5.9 Estimates of θ for the noise free case

Once the process was demonstrated to be working and repeatable, the results of this exercise can be seen in Figure 5.9, the state space second companion form transfer function was introduced with the ARMA additive noise blocks.

In the same way as the discrete time case, the estimator and model feature sampling frequency control, a forgetting factor λ, and gain control over the additive noise on $y(t_k)$. The forgetting factor allows the estimator to disregard past samples and is useful for a system that is changing, to prevent bias in the estimates of θ. The three variables are adjusted to obtain the most accurate estimates of θ.

A noticeable difference between discrete time (DT) estimation and continuous time (CT) estimation is their noise tolerance. The CT estimator is more sensitive to noise, at a sampling rate of 30Hz with a high level of noise i.e. gain factor of unity, the EN for the two estimators was found to be:

CT estimator Euclidean norm 7268.3
DT estimator Euclidean norm 1.2

However, at more realistic levels of noise the estimators are very similar in their performance.

5.2.4. Introducing faults into the model

Introducing the tyre pressure fault cannot be done in exactly the same way as the DT model because of the block diagram form of the CT model. The transfer functions are calculated for both vehicle states i.e. nominal and half tyre stiffness. Half tyre stiffness is an arbitrary quantity selected for the sake of convenience. The relationship between tyre stiffness and inflation pressure is variable depending on the particular tyre and conditions. However, the majority of authors in the field (Taylor et al. 2000, Schmeitz et al. 2005, Pillai 2006, Parczewski 2013, Smith, N. D. 2004) state that there is usually an approximately linear proportional relationship between these variables. The coefficients of the two polynomials are loaded into a MATLAB script which gives the θ values of the model for the simulation to start and end the fault at. The task of creating a fault insertion scheme is executed with the use of ramp and saturation blocks to gradually move the parameters from the nominal condition to the faulty one and then hold them at the faulty level. Details of this are shown in Figure 5.10. Note that the value for α_1 does not change for the faulty condition of deflated tyre.

As time progresses to a predetermined sample (approximately a quarter of the way in), θ starts to change from its nominal value to the system with a tyre fault. The change continues for two thirds of the simulation time at which point the parameter vector θ settles to its new value and remains constant for the remainder of the simulation. This behaviour is analogous to a vehicle with a slow puncture. In the same way as the discrete-time case, the performance of the estimator is measured by taking the average of the θ estimates for the stable regions i.e. before the fault (or after the initial estimates are made, in the fault free case) begins and after it has finished, then calculating the Euclidean norm between θ and its estimate $\hat{\theta}$ for the two periods, pre and post fault. Only the EN for the last part of the simulation is shown in Table 5.2.

The results of simulation configuration 9 are shown in Figure 5.11. The estimator accurately tracks the change in θ and converges to the true value as the fault stabilises, with a final EN value of the averaged $\hat{\theta}$ of 12.94. Contrast this with the estimates of the discrete system of Figure 5.4, the DT estimates have much more variance, although the EN value is smaller for the DT system.

An interesting property of the CT estimator is that it performs better with very low λ, 10 samples were enough for the estimator to make a good estimate, except at very low SF, as can be seen in Table 5.2, simulations 5 & 6. The extremely low SF causes very large differences between the samples and degradation of the estimates, a situation that is improved by increasing λ. In contrast, the DT estimator is more accurate with λ =0.99 for all SF.

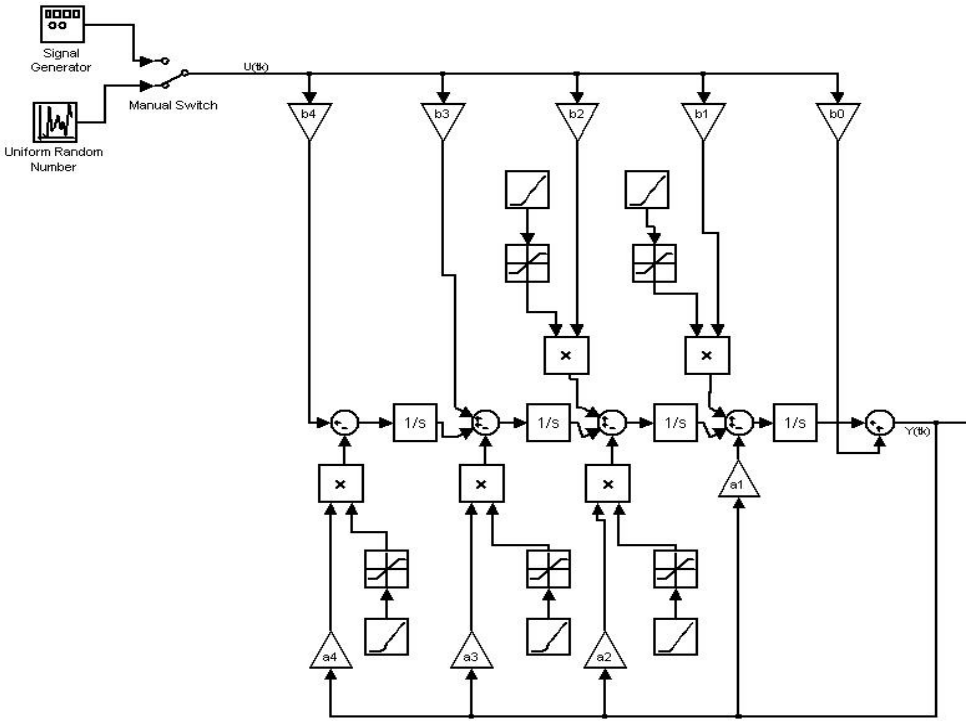

Figure 5.10 Truncated simulation showing suspension model in second companion form with blocks for fault insertion (filters are omitted). Note a variable exists for each parameter of the TF.

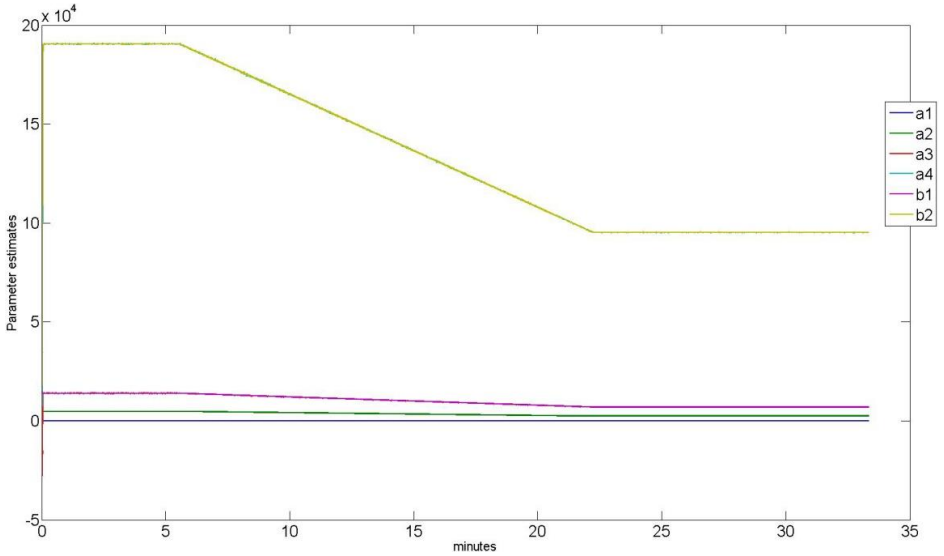

Figure 5.11 Estimates of the suspension system with a gradual decline in tyre stiffness (slow puncture)

Simulation property	Simulation Configuration Number							
	1	2	3	4	5	6	7	8
SF (Hz)	100	126	126	126	2	2	10	20
Noise ξ	0.0025	0	0	0.0025	0.0025	0.0025	0.0025	0.0025
FF λ	0.99	1	0.99	0.9	0.99	0.9	0.9	0.9
Time (s)	600	476	476	476	30000	30000	6000	3000
EN (θ)	54.033	20478	26.668	23.69	15.319	27.167	13.436	13.627
Fault type	No fault	No fault	No fault	No fault	Tyre deflated	Tyre deflated	Tyre deflated	Tyre deflated

Simulation property	Simulation Configuration Number							
	9	10	11	12	13	14	15	16
SF (Hz)	30	30	30	70	126	126	100	200
Noise ξ	0.0025	0.0025	0.0025	0.0025	0.0025	0.0025	0.0025	0.0025
FF λ	0.9	0.95	0.99	0.9	0.99	0.9	0.9	0.99
Time (s)	2000	2000	2000	857	476	476	600	300
EN (θ)	12.94	13.3	16.62	13.949	15.623	22.517	14.659	21.914
Fault type	Tyre deflated	Tyre deflated	Tyre deflated	Tyre deflated	Tyre deflated	Tyre deflated	Tyre deflated	Tyre deflated

Simulation property	Simulation Configuration Number					
	17	18	19	20	21	22
SF (Hz)	200	400	1000	3000	4500	6000
Noise ξ	0.0025	0.0025	0.0025	0.0025	0.0025	0.0025
FF λ	0.9	0.99	0.99	0.99	0.99	0.99
Time (s)	300	150	60	20	13	10
EN (θ)	25.223	37.591	172.08	213.13	615.87	1060.7
Fault type	Tyre deflated	Tyre deflated	Tyre deflated	Tyre deflated	Tyre deflated	Tyre deflated

Table 5.2 Estimation results for the CT system

Table 5.2 shows that the CT model is significantly less sensitive to the choice of sampling interval compared with the DT model. Satisfactory estimation can be achieved with sampling rate ranging from 10Hz to 400Hz, beyond which the estimates begin to degrade due to insufficient difference between successive samples. The tracking abilities of the estimators have demonstrated their appropriateness as fault detection mechanisms with the simple quarter car suspension model.

5.3. Comparison of continuous-time and discrete-time vehicle models as candidates for suspension system fault detection

This section explores the potential advantages and limitations offered by discrete-time and continuous-time model-based fault detection schemes for vehicle suspension systems (Ersanilli et al. 2008). The same suspension model of a quarter car is used from Section 5.2 to obtain transfer function models. The coefficients of the transfer function are estimated in discrete-time and continuous-time using a standard recursive least squares scheme, which provides the basis of the fault detection mechanism. The results of simulation studies indicate that continuous-time model based estimation offers benefits over discrete-time methods for fault detection in vehicle suspension systems.

5.3.1. Introduction

Model-based fault detection schemes in discrete-time (DT) and continuous-time (CT) in the context of the vehicle suspension are investigated. The choice of sampling interval is crucial when estimating DT vehicle suspension models due to the proximity of the fastest and slowest dynamic modes in the system, i.e. wheel hop and chassis displacement, respectively. When estimating DT models, a compromised sampling interval is chosen, which results from an attempt to capture both dynamic modes. Such a compromise does not arise when estimating CT models.

Fault detection in suspension systems via DT methods has been investigated by Walker (1991). It was reported that under certain conditions it was not always possible to isolate particular faults. In an attempt to increase the sensitivity whilst reducing the number of false alarms a combination of recursive least squares (RLS) and cautious least squares (CLS) was proposed (Burnham, Keith. J. 1991). Studies by Friedrich (2006) have shown that it is theoretically possible to isolate faults using CT model approaches with a state variable filter and RLS for parameter estimation.

5.3.2. Vehicle suspension model

Recall from Chapter 0, Figure 4.2 represents the quarter car vehicle suspension model. This section refers back to Figure 4.2 but for clarity and ease of reading the equations are repeated here. The vehicle data is also the same as for Chapter 0. Recall that the quarter car consists of the chassis (sprung mass, m_s), wheel assembly (un-sprung mass, m_{us}), suspension spring k_s, suspension damper B_s and tyre spring k_t is being considered, the latter replicating the effects

of tyre pressure. The input stimulus to the system is essentially a displacement, denoted x_{r}, from the road surface. Using Newton's law of motion the system may be expressed as

$$m_s\ddot{x}_s + B_s(\dot{x}_s - \dot{x}_{us}) + k_s(x_s - x_{us}) = 0 \tag{5.19}$$

$$m_{us}\ddot{x}_{us} + k_t(x_{us} - x_r) - B_s(\dot{x}_s - \dot{x}_{us}) - k_s(x_s - x_{us}) = 0 \tag{5.20}$$

where $x_s$and x_{us} denote the displacement of sprung and un-sprung mass, respectively ($\dot{x}$ and $\ddot{x}$ denote the velocity and acceleration in both cases). A convenient state space representation given by

$$\dot{\mathbf{x}} = \mathbf{A}\mathbf{x} + \mathbf{b}u \quad \text{and} \quad y = \mathbf{C}\mathbf{x} \tag{5.21}$$

with state vector

$$x = [x_s \;\; \dot{x}_s \;\; x_{us} \;\; \dot{x}_{us}] \tag{5.22}$$

leads to

$$\dot{x}_1 = x_2 \tag{5.23a}$$

$$\dot{x}_2 = -\frac{1}{m_s}[B_s(x_2 - x_4) + k_s(x_1 - x_3)] \tag{5.23b}$$

$$\dot{x}_3 = x_4 \tag{5.23c}$$

$$\dot{x}_4 = \tfrac{1}{m_s}[B_s(x_2 - x_4) + k_s(x_1 - x_3) - k_t(x_3 - u)]. \tag{5.23d}$$

Having defined the state vector, the representation takes the following state space vector-matrix form

$$\dot{\boldsymbol{x}} = \begin{bmatrix} 0 & 1 & 0 & 0 \\ \frac{-k_S}{m_S} & \frac{-k_S}{m_S} & \frac{k_S}{m_S} & \frac{k_S}{m_S} \\ 0 & 0 & 0 & 1 \\ \frac{k_S}{m_{us}} & \frac{B_S}{m_{us}} & \frac{-k_t-k_S}{m_{us}} & \frac{-B_S}{m_{us}} \end{bmatrix} \boldsymbol{x} + \begin{bmatrix} 0 \\ 0 \\ 0 \\ \frac{k_t}{m_{us}} \end{bmatrix} u(\mathrm{t}) \tag{5.24a}$$

$$\boldsymbol{y} = \begin{bmatrix} 1 & 0 & -1 & 0 \\ \frac{-k_S}{m_S} & \frac{-B_S}{m_S} & \frac{k_S}{m_S} & \frac{B_S}{m_S} \end{bmatrix} \boldsymbol{x} \qquad ; u = x_{\mathrm{r}} \tag{5.24b}$$

The output corresponding to the first row represents the suspension deflection, which is the difference between x_s and x_{us} and the output corresponding to the second row represents chassis acceleration $\ddot{x}_s$. Values of the vehicle suspension components were given earlier in Table 4.1.

The vertical acceleration $\ddot{x}_s$ of the chassis is the main output of interest for this system. This is the variable measured on the vehicle. In terms of the model this quantity is given by (5.23b). The secondary output of interest corresponding to the fast mode is that of the un-sprung mass, comprising the wheel, tyre, brake and axle assembly, given by (5.23d). Other measured outputs will not be considered here with the exception of suspension deflection as this has an impact on the sampling frequency used in the DT models and, to a lesser extent, in CT models. The outputs of the system can be expressed in terms of their transfer functions by applying

$$G(s) = c^T(sI - A)B \tag{5.25}$$

where c^T is a particular row of the output matrix C.

For the un-sprung mass this leads to an acceleration transfer function given by

$$\frac{-2222s^2}{s^4 + 27.59s^3 + 2598.4s^2 + 6984s + 95238}. \tag{5.26}$$

Similarly, for the chassis this leads to an acceleration transfer function given by

$$\frac{6984s^3 + 95238s^2}{s^4 + 27.59s^3 + 2598.4s^2 + 6984s + 95238}. \tag{5.27}$$

The poles of these transfer functions are identical and are given by two pairs of complex poles, namely

$$p_{1,2} = -12.59 \pm 48.39i \qquad p_{2,3} = -1.21 \pm 6.05i. \tag{5.28}$$

Taking the reciprocal of the real part indicates that the time constant of the fastest mode (associated with the wheel dynamics) is 80.5 ms and the slowest (associated with the chassis) is 0.725 s. These represent typical results for a vehicle suspension configuration, such as Figure 4.2. The ratio of the two dynamic modes is typically of the order 10:1 for the un-sprung and sprung mass respectively (see, for example Gillespie 1992).

5.3.2.1. Sampling interval

Measurements of the chassis acceleration are sampled at an interval T_s. This interval must be selected carefully to capture the dynamics of the dominant modes in the system. Ideally the sampling interval should be one tenth of the time constant of the fastest mode of the system (Franklin et al. 1997) to capture the dynamics of the system. This leads to a sampling interval T_s of 8.05 ms and a theoretically ideal sampling frequency of 124 Hz. However, this sampling interval is far too short for the low frequency mode (in a DT system). Indeed, herein lies the problem since a lower frequency will be too slow for the fast mode.

5.3.2.2. Modelling approaches and issues

When obtaining a DT transfer function from a frequency domain model, a conversion takes place. The transfer function is converted with a sampling interval factored into the resulting expression and usually results in a transfer function with one additional zero. The coefficients of the DT transfer function are not only dependent on the sampling interval but are usually functions of more than one CT model coefficient. Consequently, the individual DT coefficients no longer relate to meaningful individual physical quantities of the dynamic system. Local changes to a particular parameter that occur in the CT case may be distributed amongst the parameters of the DT model. This leads to a level of abstraction that is not beneficial for the purposes of fault detection and isolation. For instance, ideally, a change in tyre pressure affects a certain parameter or set of parameters in the CT model. If this change is then spread across all the parameters of a DT model, it may become problematic to differentiate tyre stiffness changes from other changes in the suspension system. Modelling in CT requires no conversion of the transfer function, the parameters are estimated directly and in the event of a vehicle fault, the link to the change in the actual vehicle sub-systems via physical laws is more direct. For most physical systems it is easier to construct models with physical insight in CT than in DT, simply because most laws of physics (Newton's law of motion, relationships in electrical circuits, etc.) are expressed in CT. Furthermore, estimating a CT model is less dependent on the sampling interval. The sampling interval is simply selected to capture the fastest mode of interest in the system, or whatever the data acquisition hardware is capable of obtaining.

5.3.3. Parameter estimation

RLS is the method used here to estimate the coefficients of the transfer functions of both DT and CT suspension models. RLS is a straightforward online estimation algorithm, yet it is optimal in the mean square error (MSE) sense when the assumptions on linearity of the model

and Gaussian properties of the measurement noise hold. ARMA additive noise has been adopted for the noise models.

5.3.3.1. The discrete-time system model

The RLS algorithm is applied to the Box-Jenkins transfer function model (5.1) with ARMA noise model (5.7) of Section 5.2 (Young, P. C. 2004).

5.3.3.2. Replicating faults in the DT system model

There are many ways in which a suspension may degrade but only tyre faults are considered here. In particular, a slow deflation which results in a gradual reduction in tyre stiffness of some 50% is considered. This fault scenario is replicated by creating a matrix of theoretical values of DT model parameters starting at sample S_1 with the nominal (no fault) values for the parameters, denoted θ_{nf}.The parameters are linearly, incrementally changed from the sample where the fault starts, denoted S_{fs} up to the sample when the fault ends, denoted S_{fe} with the faulty values of the faulty parameter vector, denoted θ_f. From the sample S_{fe} to the end of the simulation, S_e, the values remain fixed at θ_f.

5.3.3.3. Converting the CT transfer function to DT

The CT transfer function corresponding to chassis acceleration is converted to its DT counterpart using the matched pole-zero method (Franklin 1990) as an alternative approach to the Tustin transformation of Chapter 4. The transformation renders a transfer function for the fault free system

$$\frac{103.9z^3 - 300.9z^2 + 290z - 93.08}{z^4 - 3.523z^3 + 4.584z^2 - 3.131z + 0.801} \qquad (5.37)$$

for a sampling interval T_s of 8.05 ms. With the tyre spring rate set to half of the nominal value, use of the matched pole-zero procedure leads to the DT transfer function

$$\frac{52.58z^3 - 152.3z^2 + 146.8z - 47.1}{z^4 - 3.649z^3 + 5.103z^2 - 3.254z + 0.801} \qquad (5.38)$$

from which it is clear that all the model parameters change with the exception of α_1. Note that whilst a range of different sampling frequencies have been considered in this work, only the transfer functions for the theoretical ideal sampling frequency of 124 Hz (corresponding to T_s of 8.05 ms) are presented here.

5.3.3.4. The continuous-time system model

The RLS algorithm is used to estimate the coefficients of a CT differential equation model based on sampled data measurements of the input and output variables obtained in DT. Consider the linear differential equation representation

$$\frac{d^n x(t)}{dt^n} + \alpha_1 \frac{d^{n-1} x(t)}{dt^{n-1}} + \cdots + \alpha_n x(t)$$

$$= \beta_0 \frac{d^m u(t)}{dt^m} + \cdots + \beta_m u(t). \qquad (5.39)$$

Taking Laplace transforms, and assuming zero initial conditions, the transfer function corresponding to the above differential equation takes the form

$$X(s) = \frac{B(s)}{A(s)} U(s) \qquad (5.40)$$

where $X(s)$ and $U(s)$ denote the Laplace transforms of the noise free system output $x(t)$ and the available noise free input $u(t)$, respectively. The transfer function numerator and denominator polynomials are given by

$$B(s) = \beta_0 s^m + \beta_1 s^{m-1} + \cdots + \beta_m \qquad (5.41a)$$

$$A(s) = s^n + \alpha_1 s^{n-1} + \cdots + \alpha_n \qquad (5.41b)$$

where *s* is the Laplace operator. The CT system model input and noise free output $u(t)$ and $x(t)$, respectively, are sampled at discrete intervals $t_1, \ldots, t_N$.

In the case of uniformly sampled data (as in the vehicle suspension simulation) at each sampling interval Δt, where $t_k = k\Delta t$, the measured output is assumed to be corrupted by an additive measurement noise $\xi(t_k)$, i.e.

$$y(t_k) = x(t_k) + \xi(t_k) \qquad (5.42)$$

where $x(t_k)$ is the sampled CT deterministic, noise free output of the CT system and, as in the DT case, $\xi(t_k)$ is modelled as a DT ARMA process

$$\xi(t_k) = \frac{D(z^{-1})}{C(z^{-1})} e(t_k) \qquad e(t_k) = N(0, \sigma^2) \qquad (5.43)$$

The problem is to estimate the parameters of the CT differential equation (or transfer function) model from *N* sampled data pairs comprising the available noise free input and noise corrupted output, denoted $Z^N = \{u(t_k); y(t_k)\}_{k-1}^N$. The system estimation equation at the k^{th} sampling instant is expressed in the following pseudo linear regression form

$$y_f^{(n)}(t_k) = \phi_f^T(t_k)\theta_c + \xi(t_k) \tag{5.44}$$

$$\phi_f^T(t_k) = \left[-y_f^{(n-1)}(t_k) \dots - y_f^{(0)}(t_k)\ \ u_f^{(m)}(t_k) \dots u_f^{(0)}(t_k)\right] \tag{5.45}$$

$$\theta_c = [\alpha_1 \dots \alpha_n\ \beta_0 \dots \beta_m]^T \tag{5.46}$$

where the subscript *f* denotes hybrid filtering which involves a CT filter. First the pre-filtered derivatives which are sampled at instant Δt are obtained as the inputs to the integrators in the CT implementation of the state variable pre-filter $1/A\ (s)$, as shown in Figure 5.12. Ideally the coefficients of the pre-filter match those of the unknown system (Young 2006). In practice these would be initialised with approximate values and iteratively updated with the new estimates as they become available. In this work, however, rounded values close to those of the coefficients corresponding to the nominal CT suspension system are used. Further consideration would need to be given as to updating the coefficients in an application such as fault detection.

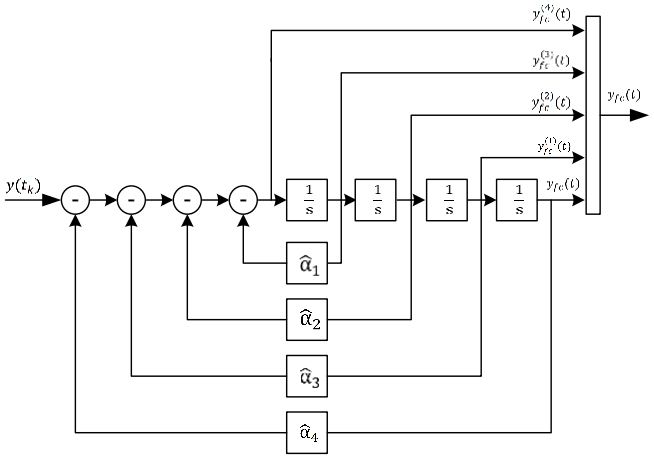

Figure 5.12 A state variable filter used to obtain derivatives of $y(t_k)$

5.3.3.5. Replicating faults in the CT system model

Similar to the DT case an equivalent fault scenario is introduced into the simulated CT system with the exception that because the model is estimated in CT the sample times S_1, S_{fs}, S_{fe}, and S_e correspond as closely as possible to those of the DT case.

5.3.4. Simulation studies

This section describes the simulation studies to compare the effectiveness of DT and CT models for their use in fault detection. As briefly introduced in Section 5.3.1, a series of trials to assess the robustness of the two approaches over a range of different sampling frequencies are carried out. As a basis for comparison the true parameters corresponding to the faulty condition are obtained theoretically and used as a benchmark to assess the accuracy of the estimation for both DT and CT over the chosen range of sampling frequencies. The performance measure in all cases is a normalised percentage Euclidean norm, denoted EN, between the true parameter vector and the mean of the estimates of the final portion of the simulation, when the fault has stabilised. This measure is expressed as

$$EN = \frac{EN_A - EN_E}{EN_A}.100 \qquad (5.47)$$

where EN_A is the Euclidean norm of the actual parameter vector and EN_E is the Euclidean norm of the estimated parameter vector. This relative percentage metric is adopted to overcome the problem of large CT parameters versus small DT parameters biasing the performance measure. Note that in all simulations reported here, the EN is calculated for the estimates of the final 3000 samples of the simulation, after the fault has been stabilised.

Attention is initially given to the DT case. To quickly gain an insight a sampling frequency of 13 Hz was chosen (approximately one-tenth of the chassis frequency) and run over *N*=10,000 samples. The trial was repeated initially three times with different noise seeds being used. In each case the variance σ^2 is taken to be $2.5.10^{-3}$. The results are given in Table 5.4. It is immediately clear that the estimated parameters vary from their true values by different amounts, as is evident from the Euclidean norm metric given in Table 5.5. This inconsistency is then investigated across a range of sampling frequencies of 10 Hz to 200 Hz. A Monte Carlo simulation is used to assess the inconsistencies, with 500 runs taking place and, once the outliers have been removed, the mean values are calculated. An outlier is defined here as a parameter set which contains one or more parameters which exceed ±10 times a given nominal value. The results are given in Table 5.6.

The consistency of the estimates in the CT case is verified by the use of a Monte Carlo simulation with simulation runs of 1, 10, 50 and 500 and the mean values of EN calculated. The resulting EN metric indicates a high degree of consistency between each simulation run, see Table 5.7. For this reason, Monte Carlo simulation for the CT models was deemed unnecessary, hence the results will feature as a single simulation run for the range of f_s between 10-200 Hz. These simulation results are given in Table 5.8.

5.3.5. Estimation results

5.3.5.1. Discussion of DT estimation results

Estimation results for sampling frequencies (f_s) in the range 10 to 200Hz are given in Table 5.4-5.5 and Figure 5.13. For each sampling frequency the true parameters and their estimates are shown with the corresponding EN and outlier count. The most accurate estimations consistently occur around 15Hz which corresponds to the ideal sampling frequency for the un-sprung mass. It is observed that for other frequencies the value of the EN metric varies.

5.3.5.2. Discussion of CT estimation results

Estimation results for sampling frequencies (f_s) in the range 10 to 200Hz are given in Table 5.7 and plotted in Figure 5.13. Since no conversion of the TF is required, there is only one set of true parameters shown on the left hand side. As in the DT case, these values represent the parameters for the final part of the simulation, after the fault has been stabilised. The mean and variance of the overall results for the DT and CT, corresponding to Tables 5.3-5.6 and 5.7,

respectively, are given in Table 5.9. This confirms that there is considerably less variability in the CT estimation performance.

Simulation run	**1**	**2**	**3**
f_s	**13**	**13**	**13**
θ	$\widehat{\boldsymbol{\theta}}$		
-0.9937	-0.993	-0.982	-0.980
-0.0595	-0.052	-0.079	-0.047
0.2928	0.298	0.287	0.284
0.1198	0.104	0.122	0.108
93.47	95.56	93.63	94.20
-219.7	-224.8	-218.0	-217.8
159.0	159.1	155.3	158.5
-32.74	-25.79	-30.25	-34.18
EN	**3.04**	**1.67**	**0.86**

Table 5.3 Single pass estimations of DT model

f_s	**10**		**15**		**30**	
	θ	$\widehat{\boldsymbol{\theta}}$	**θ**	$\widehat{\boldsymbol{\theta}}$	**θ**	$\widehat{\boldsymbol{\theta}}$
	-1.529	-1.483	-0.836	-0.833	-1.827	-1.811
	0.971	0.901	-0.423	-0.421	1.251	1.244
	-0.174	-0.137	0.416	0.418	-0.762	-0.755
	0.063	0.061	0.159	0.159	0.399	0.396
	44.47	44.91	119.01	118.4	148.6	136.8
	-100.3	-97.88	-286.0	-285.1	-391.4	-380.9
	67.21	62.67	214.9	214.6	337.1	341.0
	-11.37	-8.82	-47.95	-47.53	-94.29	-93.62
EN		4.62		0.31		3.03
Outliers		12		2		4

Table 5.4 Single pass estimations of DT model

f_s	**110**		**130**		**200**	
	θ	$\widehat{\boldsymbol{\theta}}$	**θ**	$\widehat{\boldsymbol{\theta}}$	**θ**	$\widehat{\boldsymbol{\theta}}$
	-3.589	-3.538	-3.671	-3.622	-3.810	-3.745
	4.962	4.825	5.153	5.023	5.493	5.311
	-3.150	-3.020	-3.291	-3.170	-3.554	-3.384
	0.778	0.735	0.809	0.770	0.871	0.818
	58.65	58.25	50.34	49.90	33.56	33.86
	-169.1	-166.8	-146.0	-142.8	-98.47	-94.62
	162.3	157.6	141.0	136.2	96.26	90.95
	-51.81	-48.33	-45.33	-42.97	-31.35	-29.38
EN		2.61		3.01		4.94
Outliers		5		6		3

Table 5.5 Estimation results for the DT model

Monte Carlo runs	**1**	**10**	**50**	**500**
f_s	**13**	**13**	**13**	**13**
θ	$\widehat{\boldsymbol{\theta}}$			
27.59	27.60	27.60	27.60	27.60
2598.4	2600	2600	2600	2600
6984.1	6988	6988	6988	6988
95238	95286	95286	95286	95286
6984.1	6988	6988	6988	6988
95238	95286	95286	95286	95286
EN	**0.0506**	**0.0501**	**0.0500**	**0.0500**

Table 5.6 Monte Carlo comparison for the CT model

f_s	**10**	**15**	**30**	**110**	**130**	**200**
θ	$\widehat{\boldsymbol{\theta}}$					
27.59	27.60	27.60	27.60	27.60	27.60	27.60
2598.4	2600	2600	2600	2600	2600	2600
6984.1	6988	6988	6988	6988	6988	6988
95238	95285	95286	95286	95285	95288	95288
6984.1	6988	6988	6988	6988	6988	6988
95238	95286	95286	95286	95286	95286	95286
EN	**0.0500**	**0.0505**	**0.0504**	**0.0499**	**0.0513**	**0.0511**

Table 5.7 Estimation results for the CT model

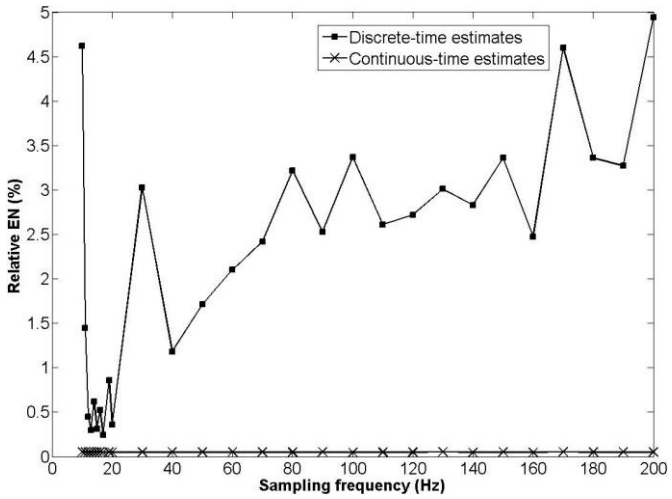

Figure 5.13 Estimation results EN comparison DT vs. CT

	Continuous-time	Discrete-time
Mean EN	0.0504	2.487
Variance EN	$0.4.10^{-6}$	2.007

Table 5.8 Mean and variance of the EN metric for estimates over a 10-200 Hz sampling frequency range

5.3.6. Conclusions

The results of extensive simulation trials of a suspension system over a range of conditions which could realistically be experienced on a road vehicle clearly indicate the superiority of CT models over DT models for online parameter estimation. The evidence suggests that the CT approach provides consistent estimates and is robust in regard to the choice of sampling frequency. It is also considered to be sufficiently accurate in order to be taken further as an approach for fault detection. The DT model on the other hand is dismissed as being inaccurate in terms of estimation consistency and unreliable in terms of robustness.

5.4. Comparison of continuous-time vehicle model estimators as candidates for suspension system fault detection

5.4.1. Introduction

Section 5.4.2, reiterates the vehicle suspension model detailed in 4.4.1, for convenience. Section 5.4.3 details the CT model and its estimation schemes. Section 5.4.4 outlines the simulation method. Section 5.4.5 gives detailed results and analyses of preliminary simulation studies. The conclusions and immediate further on-going work are presented in Section 5.4.6.

5.4.2. Vehicle suspension model

As in Chapter 4, Figure 4.2 represents the vehicle suspension model for this method. The equation for the model used are as before in Section 5.3.

5.4.3. Parameter estimation

RLS and Kalman Filter (KF) are the methods used here to estimate the coefficients of the transfer functions of the suspension model. RLS is a straightforward online estimation algorithm, yet it is optimal in the mean square error (MSE) sense when the assumptions on linearity of the model and Gaussian properties of the measurement noise hold. Although ARMA additive noise has been adopted for the noise models, the estimator is found to perform adequately, as will be demonstrated in the results presented in Section 5.4.5.

The KF estimator allows the user to leverage some *a priori* knowledge of the measurement noise and model parameter changes to give superior estimates. This makes the KF a natural choice for this type of application, where the transfer function coefficients are known to be changing in faulty conditions such as tyre deflation.

5.4.3.1. The continuous-time system model

The CT system model (5.10) is as used before in Section 5.2.2, using the state variable filter as illustrated in Figure 5.12

5.4.3.2. Cautious least squares

Cautious least squares (CLS), which is an extension of RLS, is selected as the candidate method of quantifying faults. CLS is useful in the capacity of quantifying faults because it detects, records and corrects deviations of $\hat{\theta}$ from normality. It has the additional benefit of improving the estimates of systems which temporarily experience low input excitation.

A problem associated with RLS estimators is that they need sufficient differences in measurements over time or the covariance matrix, P, experiences a condition known as 'blow up' which causes the estimates to degrade (Milek 1995). If the vehicle is traversing a motorway or a smooth road, there may be very little suspension deflection and hence low measurement activity. If the estimates deviate from the model, this could be detected as a suspension failure when in fact it is a failure of the detection system. CLS counteracts this problem by resetting the deviated parameter vector $\hat{\theta}$ generated by RLS to some pre-specified 'safe set' of parameters, denoted θ_s and the co-variance matrix is reset. This action also has the effect of artificially exciting the system, which improves the estimates in cases of low input excitation. A similar effect can be achieved with the application of a forgetting factor.

The algorithm can also log every θ estimate that departs from safe set θ_s (or stays within a pre-specified 'safe operating region', defined by the user). The rationale underlying the resets is primarily as a fault detection mechanism. When a parameter exceeds a threshold the co-variance matrix is reset and it implies something is changing in the plant e.g. a fault is occurring. Parameter drift can also be attributed other effects that are not related to faults such as model inaccuracy but it is proposed that a fault will manifest more prominently in the parameters than other effects that cause the estimates to change. The covariance matrix is set at a value of 100k in all cells. This is an arbitrary figure but in general larger numbers improve convergence time of the estimates. The parameter reset counts are intended as a guide to the type of fault that is present in the system. If a variable representing a physical property, such as spring stiffness is changed, this is reflected in a subset of the parameter values of the transfer function model that is being estimated. Table 5.9 shows the parameter values for faulty and fault-free states. The actual number of fault counts which constitutes a fault would have to be generated from practical tests on a vehicle, with the results of a particular modelling exercise representing a potential starting point.

CLS attempts to minimise the modified cost function

$$J_c(\theta) = (y - X\theta)^T \Lambda (y - X\theta) + (\theta - \theta_s)^T \Psi (\theta - \theta_s) \tag{5.48}$$

i.e. $$J_c(\theta) = J_1 + J_2 \tag{5.49}$$

The first term of which corresponds to the normal RLS cost function (and equally a KF cost function) in which $y - x^{\mathrm{T}}\theta$ is the prediction error.

The sequential operation of the CLS algorithm involves, at each time step, a further p iterations to minimise the cautious component J_2 of the cost function (5.49). For clarity, it is convenient to assume that whilst time is 'frozen' between successive iterations of RLS the discrete time index *t* is replaced by the index *j*, where *j=1,2,...p.* The sequential CLS algorithm then takes the form

$$\theta_{\mathrm{j}} = \theta_{\mathrm{j}-1} + \phi_{\mathrm{j}}\left[e_{\mathrm{j}}^{\mathrm{T}}\left(\theta_{\mathrm{s}} - \theta_{\mathrm{j}-1}\right)\right] \tag{5.50}$$

$$\phi_{\mathrm{j}} = \Phi_{\mathrm{j}-1} e_{\mathrm{j}} [1 + e_{\mathrm{j}}^{\mathrm{T}} \Phi_{\mathrm{j}-1} e_{\mathrm{j}}]^{-1} \tag{5.51}$$

$$\Phi_{\mathrm{i}} = \left[\mathrm{I} - \phi_{\mathrm{i}} e_{\mathrm{i}}^{\mathrm{T}}\right] \Phi_{\mathrm{i}-1} \tag{5.52}$$

where the e_{j} are the orthogonal unit vectors defined as

$$e_{\mathrm{j}}^{\mathrm{T}} = \left[\delta_{1j} \delta_{2j} \delta_{3j} \ldots \delta_{pj}\right] \tag{5.53}$$

in which δ_{ij} is the Kronecker delta function

$$\delta_{\mathrm{ij}} = \begin{cases} 1 & \mathrm{i} = \mathrm{j} \\ 0 & \mathrm{i} \neq \mathrm{j} \end{cases} \tag{5.54}$$

If a correction to a parameter in $\hat{\theta}$ is required a fault counter increments for that particular coefficient. The type of fault occurring in the system may be diagnosed by the pattern of corrections to the parameters. This includes changes in the vehicle sprung mass, which does not constitute a fault although it is something that arises in normal usage of a vehicle as passengers alight. In these cases, the fault detection would need to draw on other information available on the vehicle sensor data network, such as vehicle velocity, transmission status and

passenger occupancy detection (a system to detect passengers and invoke seat belt warnings if necessary).

5.4.3.3. Replicating faults in the simulation system model

Faults in the suspension system are all modelled by a gradual change from the nominal value to 50% of nominal, where the value is maintained for the remainder of the simulation.

5.4.4. Simulation studies

This section describes the simulation studies to compare the effectiveness of RLS, KF and CLS estimators for their use in fault detection. A series of trials to assess the robustness of the approaches is carried out. A comparison of RLS and KF is initially carried out and then these algorithms are enhanced by the inclusion of CLS and a second set of results is presented.

The simulations are run over *N*=10,000 samples and the additive noise variance σ^2 is taken to be $2.5.10^{-3}$.

The performance measure in all cases is a normalised percentage Euclidean norm, denoted EN, between the true parameter vector and the mean of the estimates of the final portion of the simulation, when the fault has stabilised. This measure is expressed

$$EN = \frac{EN_A - EN_E}{EN_A}.100 \tag{5.55}$$

where EN_A is the Euclidean norm of the actual parameter vector and EN_E is the Euclidean norm of the estimated parameter vector. This relative percentage metric is adopted so that different sized parameter sets can be compared. Note that in all simulations reported here, the EN is calculated for the estimates of the final 6000 samples of the simulation, directly after the fault has been stabilised.

It should be noted that it is assumed that the vehicle being modelled here is not subject to loads beyond that of two occupants and that only single faults will be considered, multiple simultaneous faults are not considered here.

The parameters the four different conditions are shown in Table 5.9, the lower part of the table is the rounded ratio of a faulty value to nominal, which indicates the relative magnitude of change occurring in the individual parameter due to the fault.

	Nominal	Tyre fault	Spring fault	Damper fault
a1	27.6	27.6	27.6	13.8
a2	4821	2598	4633	4821
a3	13968	6984	13968	6984
a4	190476	95238	95238	190476
b1	13968	6984	13968	6984
b2	190476	95238	95238	190476
Ratio				
a1	1	1	1	2
a2	1	1.9	1	1
a3	1	2	1	2
a4	1	2	2	1
b1	1	2	1	2
b2	1	2	2	1

Table 5.9 Parameter sets for the faulty conditions

5.4.5. Estimation results

Initial trials were carried out using RLS and KF. The RLS converges to the parameters as the fault stabilises with a forgetting factor of 0.99 but convergence is much faster using a KF which is tuned for the expected parameter set for a tyre fault. The result of this testing is shown in Table 5.10.

Figures 5.14 to 5.22 show the results for the same algorithms that have been enhanced by the addition of CLS. Clearly, the estimators are able to detect faults. However, when comparing the parameter values from Table 5.9 it becomes evident that the parameter resets of the CLS algorithm do not follow the actual parameter changes in the model, particularly in the case of a detuned KF. This makes it difficult for a specific fault to be identified according to the parameter changes that are occurring in the system model. Although the KF approach appears to be particularly inaccurate in terms of fault diagnosis, due to the reset count being dominated by the counts for the α_1 parameter, it is possible to tune the response using the KF correction matrix R_w and obtain reset count profiles that are characteristic of the fault that is occurring. The KF is a much more versatile approach in this respect. The tuned responses are shown in Figures 5.20 to 5.22. The fault diagnosis mechanism could be a bank of KF, each tuned for a specific fault, if the reset counts are occurring exclusively in the α_3 and β_1 parameters, this points to a change in the damper value.

	RLS	Untuned KF	Tuned KF
θ		$\widehat{\theta}$	
27.6	27.6	27.6	27.2
2598	2657	2645	2634
6984	7241	7206	6638
95238	98571	98944	98452
6984	7211	7162	7157
95238	98624	98660	95232
EN	**3.41**	**3.61**	**2.36**

Table 5.10 Comparison of RLS and KF for tyre fault

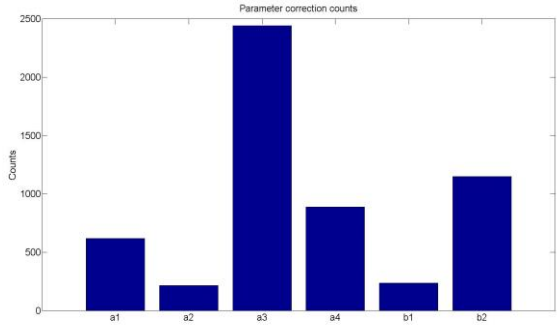

Figure 5.14 Parameter reset counts for tyre fault and RLS CLS

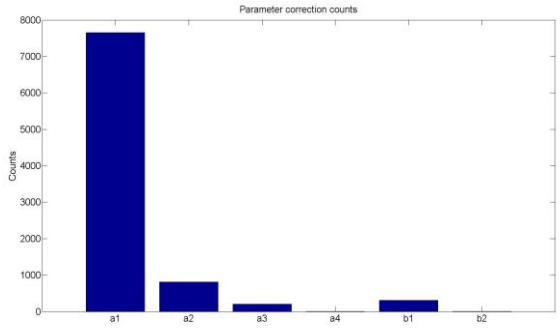

Figure 5.15 Parameter reset counts for tyre fault and detuned KF CLS

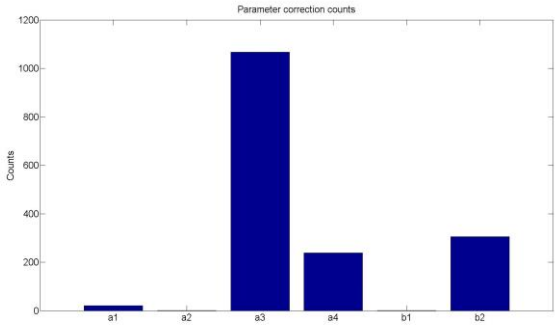

Figure 5.16 Parameter reset counts for spring fault and RLS CLS

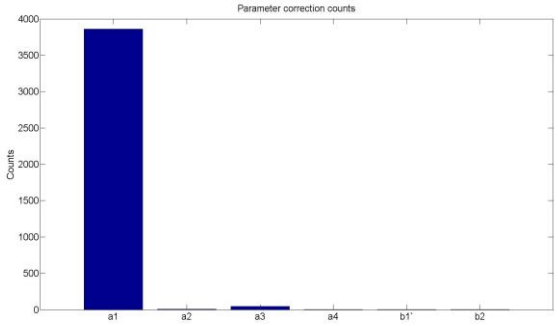

Figure 5.17 Parameter reset counts for spring fault and detuned KF CLS

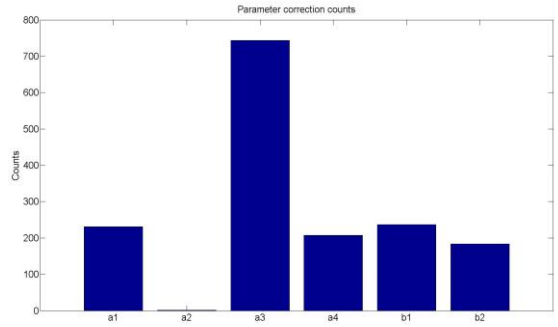

Figure 5.18 Parameter reset counts for damper fault and RLS CLS

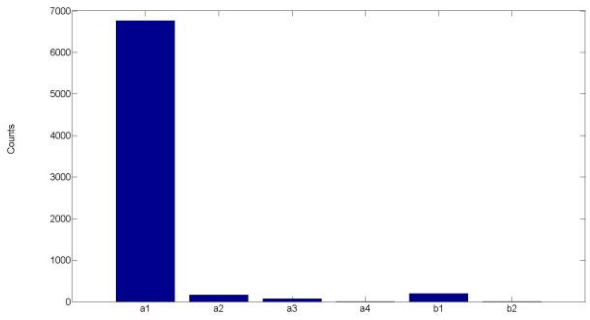

Figure 5.19 Parameter reset counts for damper fault and detuned KF CLS

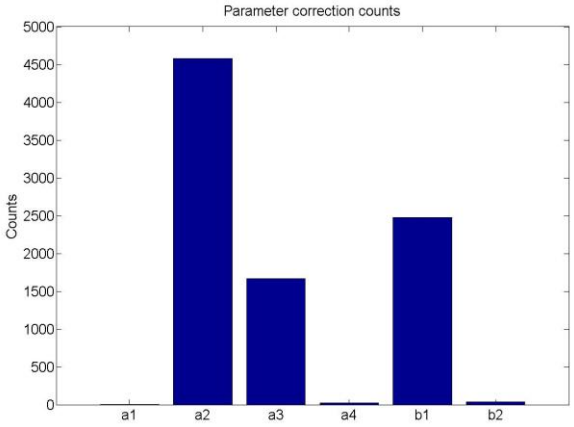

Figure 5.20 Parameter reset counts for tyre fault and tuned KF CLS

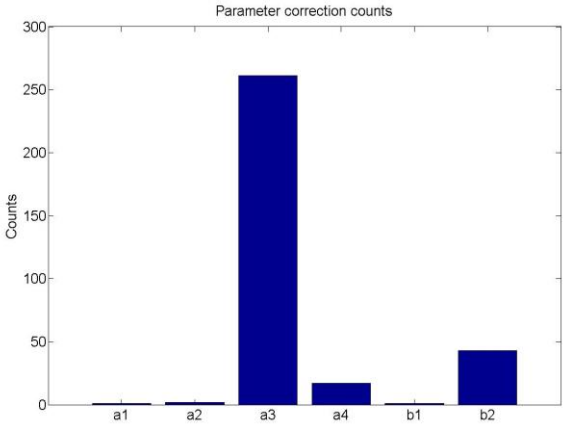

Figure 5.21 Parameter reset counts for spring fault and tuned KF CLS

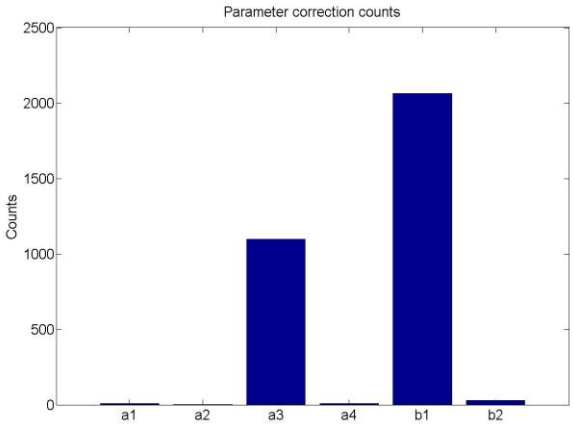

Figure 5.22 Parameter reset counts for damper fault and tuned KF CLS

5.4.6. Conclusions

It is clear that the tuned KF with CLS offers the greatest potential. While it could be argued that a similar result could be achieved by defining a safe set of parameters, estimating with a KF and monitoring-re-setting parameters, CLS is unique in its operation due to the action of the algorithm, described by Eqn 5.48-5.54.

Further work will examine the use of a bank of Kalman filters, each being tuned to detect a specific fault condition. The distribution of the reset counts for a specific type of fault is repeatable and may be developed into a positive diagnosis, possibly with the application of a fuzzy logic interpretation of the reset count, based on empirical data from testing of known faulty conditions.

5.5. A continuous-time model-based tyre fault detection algorithm utilising a Kalman state estimator approach

5.5.1. Introduction

A problem with the application of a model-based parameter estimation scheme to the suspension system, for the purpose of fault detection, is that the input to the system is unknown i.e. the road surface is not known to the algorithm in advance. The solution to this problem within this work is the utilisation of an enhanced filter which estimates the road surface input from the chassis acceleration measurement, based on knowledge of the suspension system. The relative position of the wheel to the road is also estimated and it is with these two estimates that a decision can be made about the condition of the tyre i.e. the sidewall height of the tyre changes hence implying that the pressure in the tyre changes. A more general application of this state estimation technique would be for fault detection in systems where the primary input is unknown or none of the input signals and disturbances are known at all.

The effect of tyre radius changes due to pressure is not considered in this work in order to avoid adding too much complexity to the model and obfuscating the source of tyre radius changes. The intent is the development of a tyre height estimator, not a sophisticated model of the suspension and tyre assembly. Obviously, any further work, especially involving vehicle validation, would necessitate the inclusion of this effect in the model.

This Section is organised as follows. Section 5.5.2 defines the vehicle suspension and road model and issues surrounding the selection of sampling interval. Section 5.5.3 shows how the Kalman state estimator has been implemented. Section 5.5.4 outlines the simulation studies carried out. Section 5.5.5 presents detailed results and an analysis of the simulation studies. The conclusions are presented in Section 5.5.6.

5.5.2. Vehicle suspension and road model

As in Chapter 4, Figure 4.2 represents the vehicle suspension model for this method. The input stimulus to the system is essentially a displacement, denoted x_{r}, from the road surface. The high frequency component of the road surface is modelled by a first order transfer function that is driven by band-limited white noise. The low frequency component of the road surface, denoted w_d, which represents the undulating nature of the road is generated using the method developed by Wong (2001). Using Newton's law of motion the system may be expressed as

$$m_s\ddot{x}_s + B_s(\dot{x}_s - \dot{x}_{us}) + k_s(x_s - x_{us}) = 0 \quad (5.56)$$

$$m_{us}\ddot{x}_{us} + k_t(x_{us} - (x_r + w_d)) - B_s(\dot{x}_s - \dot{x}_{us}) - k_s(x_s - x_{us}) = 0 \quad (5.57)$$

$$k(w_n - x_r) - \dot{x}_r = 0 \quad (5.58)$$

where $x_s$and x_{us} denote the displacement of sprung and un-sprung mass from the points of equilibrium, respectively ($\dot{x}$ and $\ddot{x}$ denote the velocity and acceleration in both cases).

A convenient state space representation is given by

$$\dot{\boldsymbol{x}} = \boldsymbol{A}\boldsymbol{x} + \boldsymbol{b}w_{\boldsymbol{d}} + \boldsymbol{\Gamma}w_n \quad \text{and} \quad \boldsymbol{y} = \boldsymbol{C}\boldsymbol{x} + v \quad (5.59)$$

where w_d is the low frequency road input disturbance, Γ is the input vector for the high frequency disturbance and w_{n} is the high frequency road process noise (that drives the dynamic models of interest within the system) and *v* is the additive noise that is corrupts the chassis acceleration measurement.

The state vector is defined

$$x = [x_s \;\; \dot{x}_s \;\; x_{us} \;\; \dot{x}_{us} \;\; x_r]^T \triangleq [x_1 \;\; x_2 \;\; x_3 \;\; x_4 \;\; x_5]^T$$

leading to

$$\dot{x}_1 = x_2 \quad (5.60a)$$

$$\dot{x}_2 = -\frac{1}{m_s}[B_s(x_2 - x_4) + k_s(x_1 - x_3)] \quad (5.60b)$$

$$\dot{x}_3 = x_4 \quad (5.60c)$$

$$\dot{x}_4 = \frac{1}{m_{us}}[B_s(x_2 - x_4) + k_s(x_1 - x_3) - k_t(x_3 - (x_5 + w_d))] \quad (5.60d)$$

$$\dot{x}_5 = k(w_n - x_5) \quad (5.60e)$$

where *k* defines the position of the pole in the simplified road model transfer function. Having defined the state vector, the representation takes the following state space vector-matrix form

$$\dot{\boldsymbol{x}} = \begin{bmatrix} 0 & 1 & 0 & 0 & 0 \\ \frac{-k_s}{m_s} & \frac{-B_s}{m_s} & \frac{k_s}{m_s} & \frac{B_s}{m_s} & 0 \\ 0 & 0 & 0 & 1 & 0 \\ \frac{k_s}{m_{us}} & \frac{B_s}{m_{us}} & \frac{-k_t-k_s}{m_{us}} & \frac{-B_s}{m_{us}} & \frac{k_t}{m_{us}} \\ 0 & 0 & 0 & 0 & -k \end{bmatrix} \boldsymbol{x} + \begin{bmatrix} 0 \\ 0 \\ 0 \\ \frac{k_t}{m_{us}} \\ 0 \end{bmatrix} w_d + \begin{bmatrix} 0 \\ 0 \\ 0 \\ 0 \\ k \end{bmatrix} w_n \qquad (5.61a)$$

$$\boldsymbol{y} = \begin{bmatrix} \frac{-k_s}{m_s} & \frac{-B_s}{m_s} & \frac{k_s}{m_s} & \frac{B_s}{m_s} & 0 \end{bmatrix} \boldsymbol{x} \qquad (5.61b)$$

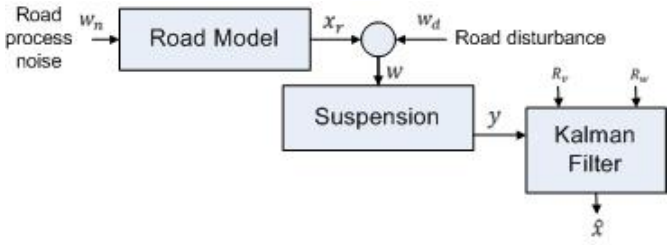

Figure 5.23 Schematic of the estimation setup

5.5.3. Kalman filter approach

A continuous-time Kalman filter provides the approach used here to estimate all of the states in the model. The standard filter has been extended to estimate the road input, denoted x_5, in (5.60d, 5.60e).

Figure 5.23 shows the schematic of the estimation setup in block diagram form. The input to the suspension system is unknown i.e. the road disturbance, denoted *w*. It is assumed that there is an underlying high frequency process noise, denoted w_n, contained within the road input and that there are additional large scale low frequency disturbances, denoted w_d, that combined with the road process noise cause the excitation of the suspension. It is assumed that w_d does not affect the tyre height ($x_{us} - x_r$), it affects all of the states ($x_{us,}\ x_{us,}\ x_r$) equally (vehicle climbing a hill) or it affects the suspension by deflecting the main spring ($x_s - x_{us}$)

The output of the suspension system is the acceleration measurement of the sprung mass, denoted *y*. The Kalman filter inputs are the noisy acceleration measurement, *y* and the user defined tuning quantities R_w and R_v for the process and output noise, respectively. The output of the Kalman filter is the estimation of the state vector, x, which includes high frequency road input, denoted x_5 (which is the extended portion of the state vector), the estimation of the states

of the suspension, denoted $\hat{x}$, includes the relative displacement of the wheel with respect to the road input and this is the variable of interest for the purposes of fault detection.

The continuous-time Kalman filter is formulated on the following basis

$$\dot{\boldsymbol{x}} = \boldsymbol{A}\boldsymbol{x} + \boldsymbol{b}w_{\boldsymbol{d}} + \boldsymbol{\Gamma}w_n \quad \text{and} \quad \boldsymbol{y} = \boldsymbol{C}\boldsymbol{x} + v \tag{5.62}$$

where w_n and v are independent zero mean Gaussian noise sources with covariance's r_w and $r_{v,}$ respectively. Γ is the process noise influence vector. The noise w_n effects the input directly where as v adds directly onto the output *y*. The state equation is usually accompanied by an assumption that the system state *x* is not directly available. In this case an optimal (in a quadratic sense) estimate of the state, $\hat{x}$, is given by a continuous time steady state filter

$$\dot{\hat{x}} = A\hat{x} + K_f(y - \hat{y}) \qquad \hat{y} = C\hat{x}$$

$$= (A - K_f C)\hat{x} + K_f y \tag{5.63}$$

where the Kalman filter gain vector K_f is given by

$$K_f = P_f C^T R_v^{-1} \tag{5.64}$$

where P_f is the positive definite solution of the algebraic Riccati equation

$$AP_f + P_f A^{\mathrm{T}} - P_f C^T R_v^{-1} C P_f + \Gamma R_w \Gamma^T = 0 \tag{5.65}$$

5.5.3.1. Replicating faults in the system model

The fault conditions are the same as in Section 5.3.3.

5.5.4. Simulation studies

The algorithm generates estimates of the road position and the wheel position using the Kalman filter applied to the augmented model of the suspension system and road. The estimates are subtracted from each other to produce a relative displacement vector which represent the tyre sidewall height. This vector of estimates is then filtered through a transfer function

$$\frac{1}{10\mathrm{s} + 1} \tag{5.66}$$

whose dynamic arbitrarily chosen to be much slower than that of the system in order to smooth the estimates into a form that is easier to observe changes occurring in the average height of the tyre. The poles of this transfer function may be moved to increase or reduce the response rate of the change detection. Increasing the rate of response would seem to have advantages over a sluggish response, in that small changes in tyre wall height would be rapidly converged on and hence will alert the motorist in good time. However, too fast a response will cause false alarms which are highly undesirable. Making the filter slower also offers benefits; the false alarm rate should be lower and it is easy to detect faults because the tyre wall height measurement is very steadily changing. However, the response may be so slow as to be of no use – the tyre is flat before the diagnostic warns the user. For the purposes of fault detection a robust diagnosis with no false alarms of faults is required.

With further testing work the value of the estimated tyre wall height could be linked directly to pressure in the tyre rather than merely an inference of some change in the tyre.

5.5.5. Estimation results

Figure 5.24 shows the difference between the road and the wheel during a drive cycle over a simulated road surface (Wong 2001) at 80km/h in the normal, no fault condition. The high density of oscillations is caused by the wheel being repeatedly displaced by the uneven road surface and oscillating in the two degrees of freedom that the suspension allows. Bounded oscillations are observed about a mean of zero, which is more readily shown by a histogram of the time series data, Figure 5.27, which exhibits normal distribution. Figure 5.30 shows the filtered (9) difference between the road and the wheel. Figures 5.26, 5.28 and 5.30 are three visualisations of the vehicle traversing a simulated road in the nominal (no fault) condition. Their counterparts, Figures 5.27, 5.29 and 5.31 show the faulty condition which starts at time reference 100s and stabilises at 150s till the end of the simulation.

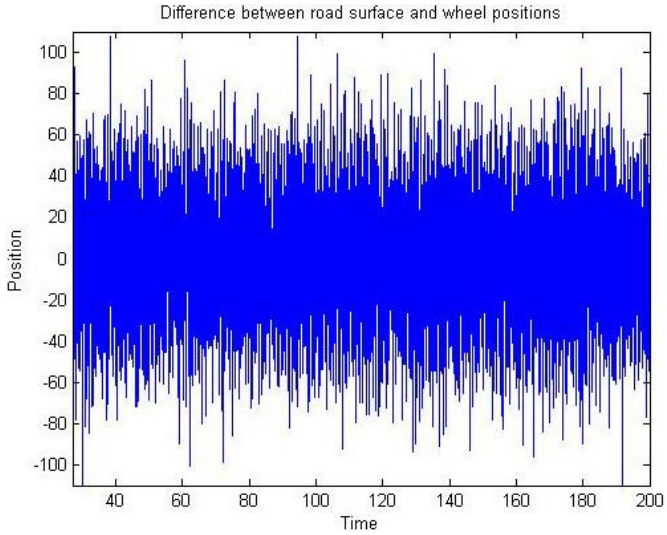

Figure 5.24 Time series difference between road and wheel position data of the vehicle on a simulated road in the nominal condition

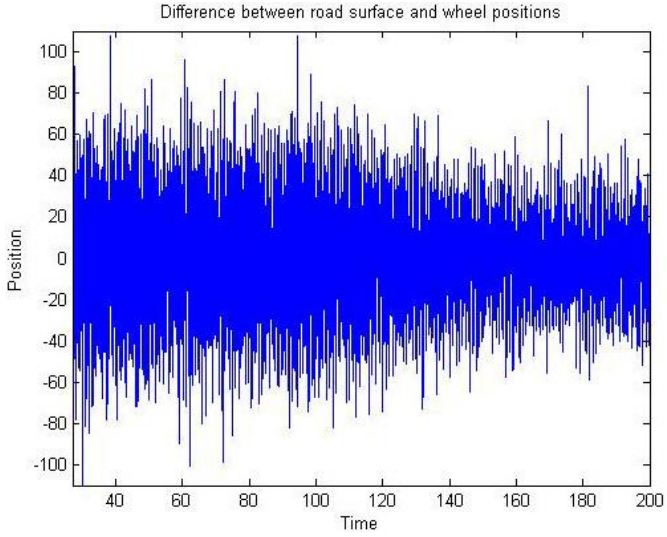

Figure 5.25 Time series difference between road and wheel position data of the vehicle on a simulated road in the faulty condition

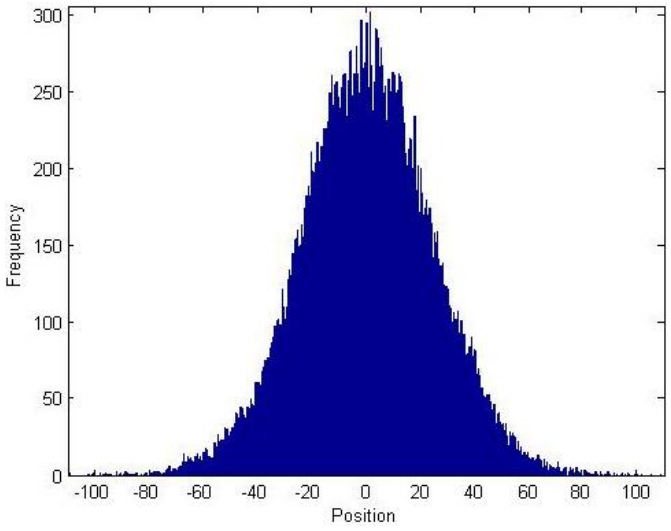

Figure 5.26 Histogram of the drive cycle time series data for the vehicle in nominal condition

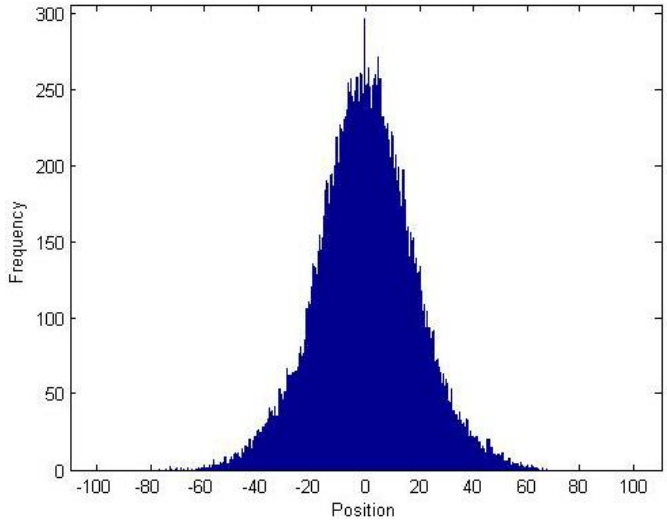

Figure 5.27 Histogram of the drive cycle time series tyre height data for the vehicle during a fault

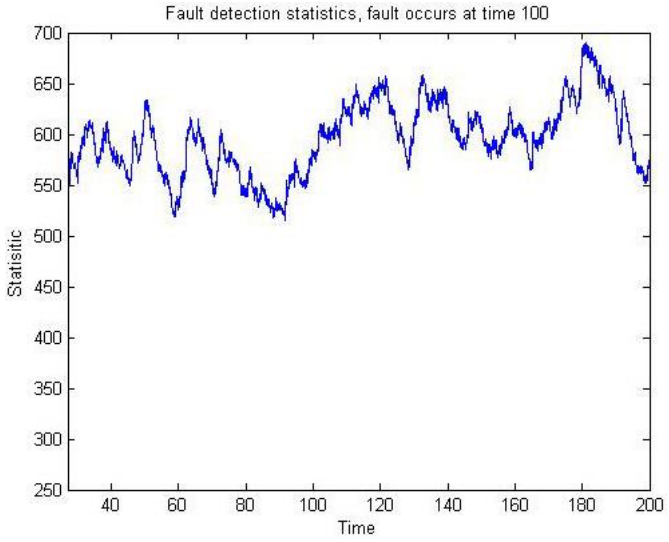

Figure 5.28 Filtered result of the drive cycle time series data for the vehicle in nominal condition

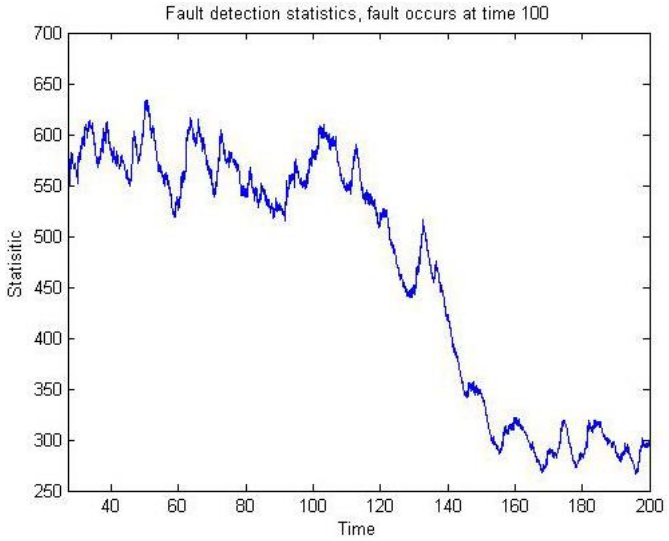

Figure 5.29 Filtered result of the drive cycle time series data for the vehicle in faulty condition

5.5.6. Conclusions

A Kalman filter was enhanced in the sense that the input was declared as a state and it was estimated along with the other states in the system. This allowed the comparison of wheel position and road position to be analysed and the analysis clearly highlights the change

happening in the system. The diagnosis cannot be considered a measurement of the tyre height (and hence tyre pressure) but it should be viewed as a method to detect change in the system. The road model is an important aspect of the fault diagnosis scheme. Contained within it is the tuning factor *k* that allows the user to adjust the model for different road surfaces and vehicle velocity. There is also the possibility to increase the order of the system from first order so that additional dynamics can be described.

5.6. A continuous-time model-based tyre fault detection algorithm utilising an unknown input observer

5.6.1. Introduction

As stated in Section 5.4, a problem with the model-based parameter estimation approach is that the input to the system is unknown i.e. the road surface is not known to the algorithm in advance. The solution to this problem within this work is the inclusion of an unknown input observer which estimates the road surface input from the chassis acceleration, based on knowledge of the suspension system (Ersanilli et al. 2009a). The design of the observer is based on the work of Sfaihi & Boubaker (2004) who developed the idea from a reduced order observer perspective.

This Section is organised as follows. Section 5.6.2 describes the vehicle suspension model. Section 5.6.3 shows how the unknown input observer is designed. Section 5.6.4 details the CT model and the estimation scheme. Section 5.6.5 outlines the simulation method. Section 5.6.6 gives detailed results and an analysis of the simulation studies. The conclusions are presented in Section 5.6.7.

5.6.2. Vehicle suspension model

As in Chapter 4, Figure 4.2 represents the vehicle suspension model for this method. The equation for the model used are as before in Section 5.3.

5.6.3. Unknown input observer

This approach to observer design divides the state vector in two parts, one part not depending on unknown inputs and the second part depending on the unknown input. The system is equivalent to

$$\dot{x} = Ax + Bu + Dv \qquad (5.67a)$$

$$y = Cx \qquad (5.67b)$$

$$T = [N\ D] \qquad (5.67c)$$

where T is a non singular matrix and $N \in \Re^{n \times (n-m)}$ and $x \in \Re^n$, $u \in \Re^n$, $v \in \Re^n$, $y \in \Re^n$, are the state, known input, unknown input and output vector, respectively. Since $p \geq m$, $rank(D)=m$, $rank(C)=p$ and the pair (C, A) are observable, one can proceed.

Suppose

$$x = Tx = T\begin{bmatrix} x_1 \\ x_2 \end{bmatrix} \tag{5.68}$$

with $x_1 \in \Re^{n-m}, x_2 \in \Re^m$and

$$A = T^{-1}AT = \begin{bmatrix} A_{11} & A_{12} \\ A_{21} & A_{22} \end{bmatrix} \tag{5.69}$$

$$B = T^{-1}B = \begin{bmatrix} B_1 \\ B_2 \end{bmatrix} \tag{5.70}$$

$$D = T^{-1}D = \begin{bmatrix} 0 \\ I_m \end{bmatrix} \tag{5.71}$$

$$C = CT = [CN \;\; CD] \tag{5.72}$$

the relation (5.69) can be written

$$\dot{x}_1 = A_{11}x_1 + A_{12}x_2 + B_1u \tag{5.73a}$$

$$\dot{x}_2 = A_{21}x_1 + A_{22}x_2 + B_2u + I_mv \tag{5.73b}$$

$$y = C_1x_1 + C_2x_2. \tag{5.73c}$$

The state x_2 is dependent on the unknown input *v* whereas x_1 is not, which makes x_1 a superior candidate for estimation. The input-free system becomes

$$\dot{x}_1 = A_{11}x_1 + A_{12}x_2 + B_1u \tag{5.74a}$$

$$y = C_1x_1 + C_2x_2. \tag{5.74b}$$

Suppose a non-singular matrix is created

$$U = [CD \;\; Q] \tag{5.75}$$

with $Q \in \Re^{p \text{ x } (p-m)}$

and denoting

$$U^{-1} = \begin{bmatrix} U_1 \\ U_2 \end{bmatrix} \tag{5.76}$$

with $U_1 \in \Re^{m \text{ x } p}, U_2 \in \Re^{(p-m) \text{ x } p}$, verifying

$$U^{-1}U = \begin{bmatrix} U_1CD & U_1Q \\ U_2CD & U_2Q \end{bmatrix} = \begin{bmatrix} I_m & 0 \\ 0 & I_{p-m} \end{bmatrix} \quad (5.90)$$

pre-multiplying both sides of measurement equation (5.75) by U^{-1} leads to

$$U_1y = U_1CNx_1 + U_1CDx_2 \quad (5.91a)$$

$$U_2y = U_2CNx_1 + U_2CDx_2 \quad (5.91b)$$

Combining (5.91a) and (5.91b) gives:

$$U_1y = U_1CNx_1 + x_2 \quad (5.92)$$

$$U_2y = U_2CNx_1. \quad (5.93)$$

The state x_2 is then deduced from (5.92) such that

$$x_2 = U_1y - U_1CNx_1 \quad (5.94)$$

hence substituting (5.94) into (5.67a) gives

$$\dot{x}_1 = \tilde{A}_1x_1 + B_1u + E_1y$$

$$\bar{y} = \tilde{C}_1x \quad (5.95)$$

where

$$\tilde{A}_1 = A_{11} - A_{12}U_1CN, \qquad E_1 = A_{12}U_1, \qquad C_1 = U_2CN$$

and $\bar{y} = U_2y$.

If the pair $(\tilde{A}_1, \tilde{C}_1)$ is observable or detectable, following the conventional Luenberger observer design procedure (Franklin et al. 1997), it is possible to design a reduced order observer for the unknown input free system (25)

$$\dot{\hat{x}}_1 = (\tilde{A}_1 - L\tilde{C}_1)\hat{x}_1 + B_1u + Ly \quad (5.96)$$

where $L \in \Re^{(n-m)\mathrm{x}(p-m)}$ $L = LU_2 + E_1$.

Then

$$\hat{x} = T\hat{x} = T\begin{bmatrix} \omega \\ U_1y - U_1CN\omega \end{bmatrix} \quad (5.97)$$

and $\hat{x} \to x$ as $t \to \infty$. Based on the reduced order observer described by (5.96) and (5.97), an estimation of unknown inputs can be obtained

$$\hat{v} = U_1\dot{y} + G_3\omega + G_4 y + G_5 u \tag{5.98}$$

where

$$G_3 = U_1 CNLU_2 CN + U_1 CNA_{12}U_1 CNN - U_1 CNA_{11} - A_{21} + A_{22}U_1 C \tag{5.99}$$

$$G_4 = -U_1 CNLU_2 - U_1 CNA_{12}U_1 - A_{22}U_1 \tag{5.100}$$

$$G_5 = -U_1 CNB_1 - B_2 \tag{5.101}$$

5.6.4. Parameter estimation

RLS is the method used here to estimate the coefficients of the transfer functions of the suspension model. RLS is a straightforward online estimation algorithm, yet it is optimal in the mean square error (MSE) sense when the assumptions on linearity of the model and Gaussian properties of the measurement noise hold. Although ARMA additive noise has been adopted for the noise models, the estimator is found to perform adequately, as will be demonstrated in the results presented in Section 5.5.6.

5.6.4.1. The continuous-time system model

As in Chapter 4, Figure 4.2 represents the vehicle suspension model for this method. The equation for the model used are as before in Section 5.3.

5.6.4.2. Replicating faults in the system model

The fault conditions are the same as in Section 5.3.3.

5.6.5. Simulation studies

For the purposes of fault detection a robust diagnosis with no false alarms of faults is required. To achieve this goal a matrix of tests is implemented and a majority voting system is proposed, similar to the type that is used in aircraft diagnostics (Yan et al. 2006). The fault decision algorithm is presented with the result of three tests and a majority verdict decides the diagnosis and hence alerts the driver of a problem with tyre pressure.

The tests are detecting changes in the system in three distinct ways. The primary approach is parameter estimation and is carried forward from the work of Ersanilli et al. (2008). This technique is augmented by analysis of the input estimation: variance and the phase portrait.

The simulation studies show that the estimated parameters no longer converge to the true model parameters. The cause of this is most likely to be the estimation of the input, which is only an approximation of the road surface. This behaviour is not particularly problematic as the estimations tend to settle to a steady value when the system is in steady state and during a fault are changing in sympathy with the actual model parameters. A persistent change in the parameters can then be deemed to be a fault. For practical applications, bounds and conditions should be placed on the variation of the estimated parameters for a diagnosis to take place. With further testing work the value of the estimated parameters could be linked directly to pressure in the tyre.

5.6.6. Estimation results

Figure 5.30 shows estimation of parameter a_1 in a typical test run with no fault. Contrast this result with Figure 5.31 which shows the fault occurring at 6 minutes and stabilising at 12 minutes. Figure 5.32 shows the mean variance of the input estimation as it evolves over time, starting with the fault free condition, with the fault being introduced at the 40% of the total test time and stabilising at around 70%. Figure 5.33 compares the phase portrait of the input estimation before and after the fault has occurred and stabilised.

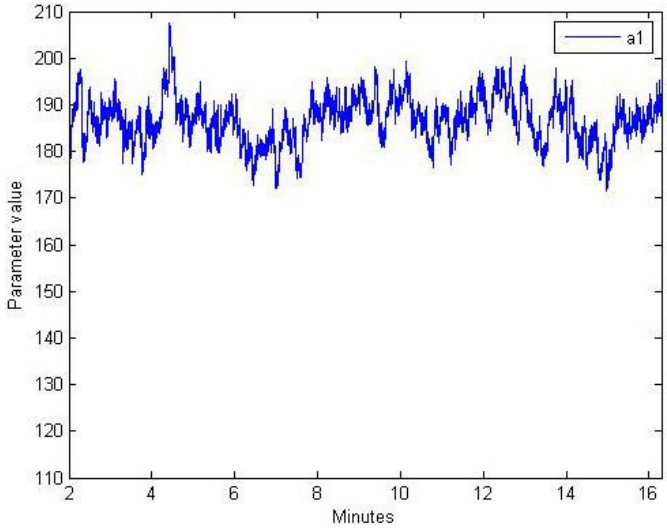

Figure 5.30 Parameter estimations of a_1 in the fault free condition

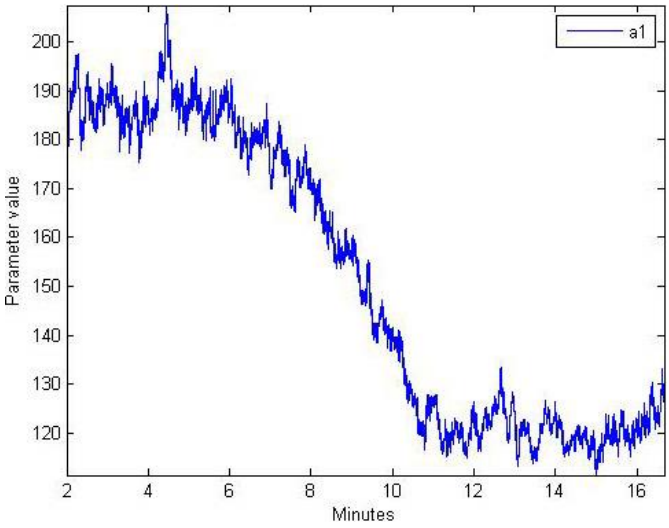

Figure 5.31 Parameter estimations of a_1 as a fault occurs at 6 minutes and stabilises at 12 minutes

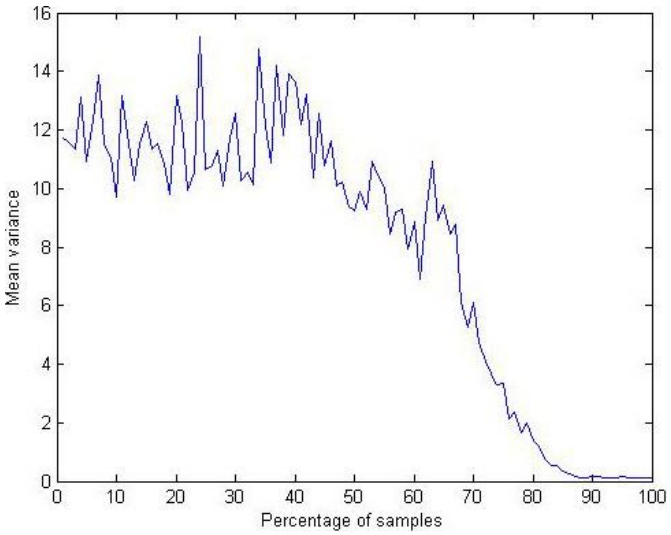

Figure 5.32 Mean input estimation variance as a fault occurs at 40% and stabilises 70%

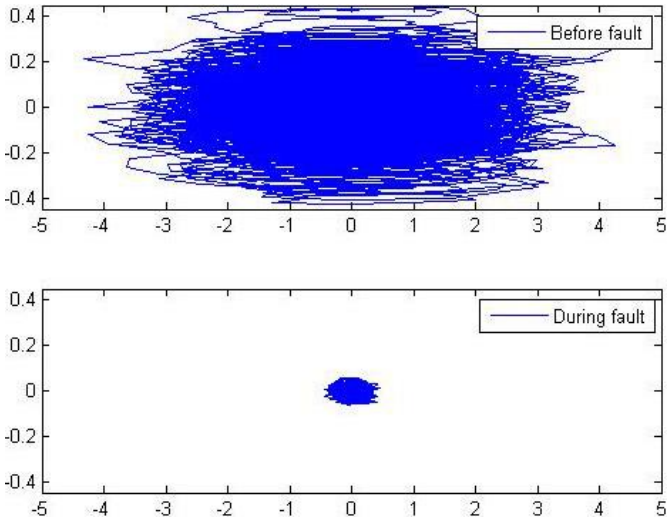

Figure 5.33 Phase portrait of the input estimation before and during a fault

5.6.7. Conclusions

A quarter car suspension model and unknown input observer was developed. The parameters of the transfer function model were estimated with no access to the real (road) input. Diagnostics were developed to identify changes in the system relating to tyre pressure decrease and a majority voting system was proposed.

The diagnostic tests show that it is possible to distinguish between the system in a nominal state and the faulty condition, by the use of three different tests. During the course of the simulation studies it became clear that tuning the observer made a significant difference to the ability of the diagnostic algorithms to track changes in the system. The observer design is dependent on the system matrix *A* and so computing the observer with modified values of tyre spring, k_t, moved the poles of the observer.

This behaviour highlights a property of the fault detector: during a fault, the configuration of the observer is no longer theoretically optimum. The solution to this problem was to start with an observer that is optimally configured for the faulty condition, which happens to work adequately for the fault free condition and is an improvement over the observer which is configured for the fault free case. Further work will include an investigation of the possibility of a multiple model approach with models for a variety of different system states.

With further testing work the value of the estimated parameters could be linked to pressure in the tyre to give an estimation of the real pressure rather than merely indicated a change in the pressure.

Majority voting is the proposed method of defining a fault and this could be further developed into a pattern matching algorithm that can match test outcomes with vehicle states i.e. change in mass, road surface, vehicle velocity to improve the accuracy over a range of driving scenarios.

5.7. Wheel angular velocity comparator

While the wheel rotation observer approach is based on the ABS wheel speed signals (decimal km/h) it is abstracted from the signal in the sense that the signal retrieved from the vehicle data bus (hexadecimal km/h) is conditioned and formatted from the raw data (voltage). Information about these signals is not in the public domain and hence must be interpreted and deduced through systematic experimentation and observation. Developing a robust and reliable ABS is not a trivial task and it took many decades to perfect for series production vehicles (Mercedes-Benz 1978; Bosch 1978). Due to this reason Vehicle OEM generally avoid development of their own ABS, and commission a system supplier for this task. The vehicle OEM specify their requirements and the supplier develops a system that will integrate with the vehicle data bus (commonly a CAN). Due to patent restrictions, each systems supplier OEM (e.g. Bosch, Continental-Teves, Denso) has its own method of acquiring and processing the data but typically this will be broadcast on the vehicle data bus in the form of a km/h value for each wheel that is updated at $10ms$ intervals. The update time is not guaranteed (due to the nature of the CAN) but testing has shown the interval does not typically exceed 30ms and mean interval to be ~14ms with standard deviation of ~5ms.

5.7.1. A simple wheel angular velocity comparator

Detection of changes in tyre pressure from the ABS wheel speed value rests on the premise that wheel radius is a function tyre pressure. As the pressure reduces, the radius of the wheel reduces in value and the wheel angular velocity must be greater for a given vehicle velocity. Herein lies the main constraint of this type of approach, in that such a system cannot detect four simultaneous changes in tyre pressure, as is commonly the case due to normal diffusion losses that occur in pneumatic tyres. It is primarily due to this reason that wheel rotation observer approaches have never been approved by the regulators in European (Regulation No. 64 - Rev.1 - Temporary Use Spare Unit, Run Flat Tyres, Run Flat-System and Tyre Pressure Monitoring System 2010) and North American (US DoT 2005) jurisdictions. In addition to this shortcoming, the algorithm represented by Eqn 5.102 cannot detect simultaneous and equal deflation on tyres sharing an axle or on one particular side of the vehicle. Table 5.11 shows the possible detection combinations. Nonetheless, the wheel rotation observer will be shown to be an effective technique for detecting the majority of puncture-related pressure loss, as this typically occurs in a single tyre. A simple algorithm based on monitoring of the inflation measure, denoted β, is defined by

$$\beta = \left| \frac{(\omega_{LF} + \omega_{RR}) - (\omega_{RF} + \omega_{LR})}{\omega_a} \right| \qquad (5.102a)$$

$$\omega_a = \frac{\omega_{LF} + \omega_{RR} + \omega_{RF} + \omega_{LR}}{4}, \qquad (5.102b)$$

where ω_{LF}, ω_{RF}, ω_{LR}, ω_{RR} denote left front, right front, left rear, and right rear wheel angular velocities respectively, and $\omega_a$is the average angular velocity. In the ideal case, for identical wheel speeds, the tyre inflation measure is

$$\omega_{LF} = \omega_{RF} = \omega_{LR} = \omega_{RR}, \qquad \beta = 0$$

The effectiveness of this algorithm is reduced due to the fact that changes in the pressure of a single tyre are diluted when the vehicle is not driven in a straight line (steering angle ≠ 0). In this context disturbances include normal driving activity such as steering and braking. For nominal tyre condition, P_{rec}, driving in a straight line and normalising the pressure values, the value of the average wheel angular velocity $\omega_a = 1$ and fault indicator $\beta = 0$. These values represent ideal conditions and in practice this value of β is only maintained during steady state cornering and straight line driving. During commencement and cessation of the manoeuvre there will be some discrepancy due to the nature of a conventional four wheel-front steering vehicle arrangement, which is dependent on the wheelbase dimension. Vehicle tests indicate that the effects described above manifests in the calculation of β as deviations from a mean somewhat akin to noise, as illustrated in Figure 5.34. On closer examination of the wheel speed signals, there exists a small amount of variance in the values that cannot be explained by the vehicle dynamics (Figure 5.34c). This may be partially attributed to the rim-tyre dynamic relationship which is exploited by (Persson et al. 2002, Umeno 2002) and it is also likely that some measurement error exists due to the nature of the Hall effect ABS wheel speed sensor that is used on this vehicle. This variance is amplified by the multiplicative nature of the calculation to arrive at a value for β . Whatever the source of this uncertainty, the value of β is close enough to a zero mean value to confirm the fault free condition, particularly in comparison to the faulty condition (Figure 5.35)

Now, suppose the tyre pressures are nominal except the left-front wheel (pertaining to the wheel angular velocity ω_{LF}), which is some value significantly lower than nominal e.g. a puncture ($P_{rec} - 20\%$). For convenience, assuming that a reduction in pressure of 20% is equal to an increase in angular velocity of 20%. In this case, ideal values provide $\omega_a = 1.05$ and $\beta =$

0.19, in theory a fault is correctly indicated. The vehicle tests confirm this result, albeit with a substantially smaller mean value for β, as can be seen in Figure 5.35

Tyre pressure state	Left-front	Right-front	Left-rear	Right-rear	Fault present?	Detect condition?	β	Pattern
All tyres pressure nominal	100	100	100	100	No	Yes	0	⊙⊙ ⊙⊙
Single deflation	-20	100	100	100	Yes	Yes	0.19	⊗⊙ ⊙⊙
Opposite diagonal pair deflated	-20	100	100	-20	Yes	Yes	0.36	⊗⊙ ⊙⊗
Same axle pair deflated	-20	-20	100	100	Yes	No	0	⊗⊗ ⊙⊙
Same side pair deflated	-20	100	-20	100	Yes	No	0	⊗⊙ ⊗⊙

Table 5.111 Percentage tyre pressure combinations and subsequent detection for basic wheel angular velocity comparator (Eqn 5.102)

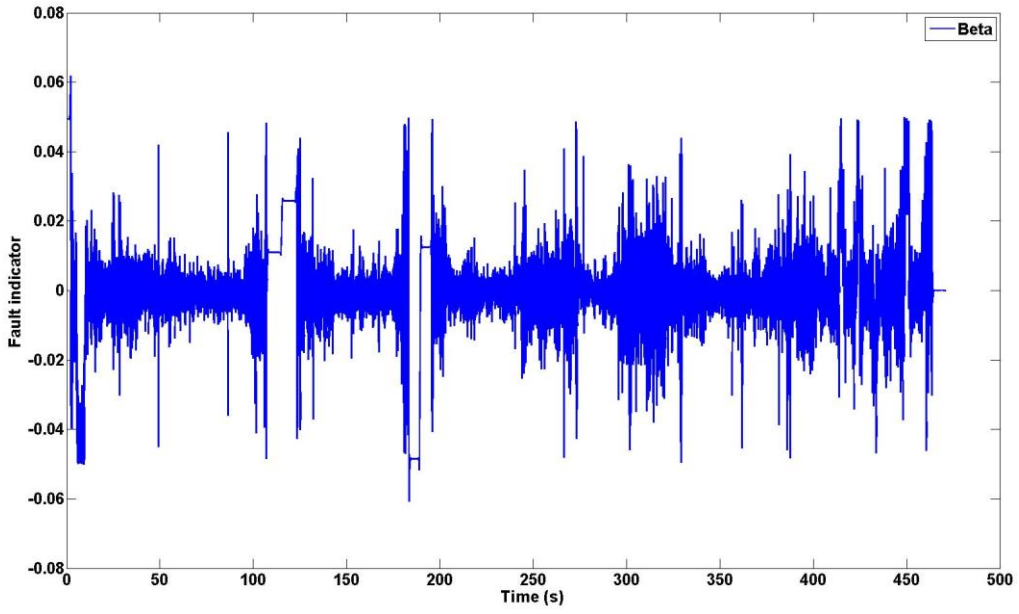

Figure 5.34a Values for β during the course of a drive cycle in the fault-free condition (nominal tyre pressure) mean value of -1.1776e-05 with standard deviation of 0.0113

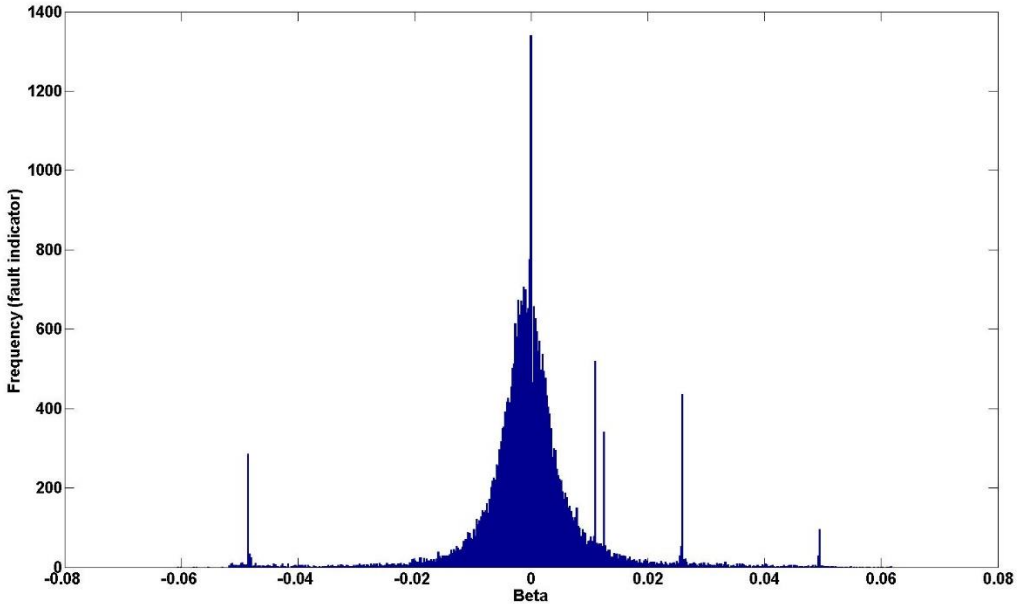

Figure 5.34b Values for β during the course of a drive cycle in the fault-free condition (nominal tyre pressure) mean value of -1.1776e-05 with standard deviation of 0.0113

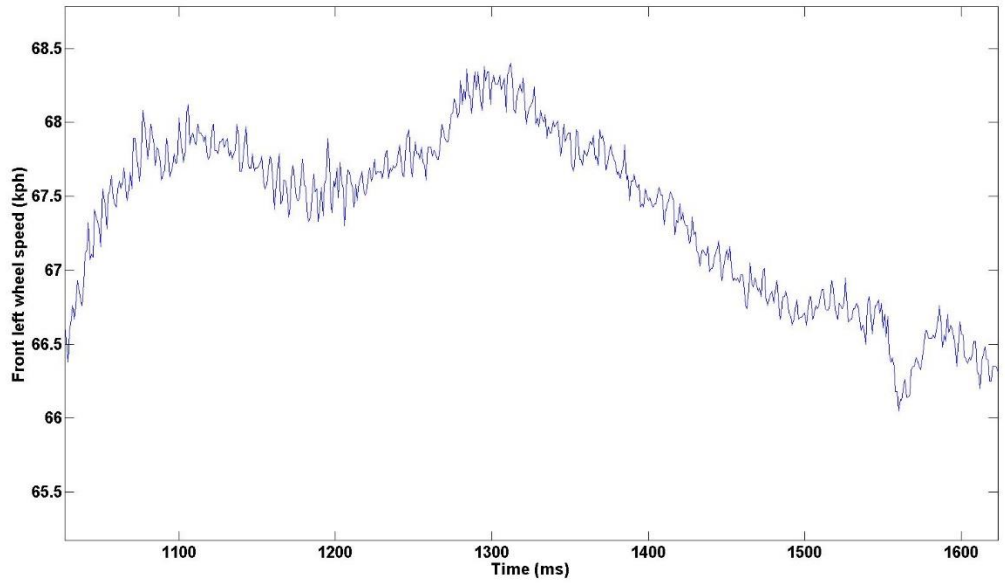

Figure 5.34c Front left wheel speed sensor noise

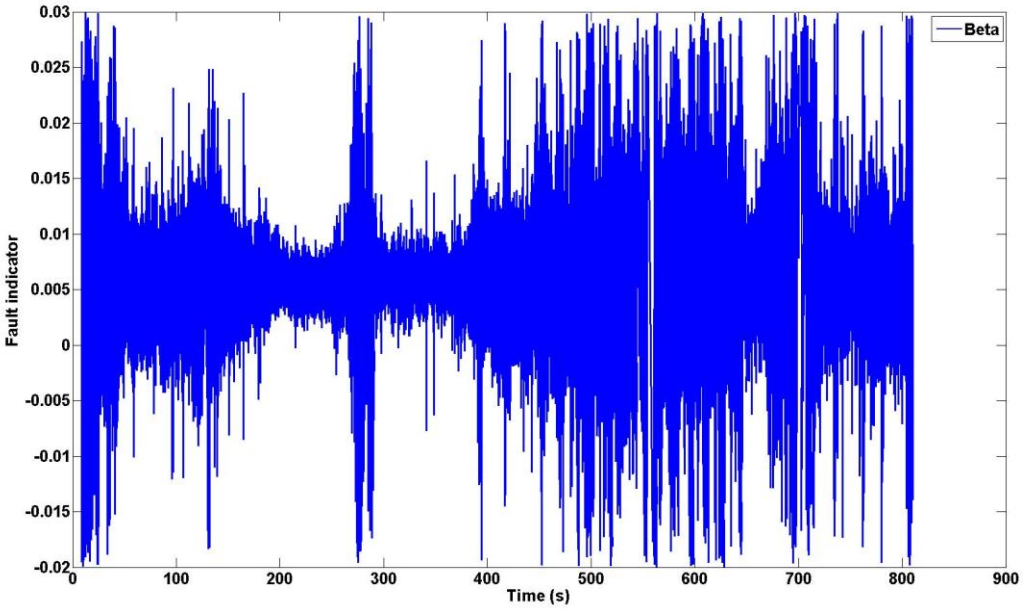

Figure 5.355a Values for β during the course of a drive cycle with a fault present on the front-left tyre (-20% pressure) mean value of 0.0056 with standard deviation of 0.0055

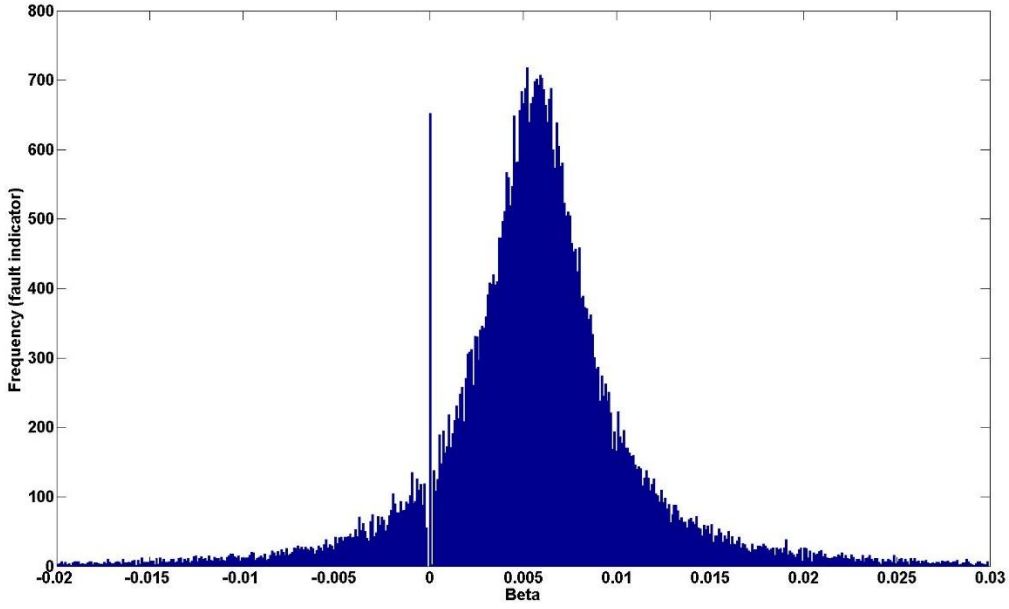

Figure 5.35b Values for β during the course of a drive cycle with a fault present on the left-front tyre (-20% pressure) mean value of 0.0056 with standard deviation of 0.0055

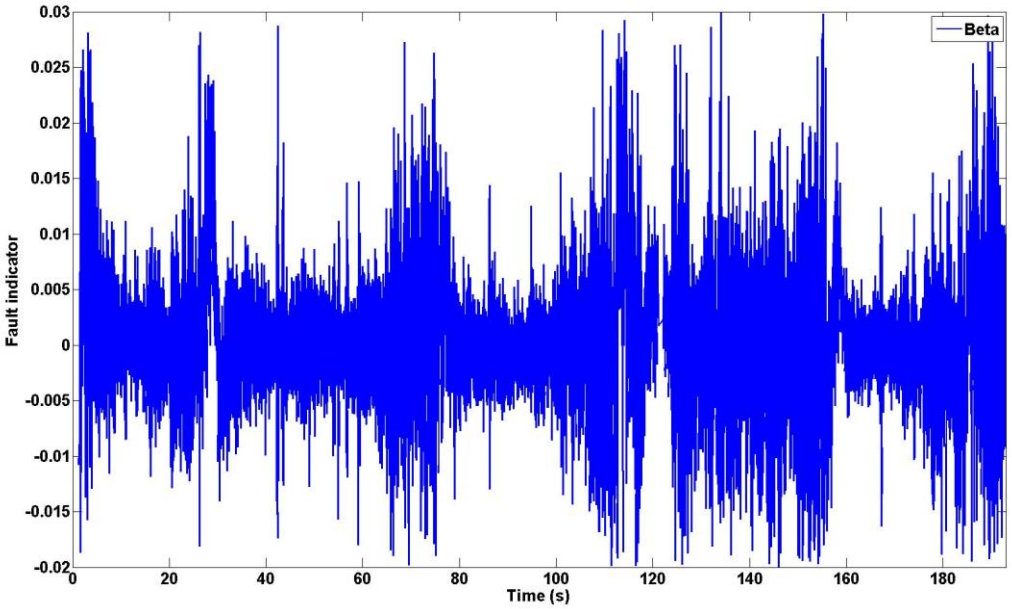

Figure 5.366a Values for β during the course of a drive cycle with a fault present on both rear tyres (-45% pressure) mean value of 3.9182e-04 with standard deviation of 0.0061

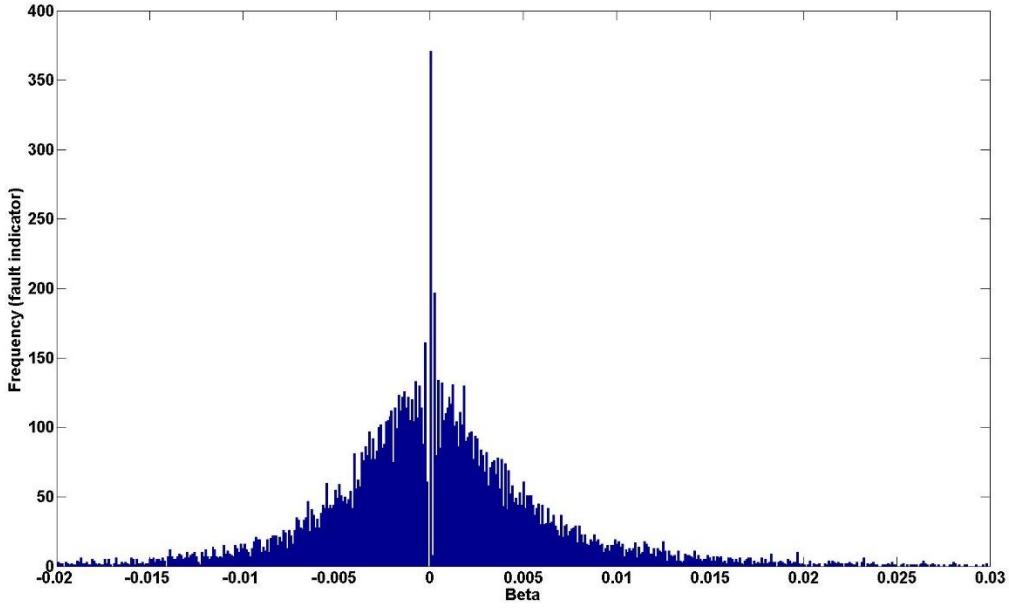

Figure 5.376b Values for β during the course of a drive cycle with a fault present on both rear tyres (-45% pressure) mean value of 3.9182e-04 with standard deviation of 0.0061

5.7.2. Improvements to the change detection method

As can be seen from Table 5.11 the basic wheel angular velocity observer has significant limitations, in terms of detecting patterns of faults, notably an inability to detect simultaneous four wheel diffusion. The problem of detecting four wheel diffusion is solved by the addition of a redundant velocity sensor and a reset mechanism. The reset mechanism may take the form of a simple switch or, with the advent of smart tyres, automatically via an embedded sensor. The premise for the reset function is that the user can know, to some degree of accuracy, what the condition of the tyres are at any given time. The likeliest opportunity to measure the air pressure presents itself at roadside vehicle services, usually attached to a fuel vending forecourt. To establish the nominal set of wheel angular velocities, the user sets the vehicle tyre air pressure in accordance with OEM recommendations and resets the tyre pressure monitoring system. Measurement error in the forecourt pressure gauge is not critical, but it must not be sporadically offset between measurement-inflation of the individual tyres. Now, with the benefit of a redundant measure of vehicle velocity from a GPS sensor, it is possible to build a relationship between the differences in vehicle velocity (a signal conditioned and reported by the ABS from individual wheel angular velocity measurements), and the vehicle velocity value generated by the GPS sensor. Since these differences are small and easily consumed by noise, the information provided by the user via the reset switch adds some additional robustness to the system. It is understood that pneumatic tyres inflated with air lose pressure at a rate typically of 1-2% per month (L. Evans et al. 2009) depending on usage, and this range of values may form the baseline for any algorithm-model that attempts to predict pressure decline in service.

The situation regarding the remaining sources of misdetection – deflations on a shared axle and deflation on the same side of the vehicle – may be improved by utilising other information about the vehicle state that exists on the data bus. It is possible to create a detection algorithm and compensation filter to remove samples that occur during cornering but a simpler approach utilises the steering wheel angle signal. The steering angle (also broadcast on the CAN) is used by the ABS-ESP system to calculate brake force required to stabilise the vehicle in the event of over/under-steer. The vehicle geometry is known and hence with the addition of the steering angle, the calculation to determine the wheel speed may be performed at any time the vehicle is in motion. Figure 5.36 demonstrates the misdetection for the twin deflation on shared axle fault condition. The value of β is clearly zero mean with very little variance despite -45% pressure from nominal on both rear tyres, with front tyre pressure set to nominal for the test.

With respect to Eqn 5.102 this is a satisfactory result, however, the algorithm requires further development as a fault detector.

5.8. Conclusions - condition monitoring and fault detection methods

It is clear from the techniques that have been developed here that no single approach is the solution to the problem of indirectly detecting changes in tyre pressure according to the rules set out by the regulators of the major vehicle markets (Directive 98/69/EC of the European Parliament and of the Council 1998, US DoT 2005).

While it is possible to give an estimate of the pressure, the accuracy of a direct sensing technique is not likely to be possible, even with perfect knowledge of the input. This constraint can, in large part, be attributed to the isolation properties of a vehicle suspension system. The ratio of 10:1 sprung mass to unsprung, which imparts the isolation properties, is a particularly effective filter of information (vibration) that would ordinarily be transmitted into the chassis. This contributes significantly to the difficulty of online estimation of parametric models. It is possible there may be a suspension system where accurate parameter estimation over a wide range of operation is possible, however, it would be an exceptional case. The suspension in racing cars are known to transmit a larger portion of the road shocks into the chassis because they are optimised for superior traction, at the expense of comfort. Regardless of the particular vehicle application, a large unsprung mass (relative to the sprung mass) is not a desirable property as this would impair the ground tracking ability of the tyre and hence is fundamentally at odds with the objectives of suspension.

A secondary obstacle to successful identification and online estimation of suspension parameters is non-linearity in the response. This is primarily attributed to the damper, whose characteristics is often asymmetric in nature, in the sense that the damping value in compression is different to that of extension. In addition to this property, some dampers feature variation of damping over the entire compression and/or extension stroke. The damping values will also change over the life of the vehicle, as the damper function deteriorates due to normal wear in the internal mechanisms. This slow, time-varying, property of the suspension will move the system response further away from any static model and associated fault detection thresholds. Other contributions to the non-linearity include the ‘bump stops’, which are devices intended to prevent suspension component clashes at the extremes of suspension travel. As the unsprung mass comes into contact with the bump stop the force required to move the unsprung mass increases rapidly as the rubber in the bump stop compresses and hardens.

Despite the above challenges, the methods which are proposed in this Chapter, form a suite of algorithms which provide the basis for a supervisory system whereby the outputs from the algorithms may be combined in a ‘data fusion’ manner. Indeed as the number of on-board control systems and communicating sensors over networks increases, the enabling technology to realise the implementation of proposed indirect approaches will have evolved to form the next development cycle.

Chapter 6.

Discussion: conclusion and further work

When this research started, it was based on the premise that if a passenger can sense the change in tyre pressure through the ride and handling characteristics of a particular vehicle, then it should be possible to devise some systematic method of determining what the character of this sensation is numerically. Initial studies showed some promise and the research proceeded to the validation stage. Tests were commissioned that have been described in Chapter 3.

An aspect of the vibration isolation properties of the suspension became obvious when testing the algorithms with data acquired from the Jaguar X-Type. It is a significant challenge to detect subtle changes in tyre pressure, purely from chassis acceleration or displacement measurement. The system is weakly identifiable due to the relatively small unsprung mass which does not cause serious perturbation of the chassis until large scale disturbances are applied to the road wheels.

6.1. Discussion: Modular approach with supervisory diagnostic

In the field of automotive engineering, the concept of a supervisory control has emerged in recent years with the advent of hybrid powertrain technology. Combining multiple sources of torque and energy storage devices to work in concert is a non-trivial task. An inevitable result of this work has been the development of an overarching controller that allows the various components to pass energy between themselves, for dissipation as drive torque in the case of motor-generators or flywheels and energy storage, in the case of batteries and flywheel. Since many of these components are costly and easily damaged (Lu et al. 2013), the supervisory control must also be a prognostic ‘health’ monitor that determines how much energy can flow through the components before damage occurs. When damage occurs the supervisory control usually attempts to limit the amount of damage (via a ‘limp-home’ reduced functionality mode) and assist in the maintenance actions in the service bay (Pisu and Rizzoni 2007).

It is envisaged that the methods outlined in this thesis could be deployed in a similar fashion, with an overarching supervisory diagnostic routine that decides upon the condition of the tyre based on data produced by the individual sub-systems. This approach is typically called ‘data

fusion' in the literature. Each diagnostic has its own 'character', that is to say, zone of operation and sensitivity to certain driving conditions such as smooth roads, which provide little information for model-based and spectral analysis methods. The vehicle may also change quite radically in terms of its physical parameters, such as added mass which may account for as much as 50% of the curb weight. Since it is not generally possible to have an exact measure of the additional mass, the supervisory diagnostic must take this into consideration in order to avoid false positives. This situation could be mitigated using a similar approach to the tyre pressure diagnostic using network-derived variables such as engine load, throttle position, vehicle position (GPS) and inertial sensors to determine vehicle mass (McIntyre et al. 2009, Winstead and Kolmanovsky 2005, Li, L. and Wang, F.-Y. 2007, Leung 2010). For the model-based and spectral approaches, the supervisory diagnostic should also consider vehicle aging properties, with respect to the gradual shift in parameters that accompanies worn and degraded components. The diagnostic system robustness is a function of careful implementation and testing of all conceivable scenarios and this includes every failure mode of the suspension system and sub-systems that the tyre diagnostic relies upon (control systems whose sensors supply data). This type of analysis is usually conducted with the support of a failure modes and effects analysis (FMEA) and a fault tree analysis. The sub-system designers play a significant part in this process, for it is they that know the system in detail. If the tyre pressure diagnostic designer is situated within a vehicle OEM, it is unlikely that any system supplier will fully disclose all aspects of their sub-system design, as this is their intellectual property. This leaves the designer with some uncertainty which will inevitably permeate the model. Since tyre pressure and general condition are regarded as safety critical and with increasing scrutiny from legislators (Directive 98/69/EC of the European Parliament and of the Council 1998, US DoT 2005, Regulation No. 64 - Rev.1 - Temporary Use Spare Unit, Run Flat Tyres, Run Flat-System and Tyre Pressure Monitoring System 2010) the burden for a robust solution intensifies.

A multiple method approach is also appealing for its flexibility. For instance, a high specification luxury vehicle may have upwards of 80 individual electronic controllers (Mercedes-Benz 2013) connected together on an array of high bandwidth data buses. This type of vehicle platform generates vast data sets from the sensors and control sub-systems. Powerful, high throughput (Muramatsu et al. 2002) and/or highly parallelised (Asano, S. et al. 2009) processors are required for image recognition driver assistance systems. CPU are rarely 100% utilised 100% of the time, when the image processing ECU is not fully utilised, the tyre pressure algorithm can be executed piecemeal.

In the case of a small inexpensive vehicle, the diagnostic would be scaled back appropriately for the sensor data that is available. As technology advances, so governmental regulation of vehicle systems inevitably increases. Since 2011 it has been mandatory for all new vehicles to be equipped with ESC, which includes ABS functionality (FMVSS 126 2011). ABS has been an EU mandated system since 2007. This situation creates a rich environment for the deployment of model-based diagnostic routines.

It is envisaged that the diagnostic would be modular for the purposes of re-use and deployed irrespective of the particular vehicle platform, configured for the particular application.

6.2. Conclusions on findings of tyre pressure monitoring systems

Following on from the literature review of existing and emerging techniques for tyre pressure monitoring, it has become apparent that, prompted largely by impending legislation, numerous ideas have been put forward. The majority of these involve direct measurement which have their immediate drawbacks and potential under certain circumstances. The work detailed in this thesis has focused on indirect measurement, this being prompted by the availability and abundance of data, as outlined in Section 6.1. The specific outcomes of this work, in order of significance, as perceived by the author, are as follows:

The most significant piece of work is considered to be that of the tyre pressure diagnosis via a wheel angular velocity comparator. Whilst earlier patents may be found (Walker, J. C. and Rehal 1993) no detailed description of the method exists in the literature. Rather this piece of work, which involved practical, experimental and deductive analysis, is original in that it makes use of an independently developed approach which acquires and interprets CAN data directly from a vehicle. The method also provides a platform from which other algorithms based on vehicle data may be created. This was achieved with basic tools and available open source software/freeware, rather than state of the art data acquisition DAQ equipment.

A further significant contribution which is considered to be marginally of a more secondary nature is the development of model-based tyre pressure diagnosis via application of an unknown input observer and a parameter estimation scheme. Research into systems described as being stiff, whereby the dynamic modes are significantly distant, yet interact with each other, has shown that continuous-time estimation methods are superior over their discrete-time counterparts. Specifically, a continuous-time, model-based tyre pressure change detector is

enhanced by the addition of an unknown input observer that simultaneously reconstructs the road profile input and provides a fault diagnostic in the form of a phase portrait.

The next contribution, in order of significance is that of model-based tyre pressure diagnosis via an enhanced filter configured to estimate states, including the input. In this work the term 'enhanced Kalman filter' has been assigned due to the inclusion of the input among the states that are estimated. The continuous-time, model-based tyre pressure change detector is enhanced by the addition of the Kalman state estimate of the road profile and gives an estimate of the tyre sidewall height, which is a function of the tyre pressure.

A further contribution is that of model-based tyre pressure diagnosis via cautious least squares (CLS). Essentially CLS is used as a fault detector by the addition of a parameter reset counter. Analysis of the fault counter provides some insight into the tyre condition. Two estimators are trialled and compared, namely recursive least squares and a Kalman filter.

A minor interesting contribution is the investigation and critique of the effects of the choice of sampling interval on discrete-time models and estimation thereof, with the corresponding continuous-time model and estimation of parameters. This underpins the work described above in model-based tyre pressure diagnosis via an enhanced filter.

In summary, the culmination of the work as outlined above provides the potential and basis for a new generation of indirect tyre pressure monitoring systems which could be migrated across the vehicle fleet. The indirect method offered by the proposed multi-modal supervisory framework is less expensive and more reliable and satisfies legislative requirements.

6.3. Conclusions of the aim and objectives

This section of the conclusions specifically addresses the overall research aim and the various objectives stated in Section 1.2, in order to discuss the outcomes.

Assess the feasibility of tyre pressure estimation – initial feasibility testing was achieved with the aid of the MEPHM (Chapter 3.1.1). The sensor module was assessed for suitability (bandwidth and sensitivity) and calibrated using a linear actuator driven by a sine function. The vehicle test results suggested that it was indeed possible to quantify the effect of tyre pressure on the ride which indicated potential for a spectral solution to the pressure estimation problem. While these tests were not exhaustive or carried out under strictly controlled conditions, it

warranted further investigation and the commitment of resources for the work of simulating the suspension.

Simulation of suspension, estimation and road – this work was realised in The Mathworks packages, MATLAB and Simulink. Due to the proliferation of the motor vehicle generally and the accompanying development of computerised design and analysis techniques, a large body of literature exists on the properties of conventional passive suspension systems with respect to modelling techniques. This situation obviated the requirement to develop a completely unique set of models for the purpose of fault detection. As a result the task was reduced to the selection and implementation of the appropriate models for the particular algorithms, in order to integrate the model into the overall scheme of the parameter or state estimator. In the initial phase of development, simple discrete-time transfer function and state space models were implemented in MATLAB which provided the I/O data streams for the RLS estimator. A white noise signal was utilised as a road input and this was enhanced with the inclusion of a quasi-random road generator. As a result of the vehicle road simulator test at the CREST facility, a drive cycle signal was obtained and used for the remainder of the research. This data set was obtained by Jaguar Land Rover engineers for the purpose of noise-vibration-harshness testing from acceleration measurements of a road-going vehicle abstracted to a vertical displacement value used to drive a set of hydraulic rams. The data represents a selection of real-world roads which improved the realism of the quarter-car simulation, particularly with respect to sensitivity testing for specific road types. For the CT model-based estimation algorithms, a state variable filter was implemented in Simulink which provided the value of the differentials that formed the observation vector for the RLS-based algorithms. The CT model is favoured over the DT counterpart due to the problems associated with estimating stiff systems. A non-linear damper with backlash was implemented in the later stages, however, this was considered an unnecessary complication for the purpose of fault detection development.

Quarter car model – Following extensive analysis of simulation and vehicle testing it is clear that the majority of the dynamics can be explained by a linear quarter car model. This is due to a number of factors. While it is true that a major contribution to non-linearity in the suspension is due to the damper's typically (in the majority of passenger vehicles) bilinear character, much of this behaviour is found at the fringe of the suspension travel and can be discounted for the majority of a typical drive cycle. It is also true that whilst measuring some state in one corner of a vehicle suspension, the effects of the road input propagate through the chassis from the other corners and effect the measurement. However, in practice this contribution is not

significant enough to cause false detection of faults, due to the overwhelming contribution to the signal power generated by the particular quarter suspension in question. This tends to be more so at the front of a typical vehicle because the front suspensions do not share an axle and many do not at the rear. Other minor contributions to the non-linearity result from the action of the bump stops, which can be disregarded for the same reasons as the damping component, effects such as stiction are minimal due to the large forces generated and backlash is not present in any significant proportion for a properly functioning vehicle. These facts pave the way for the use of transfer function models of the suspension, with all the analytical benefits this confers.

In practice, many different models were developed when the need arose, such as testing the sensitivity of individual parameters in a parameter estimation scheme. In order to achieve this in simulation, a second companion transfer function model was developed in Simulink, which allows control of individual parameter values. The same control can be achieved in the case of the suspension states using a phase variable model, as in the case of the enhanced Kalman filter of Section 5.5. Simulink was the preferred platform for these types of models, due to the complexity of implementation in a scripting language such as MATLAB.

Constraining the complexity of the models usually has the additional beneficial effect of reducing the volume of potential sources of errors in the encoding, implementation and calculation. The enhanced Kalman state estimator and phase variable model of Section 5.5 was the only algorithm to be effected by any significant computational problems, which were identified as being dependent on sensitivity to physical parameter values. The tyre damping value in particular prevented the MATLAB simulation algorithms from converging to a solution, despite solver selection and attempts to reduce the integration step size. During simulations, the tyre damping value was generally set at a small value, in keeping with the physical properties and its effects are considered to be insignificant in this application. However, the tyre dynamics with respect to pressure are an obvious target for further research, particularly with respect to the dynamical rotational relationship between wheel rim and tyre. This relationship is most readily explored via the ABS wheel speed signal (not to be confused with the wheel speed value, published on the CAN by the ABS sub-system).

Robustness and reliability – is a key area of study for any safety critical system. Since any algorithm will inevitably be implemented on a microprocessor, it is likely never to be deemed completely robust, even if the algorithm itself can theoretically be shown to be bug-free. Due

to the harsh environment that the system exists in (vehicle) and uncertainty in the measurements and disturbances (unknown road input, signal interference, vehicle degradation and modification) the challenge is to detect change in pressure in accordance with the particular regulatory thresholds without generating any false positives, over the life of the vehicle. Confidence in the reliability of the system is dependent on the thoroughness of the testing regime, which must include all conceivable and likely vehicle states and conditions, such as tyre wear or user changes the tyres, sensor and suspension hardware degradation, faults in a network node and extreme driving scenarios. It is considered that the modular approach detailed in this thesis is a mitigation for many of these sources of error because the system does not rely on a sole sensor or feedback mechanism for its operation.

Unknown road input – is the single greatest challenge for any model-based pressure change detection algorithm. As any road user can attest, the road surface can change dramatically in character and elevation over a very short period of time. This poses a problem for an algorithm that is not party to this input-disturbance and yet has a dramatic effect on any attempt to numerically determine the state of the vehicle. The situation the vehicle user finds himself in is only marginally improved. For example, there is a certain amount of trust and confidence that is required to drive a vehicle along a dark motorway at 70mph. The mitigation for this deficit in knowledge is in a modular approach that gathers all available sources of information in order to arrive at a consensus. Advances in vision systems that provide an assessment of the road surface elevation present the possibility of improving the confidence in the estimation significantly, although complete knowledge of the road is not likely to be achievable. It is the opinion of the author that it is unlikely there can be any reliable indirect tyre pressure change estimation without the inclusion of ABS wheel speed sensors. These sensors, crude as they are, form the backbone of the mitigation for unknown road disturbance and provide a more direct source of information that improves convergence time to change detection, unlike spectral or parameter estimation techniques which must gather many samples before arriving at a diagnosis of average behaviour.

Regulatory requirements – should form a useful benchmark for the algorithm developer, although only regulations for US and EU markets have been considered in this thesis. In general the regulations for automatic tyre pressure monitoring are concerned with two factors: punctures and diffusion. The definition of a puncture is not absolute but is typically interpreted as a ‘rapid reduction of pressure’, with a total rapid deflation or ‘blow-out’ at the extreme end of this spectrum. Very little research exists in the prediction of tyre blow-out failure and there

is no technology that is presently able to detect an incipient blow-out event and as such this is not considered in the EU or US regulations. Diffusion is interpreted as the natural loss in air pressure that a pneumatic tyre system undergoes during its service life. There is no definition of what constitutes normal diffusion pressure loss however, it is estimated that a typical passenger vehicle loses 0.068bar per week (Gent and Walter 2006)

For the EU market the regulation requires that the vehicle be conditioned prior to tyre pressure detection testing such that the ambient effects on the test result are minimised, with the main contribution being tyre temperature. The vehicle is subjected to a prescribed drive cycle such that the vehicle velocity is maintained for a specific duration and situations that would lead to disturbances such as wheel slip are avoided. A log is kept for the tyre pressure at the start of the test and is manipulated during the test in order to simulate the two failure modes, puncture and diffusion. The detection mechanism is given a time limit after the manual reduction of tyre pressure during the drive cycle in which it must flag a pressure drop by means of a dashboard indicator. There is no requirement for the actual pressure to be indicated, although many direct TPMS possess this feature, merely that the system detects a pressure drop of 20% of the nominal tyre pressure for the particular load state of the vehicle (the OEM tyre pressure specification typically states two conditions – single occupant and fully loaded). The pressure threshold is identical for both puncture and diffusion tests as this has been deemed to be a critical threshold for safety and rolling resistance considerations by the regulatory committee. There is a time limit of 10mins for detection of punctures and 2 hours for diffusion, although the regulation does not prescribe an upper limit.

Testing and validation – was described in Chapter 3 and comprises of three sets of tests using three candidate vehicles. The aim of the testing was twofold:

- validation of the various approaches that were developed in simulation
- analysis that would lead to improvements in the modelling of the suspension system, be it parametric or spectral.

Spectral feasibility testing

In this test a Volvo V40 was used. The tests (described in Section 3.1.1) were an attempt to analyse the effect of tyre pressure on the spectral properties of the chassis such that a numerical measure could be achieved for the driver experience when driving with one or more tyres underinflated. Subjectively, the vehicle dynamics subtly change as diffusion progresses and it may be extremely difficult for the driver to detect any change initially, particularly when these

changes are considered against a backdrop of a multitude of other disturbances such as road surface and friction coefficient, tyre temperature and wear and added vehicle mass. To further complicate matters, this subjective difference in ride and handling is a function of the particular drive cycle. For instance, changes will be significantly more difficult to detect if there are minimal cornering forces, as would be the case during motorway driving where curves in the road generally do not exceed a radius of 1km (Highways Agency 2008) and hence lateral dynamics will not be manifest. Similarly, shifts in the wheel hop frequency that accompanying tyre pressure change are likely to be completely undetectable for the majority of drivers, particularly during the initial phase of diffusion. Indeed, the shift is relatively difficult to measure as it is confined to a spectrum of approximately 5Hz (Craighead 1997), depending on the characteristics of the particular tyre, and may only be reliably detected after a substantial number of samples have been collected.

It was noted that during the testing, no significant changes in the vehicle dynamics were manifest. Due to safety considerations on the public highway, hard cornering was avoided, which diminish the lateral dynamic properties from the experience, as can be seen from the y-axis measurements in Section 3.1.1. As an initial estimate, it was satisfactorily clear that enough of a numeric change was present in the x-axis in order to proceed with the research and invest time developing sophisticated detection algorithms and commission further testing to validate the hypotheses.

CREST road simulator testing

In this test a Jaguar X-Type was used. The testing (described in Section 3.1.2) was arranged such that as many of the disturbances that could be practically avoided were eliminated from the measurements. Principle amongst these disturbances was the unknown road input itself, which was mitigated by use of the CREST road simulator at Land Rover, Gaydon. The CREST facility was configured such that only one wheel of the vehicle received the road input, in order to reduce the effect of road excitation from the other wheels.

The main aim of the test was to create a data set that could be used to access the efficacy of a given fault detection approach. A series of five tests were executed at tyre pressure levels of 100% of nominal down to 0%. During the course of the ten minute drive cycle, the road displacement was logged at 200Hz and the chassis displacement was logged at 500Hz. An attempt was made to log data using the same DAQ hardware but it was not physically possible to achieve this with the equipment that was available. The log of the road input was obtained

from the hydraulic drive controller which poses the additional problem of synchronicity of the measurements. This situation was mitigated by inserting a period of dwell time at the start of each test where the road elevation was maintained at 0mm. This dwell time is clear from the measurement log and with some experimentation it is possible to synchronise the measurement start points in the data, which is obviously of crucial importance for any system identification or fault detection algorithms. The remaining discussion on this research is continued in the final section, System identification of quarter car suspension.

ABS wheel speed testing

Due to the fact that ABS wheel angular velocity comparators were the original indirect tyre pressure change detection method and much research already exists in this area, this method was originally not targeted during this research. However, as work progressed on the other indirect methods, described in Chapter 5, it became obvious that the unknown road input is a significant problem and a method to mitigate for this unknown disturbance is necessary to improve the diagnosis to an acceptable level.

Industrial standard CAN dataloggers such as Vector CANalyzer are prohibitively expensive, yet the CAN standard itself is in the public domain and the diagnostic interface (by which the data bus is accessed) is an international standard. These facts led to the development of low cost CAN hardware and software tools in recent years that have now proliferated via the internet. This situation has provided a platform for independently created diagnostic solutions, in the vein of the approach presented in Section 5.7. The research for this approach consisted of two phases

- Identify and acquire wheel angular velocity, steering angle and brake pedal signals
- Condition the signals and develop wheel angular velocity comparator

The task of identifying the signals is onerous. The output of almost every sensor on the vehicle is broadcast on the data bus which results in approximately 20-30 individual CAN messages, each containing up to 32 individual signals. All of the signals are encoded in hexadecimal, with variable length, sign and resolution, preventing a casual inspection from determining signals of interest. To compound this situation, none of this information is in the public domain which results in a painstaking search comprised of targeted experiments in the vehicle and importation of the data log into MATLAB for analysis. Some educated guesswork is required in the initial stages (detailed in Section 3.1.4) but once the signals of interest have been identified, a series of tests are carried out under controlled conditions (tyre pressure and temperature, road type)

in order to obtain signals that represent the vehicle in various driving scenarios with various tyre pressure values. In the final analysis, the wheel angular velocity comparator is considered to be a vital component of any indirect tyre pressure estimation scheme, due to its resilience to the unknown input disturbance of the road profile and rapid convergence to diagnosis that hinders the analysis by model based approaches.

The results from the test road simulator test only partially met the aim of providing a quarter car model, for reasons that are not completely apparent, but it is likely there are some significant measurement errors in the data. When using the data to identify a model for the quarter car, there are large variances in the RLS parameter estimate and covariance blow-up phenomenon is a problem. In an attempt to identify the source of this problem, the drive cycle is split into its component parts and estimated separately. The result of this exercise revealed that highly energetic portions of the drive cycle, such as 'third world road', produced inferior estimates, when compared to 'motorway cruising'. This result is counter intuitive because estimation schemes with substantial 'information' generally have an advantage over those with a lower level of input excitation. In this case, the problem is considered a question of identifiability, due to the filtration effect of the suspension. Consider a typical wheel hop frequency of approximately 13Hz, which represents the resonance of the quarter car suspension system, the overall bandwidth is confined to approximately 40Hz. Any inputs that lie outside this frequency window are attenuated to a level that is not conducive to system identification. Anecdotally, as a witness to the testing, it was obvious that a large portion of the input was simply missing from the output, due to the effect of the damper and suspension in general. A mitigation for this effect is achieved through filtering of the signals, selecting a time constant that matches that of the suspension, thereby removing the high frequency portion of the input signal before estimation of the parameters. This approach yielded a linear model that achieved ~85% fit in terms of R_T^2. The model fit is improved marginally by constraining the estimation to the linear portion of the damper response. It is considered that the remaining ~10% can be attributed to measurement error and non-linear effects that are described in Chapters 4 and 5.

6.4. Further work

6.4.1. Sensitivity analysis

Although the algorithms have been tested for their sensitivity to faults and various inputs and parameter variations, this has been done singularly for the obvious reason that testing multiple algorithms at the same time would make judging their individual effects significantly problematic, perhaps even impossible. An area of work that warrants further study is fault detection sensitivity and range of operation. It is envisaged that this could be achieved with a vehicle test where as many of the parameters and variables of interest can be controlled or at least observed. The Crest facility detailed in Section 1.3, or a 'rolling road' would be likely candidates for the study of spectral properties and model-based parameter estimation schemes. In addition there should be a variety of normal road-going drive cycles, urban, A-road and motorway driving in order to cover the full range of driving scenarios. The threshold requirements are well understood and laid out in Chapter 1.3. A property of the vehicle that has not been studied in this thesis, is the thermal properties of the tyre. It has been noted during the course of a ~30min drive cycle that the tyres become warm to the touch, despite an ambient temperature of ~5°C. The tyre pressure was noted before and after the drive cycle and found to be 0.14bar (2psi) greater after the test. It is considered likely that the heating phenomena will cause the parameters of a transfer function model to change, which could be a source of false positives. The sensitivity analysis should address all of these points in order to guarantee the robustness of the fault detection scheme.

6.3.2. Application to blow-out prediction

A criticism of indirect approaches to tyre pressure monitoring is the uncertainty in the estimate and the algorithms ability to detect rapid pressure loss. However, continuous sampling and reporting of tyre pressure is not required (Regulation No. 64 - Rev.1 - Temporary Use Spare Unit, Run Flat Tyres, Run Flat-System and Tyre Pressure Monitoring System 2010), or particularly useful, as typical puncture dynamics are not significantly developing at the millisecond-second level, unless there is a catastrophic failure. In such a case no TPMS will detect this condition (Patwardhan et al. 1997) in a manner that the driver can make any timely or meaningful use of the information. It is debatable whether an absolute measure of tyre pressure is actually required or useful in the majority of small passenger vehicles. Many vehicle users are not aware of their tyre pressure and not curious to discover it (Singh et al. 2009) until there is a manifest problem indicated by visual inspection or degraded vehicle ride and

handling. For these reasons a simple threshold warning should be sufficient for the majority of users. The most effective way to manage tyre failure is to maintain the inflation pressure (Singh et al. 2009), a situation which is improved with automatic periodic oversight of the tyre pressure.

A possible extension of the work presented in this thesis is vibration analysis, particularly at the unsprung mass, since this is a common precursor to catastrophic failure (Modarres et al. 1999), the parametric and spectral models have potential as detection mechanisms for vibration modes associated with tyre condition. This area is considered, by the author, as being worthy of further investigation.

A method that merits further attention is the analysis of the tyre-rim dynamics. The relationship between the road surface, the tyre and the wheel rim can be modelled as a mass-spring-damper. It is known that the tyre stiffness has a significant effect on the distribution of the frequency spectrum at the axle (Umeno et al. 2002, Persson et al. 2001b) as the wheel rim angular displacement is fractionally out of phase with the tyre tread. This property is due to flexion of the tyre carcass, the extent of which is likely a function of the tyre sidewall height, and general construction of the tyre. If a transfer function model of sufficient fidelity can be calculated, the tools of system identification and spectral analysis can be applied to the problem.

6.3.3. Practical implementation

Following the experimental procedure in this work, as detailed in Appendix 2, the next phase of the development towards realising a supervisory diagnostic framework for tyre pressure monitoring, using the methods proposed in Chapter 5 and summarised in Section 6.2, it is envisaged that a vehicle manufacturer/systems supplier could readily take the work forward. As stated in Section 6.2, the culmination of the work presented in this thesis would see a new generation of tyre pressure monitoring systems which could be practically implemented by an OEM and rolled out across the vehicle fleet.

References

Asano, S., Maruyama, T. & Yamaguchi, Y., 2009. Performance comparison of FPGA, GPU and CPU in image processing. *FPL 09: 19th International Conference on Field Programmable Logic and Applications*, pp.126–131.

Atherton, J.P., 1992. Tyre deflation sensing. In *International Symposium On Automotive Technology And Automation*. FLORENCE, pp. 43–48.

Atmel, 2008. *ICs for Tire-pressure Monitoring Systems*, San Jose. Available at: http://www.prnewswire.com/news-releases/atmel-introduces-very-low-current-transmitter-ics-for-tire-pressure-monitoring-applications-72363742.html.

Basseville, M. & Nikiforov, I. V, 1993. *Detection of Abrupt Changes - Theory and Application*, Englewood Cliffs, N.J.: Prentice-Hall Inc. Available at: http://citeseerx.ist.psu.edu/viewdoc/download?doi=10.1.1.77.6896&rep=rep1&type=pdf.

Beeson, M.J. & Ishihara, H., 1998. Tyre deflation warning systems. In *European Conference on Vehicle Electronic Systems*. Coventry, pp. 8.2.1–8.2.9.

Bosch, R., 1991. *CAN Specification*, Stuttgart. Available at: http://www.bosch-semiconductors.de/media/pdf_1/canliteratur/can2spec.pdf.

Box, G.E.P. & Draper, N.R., 1987. *Empirical Model-Building and Response Surfaces.*, New York: John Wiley & Sons.

Box, G.E.P., Jenkins, G.M. & Reinsel, G.C., 2008. *Time Series Analysis*, Hoboken, New Jersey: John Wiley & Sons, Inc.

Brewer, H.K. & Rice, R.S., 1983. Tires - Stability and Control. In *International Congress & Exposition*. Detroit, USA. Available at: http://papers.sae.org/830561/.

Burnham, K.J., 1991. *PhD Thesis: Self-tuning Control for Bilinear Systems*. Coventry Polytechnic, Coventry, UK.

Burt, M., 2014. Dunlop reveals intelligent tyre concept at Geneva. *Autocar*. Available at: http://www.autocar.co.uk/car-news/geneva-motor-show/dunlop-reveals-intelligent-tyre-concept-geneva.

Carlson, C.R. & Gerdes, J.C., 2005. Consistent Nonlinear Estimation of Longitudinal Tire Stiffness and Effective Radius. *IEEE Transactions on Control Systems Technology*, 13(1), pp.1010–1020.

Chen, J., Zi, Y., He, Z., Yuan, J., 2012. Improved spectral kurtosis with adaptive redundant multiwavelet packet and its applications for rotating machinery fault detection. *Measurement Science and Technology*, 23, p.045608.

Chen, J. & Patton, R.J., 1999. *Robust Model-Based Fault Diagnosis For Dynamic Systems*, New York: Springer Science.

Choi, E.-H., 2012. Report: *Tire-Related Factors in the Pre-Crash Phase*, National Highway Traffic Safety Administration, Washington, USA

Clark, S.K. & Dodge, R.N., 1979. *A handbook for the rolling resistance of pneumatic tires*, Ann Arbor.

Continental, 2015. Intelligent Tire Systems. *Press release*. Available at: http://www.continental-automotive.com/www/automotive_de_en/themes/commercial_vehicles/chassis_safety/chassis_electronics/intelligent_tire_system_en.html?page=3.

Corona, D.L. & Komendanchik, M.E., 2008. *Bridgestone/Firestone Recall: A Case Study in Public Relations*, Louisiana. Available at: http://dcomm.cxc.lsu.edu/portfolios/09spr/dcoron1/BridgestoneFirestoneCaseStudy.pdf.

Craighead, I.A., 1997. Sensing tyre pressure, damper condition and wheel balance from vibration measurements. *Proceedings of the Institution of Mechanical Engineers, Part D: Journal of Automobile Engineering*, 211(4), pp.257–265. Available at: http://pid.sagepub.com/lookup/doi/10.1243/0954407971526416.

Csere, C., 2001. Why are Ford Explorers Crashing? *Car and Driver*. Available at: http://www.caranddriver.com/columns/why-are-ford-explorers-crashing.

Deutz, 2014. Deutz Engine Control EMR 3 CAN BUS specification. Available at: http://www.tibban.com/Parts_and_Manuals/Manuals/Engines/2013/EMR3_CAN_BUS_Specification_ver11-3.pdf.

Dixon, B. Kalinin, V. Beckley, J. Lohr, R.., 2007. A second generation in-car tire pressure monitoring system based on wireless passive SAW sensors. In *Proceedings of the IEEE International Frequency Control Symposium and Exposition*. pp. 374–380.

Ersanilli, V.E., Reeve, P.J., Burnham, K.J., 2009. A Continuous-Time Model-Based Tyre Fault Detection Algorithm Utilising a Kalman State Estimator Approach. In *IAR Workshop on Advanced Control and Diagnosis*. Zielona Góra.

Ersanilli, V.E. & Burnham, K.J., 2014. A survey of vehicle tyre pressure detection methods and related legislation. In *UKACC International Conference on Control*. Loughborough.

Ersanilli, V.E. & Burnham, K.J., 2012. Comparison of Continuous-Time Vehicle Model Estimators as Candidates for Suspension System Fault Detection. In *International Conference on Systems Engineering*. Coventry.

Ersanilli, V.E., Burnham, K.J. & King, P.J., 2009. A Continuous-Time Model-Based Tyre Fault Detection Algorithm Utilising an Unknown Input Observer. In *International Conference on Systems Engineering*. Coventry.

Ersanilli, V.E., Burnham, K.J. & King, P.J., 2008. Comparison of Continuous-Time and Discrete-Time Vehicle Models as Candidates for Suspension System Fault Detection. In *IAR Workshop on Advanced Control and Diagnosis*. Coventry.

EU, 1998. *Directive 98/69/EC of the European Parliament and of the Council*,

Eubank, R.D., Atkins, E.M. & Ogura, S., 2010. Fault Detection and Fail-Safe Operation with a Multiple-Redundancy Air-Data System. *AIAA Guidance, Navigation, and Control Conference*, (August 2010), pp.1–14.

Evans, L., MacIsaac, J., Harris, J., Yates, K., Dudek, W., Holmes, J., Popio, J., Rice, D., Salaani, K., 2009. *NHTSA Tire Fuel Efficiency Consumer Information Program Development: Phase 2 – Effects of Tire Rolling Resistance Levels on Traction, Treadwear, and Vehicle Fuel Economy*,

Forssel, U., 2009. Safety aspects of tyre pressure monitoring systems. *Vision Zero International*, pp.110–112.

Franklin, G.F., Powell, J.D. & Workman, M.L., 1997. Digital Control of Dynamic Systems. , p.382.

Freescale, 2009. *MPXY8300 Tire Pressure Monitor Sensor Specification*, Austin. Available at: http://www.freescale.com/webapp/sps/site/prod_summary.jsp?code=MPXY8300.

Friedrich, C., 2006. *Condition Monitoring and Fault Detection for Vehicle Suspension*. Coventry University.

Gent, A.N. & Walter, J.D., 2006. *The Pneumatic Tire*, Akron.

Gertler, J., 1998. *Fault Detection and Diagnosis in Engineering Systems*, New York: Marcel Dekker, Inc.

Gertler, J. & Singer, D., 1990. A new structural framework for parity equation-based failure detection and isolation. *Automatica*, 26, pp.381–388.

GIA, 2013. *Tire Pressure Monitoring Systems (TPMS) - A Global Strategic Business Report*, Available at: http://www.strategyr.com/Tire_Pressure_Monitoring_Systems_TPMS_Market_Report.asp.

Gillespie, T.D., 1992. *Fundamentals of vehicle dynamics*, Warrendale: Society of Automotive Engineers, Inc.

Golub, G.H. & Van Loan, C.F., 1996. Matrix Computation. *books.google.com*. Available at: http://books.google.com/books?hl=en&lr=&id=mlOa7wPX6OYC&oi=fnd&pg=PR11&dq=Matrix+Computation&ots=lbfsh6O3kV&sig=IbGZAjJA0yHBGVmEO9KxLCzSo0o.

Greenwald, J., 2001. Inside the Ford/Firestone Fight. *TIME Magazine*. Available at: http://content.time.com/time/business/article/0,8599,128198,00.html.

Gustafsson, F., Drevo, M., Forssell, U., Mats, L., 2001. Virtual sensors of tire pressure and road friction. In *SAE 2001 World Congress*. Available at: http://papers.sae.org/2001-01-0796/.

Halfmann, C., Ayoubi, M. & Holzmann, H., 1997. Supervision of vehicles' tyre pressures by measurement of body accelerations. *Control Engineering Practice*, 5, pp.1151–1159.

Halfmann, C., Ayoubl, M. & Holzmann, H., 1997. Supervision of vehicles' tyre pressures by measurement of body accelerations. *Control Engineering Practice*, 5(8), pp.1151–1159.

Harris, C.H., 2011. *Volkswagen Group of America, Inc., Grant of Petition for Decision of Inconsequential Noncompliance*, Washington.

Heißing, B. & Ersoy, M., 2011. *Chassis Handbook: Fundamentals, Driving Dynamics, Components, Mechatronics, Perspectives (ATZ/MTZ-Fachbuch)* 1st ed., Berlin: Vieweg+Teubner Verlag.

Highways Agency, 2008. Design Manual for Roads and Bridges: Introduction and General Requirements v. 0. Available at: https://www.tsoshop.co.uk/bookstore.asp?ACTION=ADDITEM&PRODUCTID=9780115529634.

Hill, M. & Turner, J.D., 1992. Automotive Tyre Pressure Sensing. In *IEE Colloquium "Automotive Sensors."* Solihull.

Hodge, V.J. & Austin, J., 2004. A Survey of Outlier Detection Methodoligies. *Artificial Intelligence Review*, 22(2), pp.85–126.

Hu, Y., Xu, C., Zhang, Y., Lin, L., Snyder, R., Wang, Z., 2011. A nanogenerator for energy harvesting from a rotating tire and its application as a self-powered pressure/speed sensor. *Advanced Materials*, 23, pp.4068–4071.

Isermann, R., 2006. *Fault detection and diagnosis of an automotive suspension and the tire pressures*, 401-411, Fault-Diagnosis Systems, Springer-Verlag Berlin Heidelberg

Isermann, R., 1997. Supervision, fault-detection and fault-diagnosis methods - An introduction. In *Control Engineering Practice*. pp. 639–652.

Isermann, R. & Ballé, P., 1997. Trends in the application of model-based fault detection and diagnosis of technical processes. In *Control Engineering Practice*. pp. 709–719.

Isermann, R. & Wesemeier, D., 2009. Indirect Vehicle Tire Pressure Monitoring with Wheel and Suspension Sensors. In *7th IFAC Symposium on Fault Detection, Supervision and Safety of Technical Processes*. pp. 917–922.

Kim, B.S., Chi, C.H. & Lee, T.K., 2007. A study on radial directional natural frequency and damping ratio in a vehicle tire. *Applied Acoustics*, 68(5), pp.538–556. Available at: http://linkinghub.elsevier.com/retrieve/pii/S0003682X06001654 [Accessed January 1, 2014].

Kubba, A.E. & Jiang, K., 2014. A comprehensive study on technologies of tyre monitoring systems and possible energy solutions. *Sensors (Switzerland)*, 14, pp.10306–10345.

LaHood, R. & Jackson, L.P., 2011. *Greenhouse Gas Emissions Standards and Fuel Efficiency Standards for Medium and Heavy-Duty Engines and Vehicles*,

Leung, K.T., 2010. *Road vehicle state estimation using low-cost GPS/INS*. Available at: http://linkinghub.elsevier.com/retrieve/pii/S0888327010002888.

Li, L. & Wang, F.-Y., 2007. *Advanced motion control and sensing for intelligent vehicles*, Springer US.

Li, L., Wang, F.Y. & Zhou, Q., 2005. A watch in developments of intelligent tire inspection and monitoring. In *2005 IEEE International Conference on Vehicular Electronics and Safety Proceedings*. pp. 333–338.

Ljung, L., 2006. *System Identification Theory For User*,

Löhndorf, M., Kvisterøy, T., Westby, E., Halvorsen, E., et al., 2007. Evaluation Of Energy Harvesting Concepts For Tire Pressure. In *Technical Digest PowerMEMS 2007*. Freiburg, pp. 331–334.

Lu, L., Han, X., Li, J., Hua, J., Ouyang, M., 2013. A review on the key issues for lithium-ion battery management in electric vehicles. *Journal of Power Sources*, 226, pp.272–288. Available at: http://www.scopus.com/inward/record.url?eid=2-s2.0-84869862215&partnerID=40&md5=26ff11e08cd338fe531d6ebbb3d107f7.

Lundquist, C., Karlsson, R., Özkan, E., Gustafsson, F., 2014. Tire Radii Estimation Using a Marginalized Particle Filter Tire Radii Estimation Using a Marginalized Particle Filter. , (15), pp.663–672.

Matsuzaki, R. & Todoroki, A., 2006. Passive wireless strain monitoring of actual tire using capacitance–resistance change and multiple spectral features. *Sensors and Actuators A: Physical*, 126(2), pp.277–286. Available at: http://linkinghub.elsevier.com/retrieve/pii/S0924424705005881 [Accessed January 8, 2014].

Mayer, H., 1994. Comparative diagnosis of tyre pressures. In *Proceedings of the Third IEEE Conference on Control Applications, pp* 627 - 632 vol.1, *1994*, Glasgow

Mayer, H., 1995. Model based detection of tyre deflation by estimation of a virtual transfer function. In *Control Applications, 1995, Proceedings of the 4th …*. Available at: http://archive.nbuv.gov.ua/portal/Chem_biol/infKhvor/2011_4/recvisits.pdf [Accessed January 8, 2014].

McIntyre, M., Ghotikar, T., Vahidi, A., Song, X., Dawson, D., 2009. A two-stage Lyapunov-based estimator for estimation of vehicle mass and road grade. *IEEE Transactions on Vehicular Technology*, 58, pp.3177–3185.

Mercedes-Benz, 2013. *Mercedes-Benz*, Stuttgart. Available at: http://media.daimler.com/dcmedia/0-921-1549267-1-1597451-1-0-0-1597463-0-1-12759-614216-0-0-0-0-0-0-0.html [Accessed February 1, 2015].

Microchip, 2009. Enhanced Flash Microcontrollers With 10-Bit A/D and NanoWatt Technology. , pp.1–390.

Milek, J., 1995. Stabilized Adaptive Targeting in Recursive Parameter Estimation. In *Verlag der Fachvereine Hochschulverlag*. Zurich.

Modarres, M., Kaminskiy, M. & Krivtsov, V., 1999. *Realiability Engineering and Risk Analysis: A Practical Guide*, Available at: http://books.google.com/books?id=IZ5VKc-Y4_4C&pgis=1.

Muramatsu, S., Otsuka, Y., Takenaga, H., Kobayashi, Y., Furusawa, I., Monji, T., 2002. Image processing device for automotive vision systems. *Intelligent Vehicle Symposium, 2002. IEEE*, 1, pp.121–126.

Nakajima, M., 1998. Development of a tire deflation warning system. *SEI …*. Available at: http://scholar.google.com/scholar?hl=en&btnG=Search&q=intitle:Development+of+a+tire+deflation+warning+system#1 [Accessed August 22, 2014].

Navet, N., Song, Y., Simonot-Lion, F., Wilwert, C., 2005. Trends in automotive communication systems. In *Proceedings of the IEEE*. pp. 1204–1222.

Pacejka, H.B., 2006. *Tyre Characteristics and Vehicle Handling and Stability*, Oxford: Butterworth-Heinemann.

Pacejka, H.B., 2006. *Tyre and Vehicle Dynamics*, Butterworth-Heinemann, ISBN 9780080970165

Patwardhan, S., Tan, H.S. & Tomizuka, M., 1997. Experimental Results Of A Tire-Burst Controller For AHS. *Control Engineering Practice*, 5(l), pp.1615–1622.

Persson, N., Ahlqvist, S., Forssell, U., Gustafsson, F., 2001. Low Tire Pressure Warning System Using Sensor Fusion. In *Automotive & Transportation Technology Congress & Exhibition*.

Persson, N., Gustafsson, F. & Drevö, M., 2002. Indirect Tire Pressure Monitoring Using Sensor Fusion. In *SAE 2002 World Congress*. Detroit. DOI: 10.4271/2002-01-1250

Persson, N., Gustafsson, F. & Link, S.-, 2001. Event Based Sampling with Application to Vibration Analysis in Pneumatic Tires Department of Electrical Engineering. In *IEEE International Conference on Acoustics, Speech, and Signal Processing*. Salt Lake City.

Pisu, P. & Rizzoni, G., 2007. A comparative study of supervisory control strategies for hybrid electric vehicles. *IEEE Transactions on Control Systems Technology*, 15, pp.506–518.

Pohl, A., Ostermayer, G., Reindl, L., Seifert, F., 1997. Monitoring the Tire Pressure at Cars Using Passive SAW Sensors. In *1997 IEEE Ultrasonics Symposium Proceedings. An International Symposium (Cat. No.97CH36118)*. pp. 471–474.

Pohl, A., Steindl, R. & Reindl, L., 1999. The "intelligent tire" utilizing passive SAW sensors measurement of tire friction. *IEEE Transactions on Instrumentation and Measurement*, 48(6), pp.1041–1046. Available at: http://ieeexplore.ieee.org/lpdocs/epic03/wrapper.htm?arnumber=816111.

Prolific, 2012. PL-2303HX Edition (Chip Rev D) USB to Serial Bridge Controller Product Datasheet. , (1.4.3), pp.1–30.

Pucar, P., 2011a. NIRA Dynamics NEWS Quarterly Q1 2011. *NIRA Dynamics NEWS*.

Pucar, P., 2011b. NIRA Dynamics NEWS Quarterly Q3 2011. *NIRA Dynamics NEWS*.

Pucar, P., 2012. NIRA Dynamics NEWS Quarterly Q4 2012. *NIRA Dynamics NEWS*.

Rajamani, R., 2006. *Vehicle Dynamics and Control*, Available at: http://books.google.com/books?hl=en&lr=&id=N0cVzjChUccC&pgis=1.

Rodríguez-Madrid, J.G., Iriarte, G.F., Williams, O.A., Calle, F. 2012. High precision pressure sensors based on SAW devices in the GHz range. *Sensors and Actuators A: Physical*, 189, pp.364–369. Available at: http://linkinghub.elsevier.com/retrieve/pii/S0924424712005596 [Accessed January 8, 2014].

Ryan, J. & Bevly, D.M., 2012. Tire Radius Determination and Pressure Loss Detection Using GPS and Vehicle Stability Control Sensors. In *8th IFAC Symposium on Fault Detection, Supervision and Safety of Technical Processes (SAFEPROCESS)*. pp. 1203–1208.

Schrader, 2014. Schrader TPMS products. , 49(0), pp.1–27. Available at: http://www.schraderinternational.com/Document-Library/EU-TPMS-Application-Guide?sc_lang=en-US-E.

Sfaihi, B. & Boubaker, O., 2004. Full order observer design for linear systems with unknown inputs. *2004 IEEE International Conference on Industrial Technology, 2004. IEEE ICIT '04.*, 3.

Shyrokau, B. & Wang, D., 2013. Coordination of Steer Angles, Tyre Inflation Pressure, Brake and Drive Torques for Vehicle Dynamics Control. *SAE International Journal of Passenger Cars- Mechanical Systems.* Available at: http://www.sae.org/technical/papers/2013-01-0712 [Accessed January 8, 2014].

Simani, S., Fantuzzi, C. & Patton, R.J., 2003. *Model-based Fault Diagnosis in Dynamic Systems Using Identification Techniques*, London: Springer-Verlag.

Singh, S., Kingsley, K. & Chen, C.-L., 2009. *Tire Pressure Maintenance - A Statistical Investigation*, Washington.

Sivinski, R., 2012. *Evaluation of the Effectiveness Of TPMS in Proper Tire Pressure Maintenance*, Washington. Available at: http://www-nrd.nhtsa.dot.gov/Pubs/811681.pdf.

Smith, D., 1997. Low cost tyre monitoring system using electronic article surveillance techniques. In *IEE Colloquium on Tyre Monitoring*. Iee. Available at: http://digital-library.theiet.org/content/conferences/10.1049/ic_19970277.

Smith, T. & Knight, I., 2005. *Analysis of accidents involving light commercial vehicles in the UK*, Wokingham. Available at: http://www-nrd.nhtsa.dot.gov/pdf/esv/esv19/05-0315-O.pdf [Accessed January 8, 2014].

Sturmhoebel, J., 2012. *Tire Pressure and TPMS in Consumer Practice*, Stuttgart.

Tongue, B.H., 2002. *Principles of Vibration*, New York: Oxford University Press. Available at: http://www.amazon.co.uk/Principles-Vibration-Benson-H-Tongue/dp/0195142462 [Accessed February 1, 2015].

Transport Research Board, 2006. *Tires and Passenger Vehicle Fuel Economy*, Washington. ISBN 0309094216

Tuononen, A., 2009. On-board estimation of dynamic tyre forces from optically measured tyre carcass deflections. *International Journal of Heavy Vehicle Systems*, 16, p.362.

Umeno, T., 2002. Estimation of Tire-Road Friction by Tire Rotational Vibration. *R&D Review of Toyota CRDL*, 37, pp.53–58. Available at: http://www.tytlabs.com/english/review/rev373epdf/e373_053umeno.pdf\nhttp://www.tytlabs.com/english/review/gou.html.

Umeno, T., Asano, K. & Iwama, N., 1994. Estimation of parameter variation based on the disturbance observer - Application to the estimation of the inner pressure of tires. *IEEJ Transactions on Industry Applications*, pp.268–275.

Umeno, T., Ono, E. & Asano, K., 2002. Estimation of Tire-Road Friction Using Tire Vibration Model, SAE Technical.

UNECE, 2010. *Regulation No. 64 - Rev.1 - Temporary use spare unit, run flat tyres, run flat-system and tyre pressure monitoring system*, Geneva. Available at: http://www.unece.org/trans/main/wp29/wp29regs61-80.html.

US Congress, 2000. *Transportation Recall Enhancement, Accountability, and Documentation (TREAD) Act*,

US DoT, 2000. *Federal Motor Vehicle Safety Standards; Tire Pressure Monitoring Systems; Controls and Displays*,

US DoT, 2011. *FMVSS 126*, USA. Available at: http://www.nhtsa.gov/DOT/NHTSA/Rulemaking/Rules/Associated Files/ESC_FR_03_2007.pdf.

US DoT, 2007. *National Highway Traffic Safety Administration Laboratory Test Procedure For FMVSS 138 Tire Pressure Monitoring Systems*, Washington

US DoT, 2008. *National Motor Vehicle Crash Causation Survey Report to Congress*, Virginia.

US DoT, 2005. *Tire pressure monitoring system FMVSS no. 138 - final regulatory impact analysis*, Washington

Velupillai, S. & Güvenç, L., 2007a. Tire Pressure Monitoring. *IEEE Control Systems Magazine*, (December), pp.22–25.

Velupillai, S. & Güvenç, L., 2007b. Tire Pressure Monitoring [Applications of Control]. *Control Systems, IEEE*, 27(December), pp.22–25.

VisiTyre, 2001. *The Problems with Batteries in TPMS*, VisiTyre Automotive PL, Document DMS 02062009, Battery Environmental Concerns

Walker, C.J., 1991. *A Cautious Fault Detection Algorithm*. Coventry University, UK.

Walker, J.C. & Rehal, L.S., 1993. Method Of Detecting A Deflated Tire On A Vehicle.

Wang, Y., Chen, C. & Chien, L., 2012. System Analysis of a Suitable-Weighted-Pendulum Type Power Generator for TPMS. *Journal of Science and Innovation*, 2(2), pp.77–88.

Wong, J.Y., 2008. *Theory of Ground Vehicles 4th Edition*, Wiley, ISBN: 978-0-470-17038-0

Winstead, V. & Kolmanovsky, I.V., 2005. Estimation of road grade and vehicle mass via model predictive control. *Proceedings of 2005 IEEE Conference on Control Applications, 2005. CCA 2005.*

Yan, W., Li, C. J., & Goebel, K. F. (2006, April). A multiple classifier system for aircraft engine fault diagnosis. In *Proceedings of the 50th Meeting of the Machinery Failure Prevention Technology (MFPT) Society* (pp. 271-279).

Yanase, M., 2005. Diffusion Deflation Detection Using Wheel Speed Signals. In *International Technical Conference on the Enhanced Safety of Vehicles*. pp. 1–4.

Young, P., 1981. Parameter estimation for continuous-time models—A survey. *Automatica*, 17(1), pp.23–39.

Young, P. & Garnier, H., 2006. Identification and estimation of continuous-time, data-based mechanistic (DBM) models for environmental systems. *Environmental Modelling and Software*, 21(8), pp.1055–1072.

Young, P.C., 2004. Identification and estimation of continuous-time hydrological models from discrete-time data. *International Conference on Hydrology: Science and Practice for the 21st century. Volumen I*, I, pp.406–413. Available at: http://www.hydrology.org.uk/\/Publications/imperial/3A_24.pdf.

Zhang, X. & Wang, F.Y., 2009. Design and simulation of the tire pressure sensor based on the SAW resonator and the tire capacitor impedance. In *IEEE Intelligent Vehicles Symposium, Proceedings*. pp. 1173–1178.

Appendix 1

Test vehicle specifications

1996 Volvo V40 (1995 model year)

This item has been removed due to 3rd Party Copyright. The unabridged version of the thesis can be viewed in the Lanchester Library Coventry University.

2008 Ford C-Max (2003 model year)

This item has been removed due to 3rd Party Copyright. The unabridged version of the thesis can be viewed in the Lanchester Library Coventry University.

2008 Ford C-Max (2003 model year)

This item has been removed due to 3rd Party Copyright. The unabridged version of the thesis can be viewed in the Lanchester Library Coventry University.

Table A1.2 Ford C-Max specification

2008 Jaguar X-Type (2008 model year)

This item has been removed due to 3rd Party Copyright. The unabridged version of the thesis can be viewed in the Lanchester Library Coventry University.

Table A1.3 Jaguar X-Type specification

Appendix 2

Data acquisition equipment

The following sections provide details of the equipment used for carrying out the experimental work

ELM327 CAN Microprocessor

The ELM327 is a PIC-based (Microchip 2009, PIC18F2480 programmable microcontroller by Microchip Technology) CAN interpreter and serial interface able to communicate using the RS232 serial protocol, see Figure 0.1. Contemporary PC technology usually omits a RS232 serial port in favour of USB, this means implementations of the ELM327 usually feature a serial to USB bridge (Prolific 2012). This facilitates integration with PC-based software tools such as FORScan and ELMConfig, amongst many others.

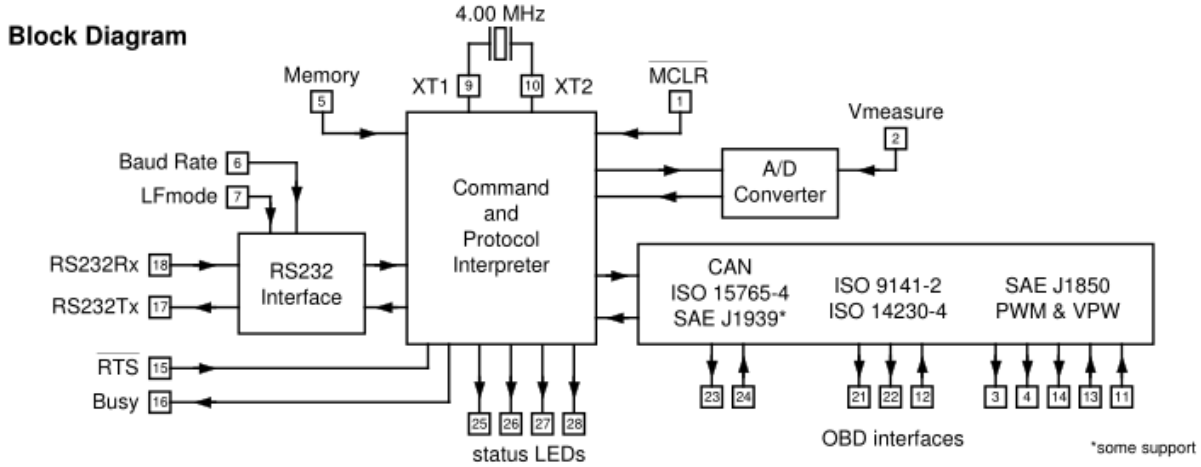

Figure A2.1 ELM327 CAN interpreter

AT commands

The ELM327 is controlled using the Hayes command set via the RS232 serial interface. The CAN message filter-mask are set using ‘AT CF hhh’ (set the CAN ID filter to hex address hhh) and ‘AT CM hhh’ (set the CAN ID mask to hex address hhh). This procedure is shown in the Table A2.1

Signal	CAN	Bit											
	ID	1	2	3	4	5	6	7	8	9	10	11	
Steer angle	**080**	0	0	0	1	0	0	0	0	0	0	0	
Wheel speeds	**4B0**	1	0	0	1	0	1	1	0	0	0	0	
		1	**1**	**0**	**1**	**0**	**1**	**1**	**0**	**0**	**0**	**0**	**0x6B0 Filter**
		0	**0**	**1**	**0**	**1**	**0**	**0**	**1**	**1**	**1**	**1**	**0x14F Mask**

Table A2.1 Configuring the filter-mask of the ELM327 for steering angle and wheel speed signals

PCL TG1 tyre pressure gauge

This item has been removed due to 3rd Party Copyright. The unabridged version of the thesis can be viewed in the Lanchester Library Coventry University.

The TPG1 is a pocket tyre pressure gauge with an angled head designed to fit onto the tyre valve at 90 degrees. It incorporates a self-adjusting friction device which enables the pressure to be read when the tyre pressure gauge is removed from the tyre valve, and a positive sealing washer to ensure measurement reliability.

Part No.	Description	Head Type	Calibration	Resolution
TPG1H01	Pocket Gauge	Angled	6-50 lbf/in² & 0.5-3.4 bar	1lb & 0.1bar units

Table A2.2 Tyre pressure gauge specification

USB Instruments DS1M12

This item has been removed due to 3rd Party Copyright. The unabridged version of the thesis can be viewed in the Lanchester Library Coventry University.

The DS1M12 is a portable, rugged oscilloscope-data logging tool for on-site data acquisition and diagnostics. The DS1M12 connects to a host PC via USB and the acquired signals are then processed and displayed by Microsoft Windows compatible software, supplied with the device. The device combines the functions of oscilloscope, data logger, spectrum analyser and frequency meter. The oscilloscope and spectrum analyser functions allow the user to quickly identify the signal of interest and select an appropriate sampling interval for the data logging application.

The DS1M12 has two independent input channels with capability to simultaneously acquire signals on both channels with 12-bit resolution. With the specification $20V$ input range this implies a voltage resolution of $\frac{20}{2^{12}} = 4.9mV$, confirmed by testing. The unit is capable of sample rates up to a theoretical $1MS/s$ (million samples per second) and in practice the device is able to capture signal dynamics at $100kHz$.

The signals are acquired and the data are stored in a variety of formats with a time stamp per sample, optimised either for compactness (binary format) or compatibility (CSV format) with processing and analysis software such as MATLAB and Excel.

Micro-Electronic Prognostic Health Monitor (MEPHM)

As stated in Chapter 3, the MEPHM module is a device produced by BAE Systems. It is designed to monitor environmental and electronic data from a host system. This data can then be processed, analysed and either stored within the module's non-volatile EEPROM, or accessed/transmitted via one or more of the interfaces shown in Figure A2.2. The architecture, illustrated in Figure A2.2, comprises the DSC Core, containing the system RAM, Timers, Interrupt Controller, Program Store, Non-Volatile EEPROM Memory, Temperature Sensor and the Vibration Sensor together with associated signal conditioning hardware.

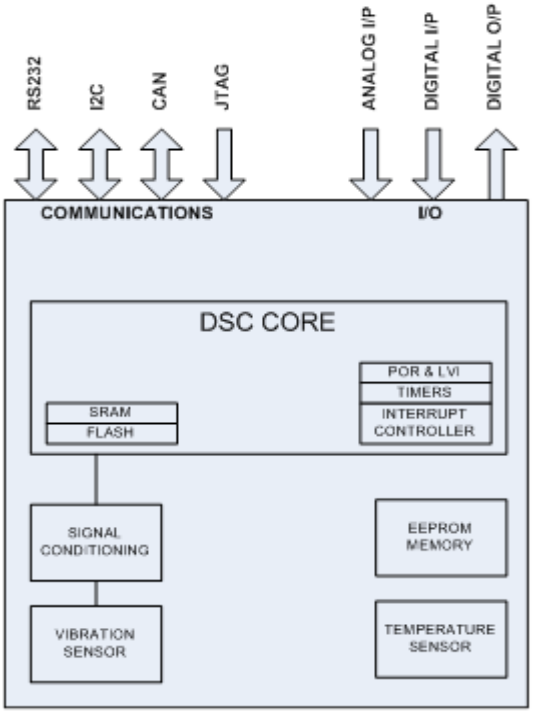

Figure A2.2 MEPHM architecture and I/O

Vibration is measured using a 3-axis MEMS accelerometer, to a maximum of +/-10g. The low-pass filter provides a roll-off of 40dB per decade to reduce aliasing, with a knee-point at 1000Hz. The time series accelerometer data is converted into spectral data via a FFT and output in 8 byte messages on the CAN bus. It can also be acquired via the RS232 serial interface. Since the data acquisition laptop PC was equipped with Vector CANalyzer, this was the most convenient way to acquire and store the data as compact log files for later analysis. The Controller Area Network (CAN) bus interface provides connectivity for using the MEPHM in an automotive environment at the 'high speed' 500kbit data rate that is common to most vehicle powertrain distributed control systems. In this application the data was captured by a Vector CANalyzer, installed in a laptop PC.

Data acquisition-processing software

FORScan

FORScan is Windows compatible software for diagnostics and data logging of CAN based vehicle control systems. Compatibility is limited to Ford, Mazda, Lincoln and Mercury vehicle brands. Within this software is a data logging facility that allows the user to specify OBD (Directive 98/69/EC of the European Parliament and of the Council 1998) sanctioned parameters and create a time series measurement file in CSV format. The creators of the software have avoided the problem of unknown message ID, format and location by restricting the available parameters to the OBD sub-set. In many cases this results in reduction of the parameter resolution and increased sampling interval. These constraints are attributed to the retrieval mechanism (the OBD protocol and ECU diagnostic function/interface) which has low network priority. See the CAN section for more details.

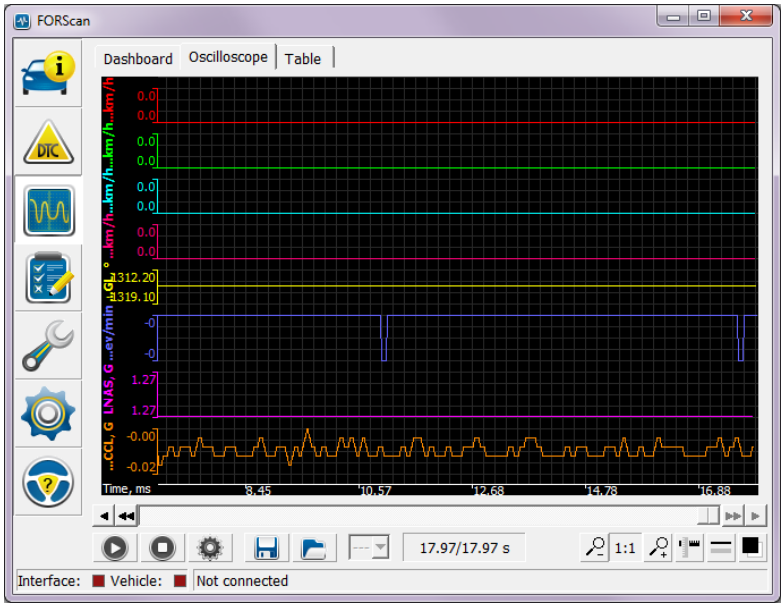

Figure 0.1 The data logging interface of FORScan

The contents of a typical ‘connection log’ are shown below. Note the presence of Diagnostic Trouble Codes (DTC) for ABS and EPS. DTC are designed as an indicator of degraded vehicle/control function and as an aid for fault diagnosis.

```
(OK) [12:36:07.183] Connection to adapter is established on COM5
(OK) [12:36:07.183] Adapter:  ELM327 v1.5
(OK) [12:36:07.396] Connection to vehicle is established
(OK) [12:36:11.590] Vehicle: Ford Focus C-MAX DURATEC-HE / I4 2.0L
2008.25 MY, VIN: WF0*********31973
(OK) [12:36:12.563] Found module:  TCM - Transmission Control Module
```

```
(OK) [12:36:13.869] Found module:  PCM - Powertrain Control Module
(OK) [12:36:14.110] Found module:  OBDII - On Board Diagnostic II
(OK) [12:36:15.615] Found module:  ABS - Anti-Lock Brake / Traction
Control Module
(WARN) [12:36:15.747] DTCs in ABS: C1165-E0
(OK) [12:36:16.480] Found module:  EPS - Electronic-Controlled Power
Steering
(WARN) [12:36:16.554] DTCs in EPS: U1900-20
(OK) [12:36:17.361] Found module:  IC - Instrument Cluster
```

ELMConfig

ELMconfig is Windows compatible software for configuration, diagnostics and data logging of CAN based vehicle control systems. As the name suggests, its main purpose if configuration of the electronically controlled systems present on a vehicle. In addition to the configuration functions, a CAN data logging function allows the user to capture any or all CAN data frames that are broadcast by the vehicle controllers. Due to the baud rate of a high speed CAN and the limited internal memory of the ELM327 PIC, it is not possible to log all frames indefinitely, a buffer over-run occurs after approximately 2 seconds (in the case of data logging of the Ford C-Max HS-CAN). This constraint is mitigated by a filter-mask configuration, whereby only specific sets of messages are logged and committed to the log file, the remainder are immediately discarded.

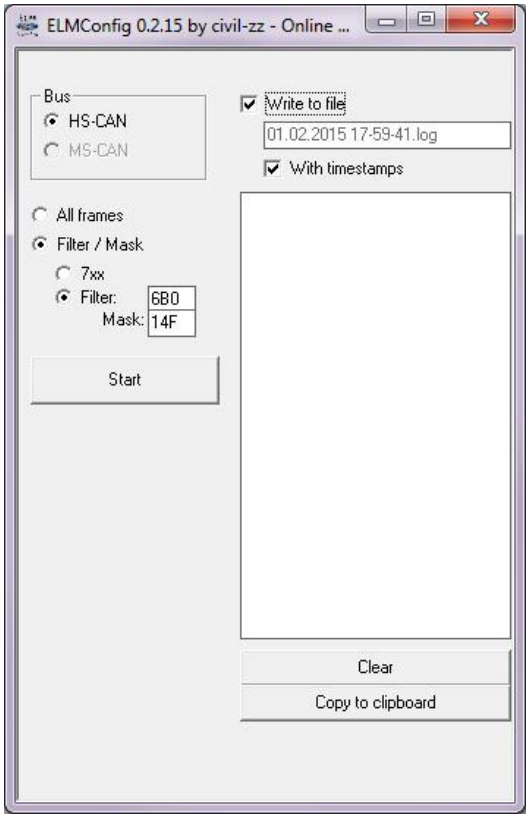

Figure 0.2 ELMConfig in data acquisition mode with filter-mask set to obtain

A snippet of a typical vehicle data log from the CAN bus is shown below

```
Version: ELMConfig 0.2.15
Adapter: ELM327
Driver: VCP
Baudrate: 500000
Connection: Scan

14:20:28.201 220 02 0D 00 00 00 00 11 19
14:20:28.201 200 27 33 27 EA 27 EA 80 18
14:20:28.201 430 5B 4C
14:20:28.201 080 13 8A 75 30 01 32 E9
14:20:28.217 090 97 02 D7 08 C7 D3 07 D0
14:20:28.217 4B0 27 10 27 10 27 10 27 10
14:20:28.217 220 02 0D 00 00 00 00 11 19
14:20:28.217 200 27 33 27 EA 27 EA 80 18
```

In this example, the so-called ‘high speed’ bus of a 2008 Ford C-Max is sampled. The network is given the name ‘high speed’ or HS-CAN simply to differentiate it from the other CAN present on this particular vehicle, a reduced baud (256kbit) ‘medium speed’ or MS-CAN network. HS-CAN connects engine management, transmission, ABS, electronic-controlled power steering, instrument cluster and facilitates the distributed functionality of the vehicle control. The data log starts with a header describing the software version number, interface hardware type, software driver type, vehicle network baud rate (bits/s) and the ELMconfig mode of operation. ELMConfig may be configured to timestamp each message it detects on the network but the time is not associated with the vehicle controllers, each of which is keeping an internal clock, not visible on the network. The Timestamp relates to the internal clock of the host PC.

The major obstacle to overcome by logging raw data is, unlike the OBD parameters, there is no definition for the data. Targeted experimentation is required to interpret the data into a meaningful signal.

Controller Area Network

The Controller Area Network (CAN) is a serial communications protocol which facilitates distributed real-time control with a very high level of resilience to data corruption and degradation of the physical layer (electrical faults). Its domain of application ranges from high speed networks to low cost multiplex wiring. In automotive electronics, engine control units, sensors, anti-skid-systems, for example, are connected using CAN with bitrates up to 1 Mbit/s (Bosch 1991). A typical data frame is shown in Figure X.X, these frames are the primary source of information on the data bus.

Arbitration (handling transmitter conflicts)

Whenever the bus is free, any unit may start to transmit a message. If 2 or more units start transmitting messages at the same time, the bus access conflict is resolved by bitwise arbitration using the identifier (ID). The mechanism of arbitration guarantees that neither information nor time is lost. If a data frame and a remote frame with the same identifier are initiated at the same time, the data frame prevails over the remote frame. During arbitration every transmitter compares the level of the bit transmitted with the level that is monitored on the bus. If these levels are equal the unit may continue to send. When a ’recessive’ level is sent and a ’dominant’ level is monitored (see Bus Values), the unit has lost arbitration and must withdraw without sending one more bit (Bosch 1991).

Consider an 11-bit ID CAN network, with two nodes with IDs of 15 (binary representation, 00000001111) and 16 (binary representation, 00000010000). If these two nodes transmit at the same time, each will first transmit the start bit then transmit the first six zeros of their ID with no arbitration decision being made. In the following example of an 11-bit (CAN 1.2) ID network, with constituent nodes 15 (0x00F) and 16 (0x010), both are attempting to transmit at the same time. This situation will continue until node sixteen transmits a ‘1’ in bit position four and node fifteen a ‘0’. It is in this way identifiers with a smaller value are given priority (typically safety and mission critical systems such as ABS and powertrain). This must also be balanced with periodicity of the messages. If a message is important but does not occur very often, this is usually assigned a low ID value. If the message is important and occurs very frequently, it may be assigned a middle range value in order to avoid monopoly of the data bus (it will lose in arbitration).

	Start Bit	ID Bits										The Rest of the Frame
		10	9	8	7	6	5	4	3	2	1	0	
Node 15	0	0	0	0	0	0	0	0	1	1	1	1	
Node 16	0	0	0	0	0	0	0	1	Stopped Transmitting				
CAN Data	0	0	0	0	0	0	0	0	1	1	1	1	

Table 0.1 Arbitration between two CAN nodes

Overload

Overload of the CAN bus can occur if there are too many ECU attempting to transmit this is signalled by the transmission of an overload frame. It is primarily for this reason that diagnostic messages are confined to the 0x7xx range.

Diagnostic interface

A diagnostic interface is not specified in the CAN standard, despite the dependence of modern diagnostics on CAN. The standard method for interrogation of vehicle control systems, in order to obtain DTC and other parameters is via the diagnostic interface, commonly referred to as the 'J1962 connector' that exists in the drivers footwell. In most vehicles, there will be an access point to other non-OBD networks, present in the J1962 connector.

A typical vehicle ECU parameter specification can be seen in (Deutz 2014) which lists the available signals and their composition and location

This item has been removed due to 3rd Party Copyright. The unabridged version of the thesis can be viewed in the Lanchester Library Coventry University.

Table 0.2 CAN data frame composition (Bosch 1991)